Rockefeller University
Digital Commons @ RU

Student Theses and Dissertations

2008

Visualizing Dendritic Cells In Vivo

Randall L. Lindquist

Follow this and additional works at: http://digitalcommons.rockefeller.edu/student_theses_and_dissertations

Part of the Life Sciences Commons

Recommended Citation
Lindquist, Randall L., "Visualizing Dendritic Cells In Vivo" (2008). *Student Theses and Dissertations.* Paper 200.

This Thesis is brought to you for free and open access by Digital Commons @ RU. It has been accepted for inclusion in Student Theses and Dissertations by an authorized administrator of Digital Commons @ RU. For more information, please contact mcsweej@mail.rockefeller.edu.

VISUALIZING DENDRITIC CELLS *IN VIVO*

A Thesis Presented to the Faculty of
The Rockefeller University
in Partial Fulfillment of the Requirements for
the degree of Doctor of Philosophy

by
Randall L. Lindquist
June 2008

© Copyright by Randall L. Lindquist 2008

ABSTRACT

Cell:cell interactions are critical at all stages of the immune response, yet relatively little is known about their dynamics *in vivo*. We set out to visualize in intact, living lymphoid tissue the physiological role of dendritic cells in tolerance and immunity; this was achieved by intravital microscopy of fluorescently-labeled DCs and lymphocytes in the inguinal lymph nodes. We generated mice that specifically expressed EYFP in their dendritic cells and observed their behavior in living LNs; we found that in the steady state, DCs formed sessile networks and largely restricted their movements to probing with their dendrites. We next observed dendritic cells' interactions with transferred fluorescently labeled T cells under conditions of tolerance and immunity, and found both were characterized by similar activation, proliferation, and early antigen-dependent T cell arrest. Based on our initial observation that early tolerogenic and immunogenic interactions are similar, we investigated the role of TCR affinity for MHC:peptide complexes (pMHC) in these interactions during tolerance induction. We observed that pMHC potency correlates with T cell proliferation, Ca^{2+} flux and with early antigen-specific arrest; T cell anergy was induced by all ligands that activated T cells, and was independent of T cell proliferation, Ca^{2+} flux, and early arrest *in vivo*. We further examined the *in vivo* dynamics of germinal center reactions, and observed that germinal centers are dynamic structures, with nearly all GC B cells remaining motile and restricted to the germinal center, migrating bidirectionally between dark and light zones. Follicular B cells passed through the GC compartment easily, and were able to join ongoing GC reactions in an affinity-dependent fashion.

Acknowledgments

I would first like to thank Michel Nussenzweig, for all of his mentorship, advice, and help. He welcomed me into his laboratory right away, and handed me the greatest project ever, on a silver platter. He is an excellent mentor, and a wonderful teacher; I cannot begin to imagine a better laboratory in which to train as a scientist, and cannot begin to express how indebted to him I am.

I would also like to thank our collaborator Mike Dustin at NYU, who has been an integral part of every experiment in this body of work. Without his expertise, unflagging cheerfulness, or willingness to let us use his microscope, none of this could have been accomplished.

I worked more closely with Guy Shakhar, then in Mike's lab at NYU, than with anyone else on these experiments. Guy was always a pleasure to work with, even while tracking T cells in Volocity at ungodly hours of the night; none of these experiments could have been performed without his expertise or attitude.

I would like to thank everyone in the Nussenzweig Lab for making it such an enjoyable place to work. I would specifically like to thank Hedda Wardemann for beginning the project by generating the CD11c-EYFP transgene, and for showing me how to use our FACSCalibur. I would like to thank Diana Dudziak for her friendship, for help with the T cell responses and for sharing her antibodies. Dimitris Skokos introduced me to the TCR affinity project and helped with the T cell responses, and was always willing to go to the Faculty Club when experiments were not working. Tanja Schwickert introduced me to the GC project, which has turned out well so far and promises to be even more productive. Anna Gazumyan was a wonderful baymate, always full of suggestions for experiments, concerts, museum exhibitions, and apples or assorted Russian delicacies. Revati Masilamani and I had many 3 AM conversations about our experiments, and possibly more 3:15 conversations about everything else; these were invaluable in maintaining my sanity, such as it is. Kevin McBride was a valued colleague and participant in a select few of the above conversations.

Other lab members to whom I am grateful include Tom Eisenreich for making the CD11c-EYFP mouse that served as a foundation for this work, and for additional

invaluable assistance with mice; Tanya Obukhanych showed me how to use the cryostat to cut frozen sections; Almudena Ramiro supervised my first six months in the lab, and helped me get grounded and find my way around; Klara Velinzon kindly helped me with the first FACS experiments; I am also grateful to Zoran and Virginia for keeping everything astonishingly well-organized and smoothly running.

I would also like to thank my thesis committee members: Ralph Steinman, Jeff Ravetch, and Eric Pamer, for their invaluable comments and criticisms at all stages of my research, and Thorsten Mempel, for kindly traveling from Boston to participate in my thesis defense.

Lastly, I would like to thank my parents und mein liebchen for their love and support.

Table of Contents

Chapter 1: Introduction 1

Establishment of self-tolerance 4

Maintenance of self-tolerance 5

Initiation of adaptive immune responses 6

Dendritic cells and self-tolerance 9

Leukocyte trafficking and function 11

Leukocyte migration within tissues 16

In vivo imaging of immune responses 17

Steady-state behavior of dendritic cells 21

Comparison of tolerogenic and priming T cell responses 22

TCR affinity for pMHC and T cell dynamics *in vivo* 24

Dynamics of germinal center reactions 25

Summary 26

Chapter 2: Methods 27

Transgenic mice 27

Immunofluorescence 28

Confocal microscopy 29

Flow cytometry analysis of DCs 29

Recombinant antibody production 30

Cell transfer, labeling, and antigen delivery for imaging experiments 30

In vivo OT-II T cell responses 32

In vivo B cell experiments - Germinal Center joining and affinity 32

In vivo AND T cell responses 33

Surgery for intravital imaging of inguinal LN 33

Intravital microscopy 34

Data analysis 35

Altered peptide ligand synthesis 37

In vitro T cell responses 38

In vitro calcium measurements 39

Chapter 3. Imaging DCs *in vivo* 41
CD11c-EYFP mice express EYFP specifically in their dendritic cells 41
Blood and lymph flow are preserved during intravital imaging 42
Dendritic cell movement varies by microanatomical location 42
Dendritic cells form clusters with B and T lymphocytes at the B-T interface 43
Migrant DCs join the endogenous DC network 44

Chapter 4. DC:T cell interactions under tolerizing and immunizing conditions 59
Tolerance and priming are characterized by similar retention near HEVs 60
Imaging tolerance and immunity 60
Analysis of cell motility parameters 61
Tolerized T cells rapidly undergo an antigen-specific arrest 62
Priming yields an antigen-specific arrest similar to that observed in tolerance 63

Chapter 5. pMHC potency in DC:T cell interactions 86
pMHC potency correlates with activation and proliferation *in vitro* 86
pMHC potency correlates with activation and proliferation *in vivo* 87
pMHC potency correlates with early antigen-specific T cell arrest 88
pMHC potency correlates with Ca^{2+} flux *in vitro* 90
pMHC potency correlates with Ca^{2+} flux *in vivo* 91

Chapter 6. Imaging Germinal Center Reactions 109
GCs are open structures in which antigen-specific B cells are retained 110
There is no net B cell migration between GC light and dark zones 112
GC B cells decelerate upon making antigen-specific contacts but do not arrest 112
B cells compete on the basis of affinity for antigen to join ongoing GC reactions 113

Chapter 7. Discussion 128
T cell Antigenic Search Algorithm 128
Initial stages of priming and tolerance induction are similar 130
pMHC potency, Ca^{2+}, and the dynamics of DC:T cell interactions 136
Dynamics of germinal centers *in vivo* 138
Antigen recognition and cellular dynamics 142
Appendix: Movie Legends 144
References 155

List of Figures

Figure 3.1	Brightness and surface markers of CD11c-EYFP cells	45
Figure 3.2	Flow cytometric analysis of EYFP cells visible by two-photon microscopy	47
Figure 3.3	CD11c-EYFP mice examined by immunofluorescence	49
Figure 3.4	Anatomic distribution and behavior of DCs within the lymph node	51
Figure 3.5	$CD11c^+$ DCs form clusters with T and B cells in the steady state	53
Figure 3.6	DC clusters include more than one DC	55
Figure 3.7	Transferred ECFP DCs gradually incorporate into the endogenous DC network	57
Figure 4.1	OT-II T cell activation and tolerance induced by α-Dec-Ova	66
Figure 4.2	T cells are retained antigen-specifically near HEVs early in tolerance and priming	68
Figure 4.3	Experimental timeline for imaging T cell tolerance and priming	70
Figure 4.4	T cell velocity under tolerizing conditions	72
Figure 4.5	T cell arrest under tolerizing conditions	74
Figure 4.6	T cell directionality under tolerizing conditions	76
Figure 4.7	T cell velocity under priming conditions	78
Figure 4.8	T cell arrest under priming conditions	80
Figure 4.9	T cell directionality under priming conditions	82
Figure 4.10	Normalized mean cell velocities under tolerizing and priming conditions	84
Figure 5.1	Differential activation of $CD4^+$ AND T cells by APLs	93
Figure 5.2	Anti-DEC delivers antigen to DCs *in vivo*	95
Figure 5.3	Activation of AND T cells *in vivo* by α-DEC-MCC and α-DEC-APL constructs	97
Figure 5.4	T cell proliferation is not required for anergy induction *in vivo*	99
Figure 5.5	pMHC potency drives early T cell deceleration	101
Figure 5.6	pMHC potency drives Ca^{2+} flux and arrest *in vitro* in T cell blasts	103

Figure 5.7	pMHC potency drives Ca^{2+} flux and arrest *in vitro* in naïve T cells	105
Figure 5.8	pMHC potency drives Ca^{2+} flux and arrest *in vivo*	107
Figure 6.1	Transferred B cell frequency and oligoclonal generation of GCs	114
Figure 6.2	Flow cytometric and histological analysis of NP/B1-8^{hi} GC kinetics	116
Figure 6.3	FDC-M1 *in vivo* staining	118
Figure 6.4	Behavior of GC and naïve B cells in secondary follicles	120
Figure 6.5	Analysis of B cell behavior in GC LZ and DZ	122
Figure 6.6	Analysis of contacts between B cells and FDC-$M1^{+}$ cells	124
Figure 6.7	B cell entry into ongoing GC reactions is affinity-dependent	126

List of Movies

Movie 3.1 Anatomic location of $EYFP^+$ DCs within the LN

Movie 3.2 Reconstruction of $EYFP^+$ DCs within the LN

Movie 3.3 Blood flow remains intact during intravital imaging

Movie 3.4 Lymph flow remains intact during intravital imaging

Movie 3.5 Extravasation is occasionally observed

Movie 3.6 Example of phototoxicity

Movie 3.7 Subcapsular sinus DCs and macrophages

Movie 3.8 Subcapsular DCs probing movement

Movie 3.9 T cell zone DCs form an extensive network

Movie 3.10 T cell zone DC network dynamics

Movie 3.11 Perifollicular DCs in relation to the LN capsule

Movie 3.12 Movement patterns of follicular and perifollicular DCs

Movie 3.13 DC clusters observed at the T-B interface

Movie 3.14 Z-stack through DC clusters in Movie 3.13

Movie 3.15 The behavior of DC clusters in the T-B interface zone.

Movie 3.16 Resident LN DCs and transferred mature DCs of splenic origin

Movie 3.17 DC intravasation into HEV

Movie 4.1 Tolerizing interactions 1-6 h after T cell transfer

Movie 4.2 Tolerizing interactions 6-12 h after T cell transfer

Movie 4.3 Tolerizing interactions 12-18 h after T cell transfer

Movie 4.4 Priming interactions 1-6 h after T cell transfer

Movie 4.5 Priming interactions 6-12 h after T cell transfer

Movie 4.6 Priming interactions 12-18 h after T cell transfer

Movie 4.7 T cell cluster

Movie 4.8 T cell swarming without YFP DC

Movie 5.1 T cells arrest upon recognizing the high-potency pMHC L98A

Movie 5.2 T cells do not arrest upon recognizing the medium-potency pMHC Y97K

Movie 5.3 T cells do not arrest upon recognizing the low-potency pMHC T102L

Movie 5.4 *In vitro* Ca^{2+} flux in response to unloaded GPI–I-E^k

Movie 5.5 *In vitro* Ca^{2+} flux in response to L98A
Movie 5.6 *In vitro* Ca^{2+} flux in response to Y97K
Movie 5.7 *In vitro* Ca^{2+} flux in response to T102L
Movie 5.8 *In vivo* Ca^{2+} flux in response to α-Dec-L98A
Movie 5.9 *In vivo* Ca^{2+} flux in response to α-Dec-Y97K
Movie 5.10 *In vivo* Ca^{2+} flux in response to α-Dec-T102L
Movie 5.11 *In vivo* Ca^{2+} flux in untreated control
Movie 6.1 Overview of a germinal center
Movie 6.2 Dynamics of GC B cells
Movie 6.3 Dynamics of GC B cells without antigen boost
Movie 6.4 Dynamics of a GC without FDC labeling
Movie 6.5 Dynamics of specific B cell:FDC contacts
Movie 6.6 Dynamics of nonspecific B cell:FDC contacts

CHAPTER 1. INTRODUCTION

The immune system has fascinated people since antiquity. The first written description of immune memory is from Thucydides, describing the plague of Athens in 430 B.C.: those people who recovered from the plague, himself included, could care for the sick without becoming ill again (Thucydides and Warner, 1954). Inflammation was recognized as a response to illness not long after, and the cardinal signs were described by Celsus in the first century A.D.: rubor (redness), tumor (swelling), calor (heat), and dolor (pain) (Celsus and Spencer, 1938). Since immune responses were recognized, the question of how the body could tell self from non-self has been the primary focus of immunology.

Much of the interest in immunology has been due to its obvious immediate clinical applications, such as vaccination. From the time of Edward Jenner's smallpox vaccine, nothing was known about the mechanism by which hosts were protected until Behring and Kitasato demonstrated antitoxins against diptheria. Although Metchnikoff showed that macrophages could phagocytose bacteria, it proved too difficult to "stimulate the phagocytes", (Shaw, 1906), and cellular immunity fell out of favor, as the humoral theories proved themselves with antisera.

One of the fundamental conceptual leaps in immunology was made by Karl Landsteiner, with the discovery that antibodies could be generated to chemically synthesized organic molecules if they were attached to a protein carrier. If the immune system can specifically recognize arbitrary, synthetic molecules that have not previously existed in nature, then antigenic space is not inherently limited to pathogens, which

implies that the immune system is capable of generating reactions against self as well as non-self. The rarity of autoimmunity implies a strong suppression of reactivity against self antigens, something noted by Paul Erlich in his writings marveling that the body manages to avoid a “horror autotoxicus” (Himmelweit, 1956-1960).

The mechanism of immune specificity was controversial, with arguments being made for both “instructive” and “selective” theories. In the former, the antigen served as a template for the folding of antibody; antibodies obtained specificity from their interaction with antigen. The selective theories postulated that specific antibodies were formed and reaction with antigen stimulated the production of that antibody. The best-formulated selective theory was Ehrlich’s “side-chain” theory, which said that “side chains” were preformed and secreted in response to antigen. As people found it difficult to conceive that the body could have preformed antibodies against chemically synthesized molecules that did not previously exist in the environment, instructive theories became more accepted, and selective theories were largely ignored, until the question of self-tolerance was raised by Medawar’s experiments showing transplantation tolerance (Billingham et al., 1953).

As self-tolerance came into focus, selective theories seemed more reasonable. Niels Jerne put forth a reformulation of Ehrlich’s side-chain theory (Jerne, 1955), which was expanded on by David Talmage (Talmage, 1959) and Macfarlane Burnet (Burnet, 1959). Burnet most clearly formulated the theory of clonal selection, which which postulated that immune cells each expressed one unique, randomly-generated receptor, that cells are only active after encountering their cognate antigen, and that self-reactive clones are deleted during development (Burnet, 1959). Others contributed to the

formulation of this theory as well, with Joshua Lederberg proposing "random assembly of the DNA of the globulin gene during certain stages of cellular proliferation" (Lederberg, 1959); this was proven correct seventeen years later, with the demonstration that antibody diversity is generated somatically, through recombination (Brack et al., 1978; Hozumi and Tonegawa, 1976).

The general paradigm of self and non-self does not completely describe the immune system, however. Charles Janeway observed that the adaptive immune response has evolved to protect its host from pathogenic non-self, and postulated that receptors existed that could distinguish pathogenic molecules from non-pathogenic molecules (Janeway, 1989): as the non-self molecules that threaten the host are pathogens, there must be some way to differentiate between pathogenic non-self and irrelevant non-self. This idea of pattern recognition receptors was proven right shortly thereafter with the discovery that Drosophila *toll* is necessary for defense against fungi but not bacteria (Lemaitre et al., 1996). The first mammalian innate receptor to be functionally characterized was toll-like receptor 4 (TLR4), which recognizes lipopolysaccharide, a component of the cell wall of gram-negative bacteria (Hoshino et al., 1999; Poltorak et al., 1998; Qureshi et al., 1999). Since then, the critical importance of a second, antigen-independent, pathogen-derived signal in initiating immune responses has become more evident (Janeway and Medzhitov, 2002); it is now known that TLRs are just one of the signaling mechanisms by which pathogens are detected (Gavin et al., 2006; Inohara and Nunez, 2003).

Initiation of adaptive immune responses

Adaptive immune responses begin with antigen presentation to naïve T cells in the lymph node paracortex; dendritic cells engulf antigenic particles and degrade proteins into short peptides which are presented on MHC class I and II molecules (Itano and Jenkins, 2003). Some reports have suggested that the extent of antigen processing and presentation by DCs is influenced by TLR-mediated pathogenicity sensing (Blander and Medzhitov, 2004; Blander and Medzhitov, 2006), but this remains controversial, as these experiments were done *in vitro* and conflict with much *in vivo* data showing that DCs constantly process and present self antigens to T cells in the draining lymph node(Scheinecker et al., 2002; Steinman et al., 2003b; Wilson et al., 2004). DCs from gastric LNs were found to present peptides from gastric parietal cell H^+/K^+ ATPase, while DCs from skin-draining and mesenteric LNs did not, indicating that DCs present endogenous self-antigens in non-inflammatory conditions *in vivo* (Scheinecker et al., 2002). Subsequently, immature, endogenous DCs were shown to process and present membrane-bound antigen to transgenic T cells, in the absence of any inflammatory state (Wilson et al., 2004). Furthermore, numerous studies delivering antigen to multiple endocytic receptors on DCs has demonstrated that antigen is processed and presented to T cells efficiently in the absence of any priming stimulus (Bonifaz et al., 2002; Dudziak et al., 2007; Hawiger et al., 2001; Idoyaga et al., 2008). The inconsistency between these studies and the *in vitro* data may be due in part to differences between bone-marrow derived macrophages and DCs *in vitro* and the physiological setting of intact lymphoid

organs, with multiple subtypes of dendritic cells, other immune cells, stromal cells, and a more diverse cytokine milieu.

Naïve T cells require more than antigenic stimulation through their TCR ("signal 1") to generate immune responses; in the absence of T cell CD28 signaling ("signal 2", mediated through costimulatory molecules such as CD80 and CD86 on APCs), naïve T cells are anergized (Bretscher and Cohn, 1970; Janeway, 1989; Jenkins et al., 1987; Lenschow et al., 1996). The upregulation of costimulatory molecules on APCs is rapidly induced by innate responses, including TLRs (Medzhitov et al., 1997); this prevents non-pathogenic antigens from inducing potentially harmful immune responses.

T cells that recognize their cognate pMHC and receive the proper costimulatory signals upregulate molecules that increase their sensitivity to proliferative cytokines (Leonard et al., 1984; Leonard et al., 1983) and that inhibit their ability to leave the lymph node (Shiow et al., 2006). Activated T cells proliferate in the lymph node over a three-day period, and eventually leave the lymph node through efferent lymphatics, to re-enter the circulation via the thoracic duct (Gowans and Knight, 1964). Relatively little is known about how lymphocytes exit from LNs, but it is a highly regulated process that requires sphingosine-1-phosphate receptor-1 ($S1P_1$) signaling (Mandala et al., 2002; Matloubian et al., 2004).

Establishment of self-tolerance

Both T and B cell antigen receptors are assembled somatically by random recombination of gene segments, which leads to both self- and non-self-reactivity (Janeway et al., 2001); to avoid autoimmunity and horror autotoxicus, self-reactive cells

must be purged. Most immunologic tolerance to self antigens is established centrally, during T cell development in the thymus and B cell development in the bone marrow; this prevents most autoreactive cells from ever encountering self antigens. Developing $CD4^+CD8^+$ thymocytes are first positively selected for recognition of host antigen-presentation molecules in the thymic cortex, with cells that fail to bind MHC dying by apoptosis, and surviving cells undergoing lineage commitment to the $CD4^+$ or $CD8^+$ single-positive thymocytes (Starr et al., 2003). Surviving single-positive thymocytes then migrate to the medulla and are negatively selected for recognition of self antigens, with cells that bind self-pMHC too tightly dying by apoptosis. The migration of single-positive cells to the medulla is driven by their upregulation of CCR7 (Kwan and Killeen, 2004; Misslitz et al., 2004; Ueno et al., 2004); although negative selection can occur at the double-positive stage, the thymic cortex has a very limited peptide repertoire, and DP thymocytes do not effectively undergo negative selection. Single-positive thymocytes remain in the medulla for 1-2 weeks while they undergo negative selection (Starr et al., 2003); this serves to ensure that all T lymphocytes that exit to the periphery recognize only foreign pMHC, preventing autoreactivity.

However, the mechanism of negative selection seems to be incomplete: if some proteins (i.e. tissue-specific hormones like thyroxin or insulin) are only expressed in the periphery and not in the thymus, autoreactive T cells can not be negatively selected against those antigens and autoimmunity should develop. One way this problem is avoided is by expressing many "peripheral, tissue-specific" antigens at low levels in the medullary thymic epithelial cells that are responsible for negative selection (Anderson et al., 2002; Liston et al., 2003; Villasenor et al., 2005). The protein AIRE (autoimmune

regulator) is expressed in these cells and is required for the ectopic expression of mRNAs encoding peripheral tissue-restricted antigens (Anderson et al., 2002; Liston et al., 2003); defects in this protein cause severe autoimmune endocrinopathy in both mice (Anderson et al., 2002; Ramsey et al., 2002) and people (known as autoimmune polyendocrinopathy syndrome-1 [APS-1] or autoimmune polyendocrinopathy-candidiasis-ectodermal dystrophy [APECED]; OMIM #240300) (Consortium, 1997; Nagamine et al., 1997). The precise mechanism by which the AIRE protein contributes to central tolerance remains somewhat controversial, with evidence suggesting that it can function both as a transcriptional transactivator (Bjorses et al., 2000; Pitkanen et al., 2000) and as an E3 ubiquitin ligase (Uchida et al., 2004).

Maintenance of self-tolerance

It is important to note that not all tolerance is established centrally, by deletion of autoreactive T cells from the immune repertoire. Self-reactive T cells can be found in the peripheral blood of most healthy humans, at low but detectable frequencies (Liblau et al., 1991; Sun et al., 1991). The forkhead box transcription factor FoxP3 is necessary for the development of regulatory T cells with an immunosuppressive function (Tregs) (Hori et al., 2003); inactivating mutations in FoxP3 cause fatal autoimmune disease very early in life in both mice (Brunkow et al., 2001) and humans (Bennett et al., 2001; Chatila et al., 2000; Wildin et al., 2001). A spontaneous frameshift mutation causes the scurfy phenotype in mice, which is similar to the human disease immune dysregulation, polyendocrinopathy, enteropathy, X-linked syndrome (IPEX), also called X-linked autoimmunity–allergic disregulation syndrome (XLAAD; OMIM reference #304930).

Further evidence that Tregs are critical in maintaining immune tolerance is provided by their ability to suppress pathogenic responses against normal GI flora. SCID mice that are given Treg-depleted $CD4^{+}CD45RB^{high}CD25^{-}$ T lymphocytes develop autoimmune gastritis and inflammatory bowel disease (Read et al., 2000; Suri-Payer and Cantor, 2001); concurrent transfer of Tregs protects against this (Hori et al., 2003). Recently, Rudensky's group showed that $FoxP3^{+}$ Tregs are necessary to maintain peripheral tolerance by using knock-in mice that express a receptor for diptheria toxin (huEGFR) specifically in $FoxP3^{+}$ cells (Kim et al., 2007). Injection of diptheria toxin causes a specific depletion of Treg cells and leads rapidly to severe lymphoproliferation. Deletion of Tregs neonatally leads to neonatal lethality similar to that observed in scurfy mice, while deletion of Tregs at later ages leads to rapid lymphoproliferation and morbidity. This requirement for Tregs to suppress pathologic responses in normal, healthy animals indicates that central tolerance alone is not sufficient to avoid immunopathology, and that peripheral tolerance mechanisms are critically important.

Dendritic cells and self-tolerance

Over the last five-ten years, a growing body of evidence has indicated that dendritic cells play significant roles in inducing tolerance in the absence of inflamation; it is generally believed that the outcome of antigen presentation by DCs depends on the state of DC maturation (Liu, 2001; Mellman and Steinman, 2001; Steinman et al., 2003a; Steinman et al., 2003b). Immature DCs capture, process, and present a variety of self antigens to T cells; sources of antigen include serum and environmental proteins (Holt et al., 1988; Liu and MacPherson, 1993; Vermaelen et al., 2001), extracellular matrix

components, and dead cells (Belz et al., 2002; Huang et al., 2000). Antigen presentation by steady-state DCs establishes T cell tolerance to prevent adverse reactions to self when the same antigens are presented in immunizing conditions (Brimnes et al., 2003; Steinman et al., 2003a; Steinman et al., 2003b).

The first evidence that dendritic cells were capable of inducing antigen-specific tolerance was obtained by injecting mice with an antibody to the dendritic cell surface receptor 33D1; these mice were subsequently resistant to immunization with other rat IgG2b antibodies, but generated normal responses to antibodies of other isotypes (Finkelman et al., 1996). Simultaneous administration of inflammatory stimuli led to heightened responses to subsequent IgG2b challenge. Subsequent, more sophisticated experiments have suggested that the default state of antigen presentation by DCs is T cell tolerance. Injection of mice with antigens coupled to a Dec-205-specific antibody either by engineering them into the antibody C-terminus (Hawiger et al., 2001) or by chemical conjugation (Bonifaz et al., 2002) led to antigen-specific T cell proliferation and subsequent tolerance. Simultaneous administration of adjuvant and DC-targeted antigen led to strong T cell responses to subsequent antigenic challenge (Bonifaz et al., 2002; Bonifaz et al., 2004; Hawiger et al., 2001; Hawiger et al., 2004).

The mechanism by which steady-state tolerance is achieved seems to vary between transgenic T cells, as tolerized HEL- and ovalbumin-specific T cells on a C57/B6 background are deleted (Bonifaz et al., 2002; Hawiger et al., 2001), while MOG-specific T cells on the same background are not deleted but anergized, in a CD5-dependent manner (Hawiger et al., 2004). Moth cytochrome c-specific AND T cells on the B10/BR background are also anergized, not deleted (Skokos et al., 2007).

Other groups have shown that dendritic cells can induce antigen-specific tolerance by using mice that express foreign antigens in dendritic cells upon administration of tamoxifen (Probst et al., 2003). Induction of LCMV epitopes under steady-state conditions led to T cell tolerance to the induced epitopes, but not to an uninduced LCMV epitope; challenge with LCMV resulted in rapid viral dissemination to the spleen. In contrast, induction of LCMV epitopes concurrently with administration of agonistic α-CD40 antibody led to the development of T cell immunity strong enough to rapidly clear virus (Probst et al., 2003). Further work from this group indicated that steady-state DC-induced $CD8^+$ T cell tolerance is T cell-intrinsic and requires the costimulatory molecules PD-1 and CTLA-4 (Probst et al., 2005). T cells deficient in PD-1 were not tolerized upon induction of LCMV epitopes, but wild-type congenic T cells in the same animals were tolerized normally. Treatment of mice with a neutralizing antibody to CTLA-4 concurrent with induction of LCMV epitopes also led to incomplete tolerance induction.

The inducible model of Probst *et al*. has some imperfections – most notably, the fact that tamoxifen and other estrogen receptor modulators used to induce antigen expression are not entirely without effect on immune cells – but it complements the studies that targeted DCs with modified antibodies to induce tolerance. The general hypothesis that dendritic cells induce T cell tolerance as the default pathway, with inflammatory stimuli required to induce priming, is well supported.

There is some evidence that stromal cells in peripheral LNs can induce tolerance, although this remains controversial (Lee et al., 2007). LN stromal cells expressed peripheral tissue antigens and presented them to $CD8^+$ T cells, leading to deletional

tolerance (Lee et al., 2007). This tends to support the hypothesis that tolerance is an actively maintained process, not simply the absence of inflammation.

Although both DCs and Tregs contribute to and maintain peripheral tolerance, to date, only Tregs have been shown to be necessary to avoid immunopathology. Attempts to delete DCs and induce a loss of self-tolerance are hampered by the corresponding loss of antigen presentation after DC deletion, which prevents the subsequent development of autoimmunity. The more subtle experiment of inducibly inhibiting the ability of DCs to tolerize T cells has not yet been performed, as the mechanism by which DCs induce tolerance in T cells remains unclear, although PD-1:PD-L1 interactions seem to be necessary (Probst et al., 2005).

Leukocyte trafficking and function

As an organ system, the immune system is unique in that cells transit extensively between organs and the bloodstream. Lymphocytes enter lymph nodes through specialized vascular structures known as high endothelial veins, migrate to their appropriate location within the LN, and search the parenchyma for their antigen (Girard and Springer, 1996; Marchesi and Gowans, 1964). Lymphocytes that fail to find their antigen within two or three days exit the LN and enter the efferent lymph, to re-enter the circulation through the thoracic duct (Gowans and Knight, 1964). Lymphocytes typically spend less than 30 min in the circulation before re-entering another lymphoid organ (Pabst, 1988). Removal of recirculating lymphocytes via thoracic duct cannulation leads to almost complete depletion of lymphocytes, indicating that the vast majority of lymphocytes actively recirculate (Geener and Gowans, 1962).

Leukocyte extravasation is a multistep process, with each process involving interactions between different leukocyte and endothelial cell proteins (von Andrian and Mempel, 2003). Leukocytes first loosely roll along the vessel endothelium, leading to chemokine receptor-mediated activation of integrins, which firmly adhere the leukocyte to the vessel wall. Firmly adhered leukocytes can then diapedese across the endothelium, pass through the basement membrane, and migrate into the tissue parenchyma. The specific adhesion molecules and ligands differ among leukocytes and specialized vasculature (von Andrian and Mempel, 2003); for simplicity, the entry of naïve T and B lymphocytes into LNs through HEVs will be focused on here. The first step in leukocyte extravasation, rolling, is mediated by L-selectins on lymphocytes, which adhere to peripheral node addressins (PNAd), O-linked oligosaccharides related to sialyl-lewis^X (Berg et al., 1991; Streeter et al., 1988a; Streeter et al., 1988b). The L-selectin-mediated interactions are not strong enough to fix the cell directly to the vessel wall, so shear forces from blood flow push the leukocyte along, leading to rolling. As a lymphocyte rolls, CCR7 is activated by HEV-bound CCL21 and CCL19, displayed on the endothelial surface (Campbell et al., 1998a; Campbell et al., 1998b; Gunn et al., 1998); the $G_\alpha i$-linked signaling induced by CCR7 activates the integrin leukocyte function-associated antigen 1 (LFA-1) (Stein et al., 2000), which binds to intercellular adhesion molecule 1 (ICAM-1) on the endothelial wall (Hamann et al., 1988; Warnock et al., 1998). Interactions between LFA-1 and ICAM-1 mediate firm adhesion, which fixes the lymphocyte in place, allowing CD31-mediated diapedesis to occur. Once the cell has crossed the basement membrane and entered the LN parenchyma, it can follow guidance cues directing it to the B or T cell area, as appropriate. As an example of how homing

receptor molecule expression controls trafficking, most myeloid cells express L-selectin, but not CCR7, so they roll in HEVs but fail to arrest; conversely, activated effector T cells or effector memory T cells lack L-selection and do not roll, precluding them from homing through HEVs to LNs (Sallusto et al., 1999; von Andrian and Mempel, 2003).

Intact lymphocyte trafficking and migration is required for proper immune function; defects in homing molecules or their ligands result in immunodeficiencies (Etzioni and Harlan, 1999). Leukocyte adhesion deficiency type 1 (LAD 1, MIM#116920), characterized primarily by a defect in neutrophil adhesion, is caused by deficiencies in the beta-2 integrin CD18, which is necessary for cell-surface expression of its dimerization partners, the alpha integrins CD11a, CD11b, and CD11c (Anderson et al., 1984; Bowen et al., 1982; Crowley et al., 1980; Dana et al., 1984; Springer et al., 1984). All of the L-selectin ligands require significant post-translational modifications by glycosyl- and sulphotransferases for effective L-selection recognition; defects in the Golgi-bound GDP-fucose transporter FucT1 lead to leukocyte adhesion deficiency type II, or Rambam-Hasharon syndrome (MIM#266265 and #605881) (Etzioni et al., 1992; Frydman et al., 1992; Karsan et al., 1998).

Leukocyte trafficking is not simply restricted to movement from the blood into tissue, however; the development and life cycle of lymphocytes involve many homing and migratory events. T cells originate as precursors in the bone marrow, enter the bloodstream, migrate through the bloodstream into the thymus, migrate within the thymic cortex to be positively selected and to the medulla to be negatively selected, leave the thymus and enter the circulation as naïve T cells, enter lymph nodes through high endothelial veins, migrate within the T cell area until it finds a dendritic cell presenting

its cognate antigen or exit through the lymph, re-enter the circulation, and enter another lymph node to repeat the last few steps. Upon antigen encounter, T cells are activated as above, and ultimately exit the lymph node in the efferent lymph, to re-enter the circulation via the thoracic duct (Gowans and Knight, 1964).

Lymphocyte homing receptors change as a function of the developmental stage; afferent lymph contains memory, but not naïve T cells, indicating that naïve T cells can only home to LNs through HEVs, while (some) memory T cells home from the blood to peripheral tissues, and can travel in afferent lymph to LNs (Klonowski et al., 2004; Mackay et al., 1990). Antigen-experienced memory T cells may be classified as effector (T_{EM}) or central memory (T_{CM}) T cells, based on their expression of the cell surface homing receptors CCR7 and CD62L (Sallusto et al., 1999). Central memory cells, like naïve T cells, are $CCR7^+$ and home to lymphoid tissues through HEVs in a CD62L-dependent manner. Effector memory T cells are $CCR7^-$ $CD62L^-$ and therefore cannot home to LNs through HEVs; they home to peripheral tissues through tissue-specific homing receptors or through receptors for inflammation-induced adhesion molecules. Interestingly, the homing specificity of T cells is 'imprinted' when they are primed with antigen (Agace, 2006; Kantele et al., 1999); one elegant study showed that intraperitoneal injection of antigen induced both skin-homing effector cells in peripheral LNs and gut-homing effector cells in gut-associated lymphoid tissues (Campbell and Butcher, 2002).

T cells home to the gut (mesenteric LNs, peyer's patches) through receptors including the integrin $\alpha4\beta7$ and CCR9, a receptor for the intestinal epithelium chemokine CCL25 (Hamann et al., 1994; Kantele et al., 1999; Svensson et al., 2002). These receptors are upregulated by retinoic acid, which is produced by by gut-associated DCs

from vitamin A (Iwata et al., 2004; Mora et al., 2003; Stagg et al., 2002). T cell homing to skin has also been extensively studied. One skin-specific chemokine is CCL27, which attracts the $CCR10^+$ subset of memory T cells (Homey et al., 2002; Morales et al., 1999; Reiss et al., 2001). The active form of vitamin D3, $1,25(OH)_2D_3$ was found to induce CCR10 expression on T cells and to suppress the gut-homing receptors CCR9 and $\alpha4\beta7$ integrin (Sigmundsdottir et al., 2007). Interestingly, DCs were found to metabolize the inactive prohormone vitamin D3, which is generated in the skin upon UV exposure (Holick et al., 1980; MacLaughlin et al., 1982), to the biologically active form (Sigmundsdottir et al., 2007). This is consistent with the emerging paradigm that DCs activate locally generated signaling molecules to program T cell migration and trafficking behavior.

Leukocyte migration within tissues

Migration within tissues is also critical for proper immune function – many fundamental immune processes depend on interactions between cells, requiring that both interacting cells find and contact each other. Naïve T cells must find their antigen on DCs (Itano and Jenkins, 2003), Th2 cells must find their antigen on B cells (Abbas et al., 1996; Garside et al., 1998), T_{FH} cells must find their antigen on GC B cells (Campbell et al., 2001; Kim et al., 2001), and B cells find their antigen on FDCs (Kosco et al., 1992; Kosco-Vilbois, 2003) or, controversially, conventional DCs (Qi et al., 2006). For lymphocytes to find their antigenic needle within the lymph node haystack requires efficient search algorithms that enable cells to rapidly sample all of the incoming antigens, as fewer than 1 in 10^5 cells is specific for any epitope on most pathogenic

molecules (Janeway et al., 2001). This occurs both through distribution of antigen throughout the lymph node, and movement of lymphocytes within the lymph node. Soluble antigen is rapidly distributed to dendritic cells (Itano et al., 2003) through afferent lymphatic conduits (Sixt et al., 2005), and migrating DCs carrying larger, particulate antigens arrive over the course of hours to days and distribute themselves throughout the T cell area (Itano et al., 2003; Kissenpfennig et al., 2005; Lindquist et al., 2004). The migrating dendritic cells comprise two populations: $CD205^{int}$ $CD207^{lo}$ dermal dendritic cells, which arrive in the shallow paracortex of the LN between 6-12 hours, and $CD205^{hi}$ $CD207^{hi}$ Langerhans cells, which arrive in the deep paracortex after at least 24 hours (Kissenpfennig et al., 2005).

Migrating DCs further distribute antigen throughout the lymph node by transferring it to lymph node resident DCs (Allan et al., 2006; Fleeton et al., 2004; Inaba et al., 1998); recent data has indicated that priming of T cell responses occurs through LN resident DCs in addition to or instead of the migratory DC that brought antigen to the LN (Allan et al., 2003; Allan et al., 2006; Belz et al., 2004; Zhao et al., 2003). HSV infection of the epidermis leads to MHC Class I-restricted priming through antigen presentation by LN-resident $CD8\alpha^+$ DCs, not Langerhans cells (Allan et al., 2003; Smith et al., 2003). Airway infection with influenza or HSV-1 leads to MHC Class I-restricted antigen presentation by both airway-derived $CD8\alpha^-CD11b^-$ DCs and $CD8\alpha^+$ lymph-node resident DCs (Belz et al., 2004). Vaginal infection by HSV-2 leads to MHC Class II-restricted antigen presentation only by $CD11b^+$ submucosal DCs, not Langerhans cells or $CD8\alpha^+$ DCs (Zhao et al., 2003).

Antigen transfer between DC populations does not occur in a vacuum – T cell priming by lymph node resident DCs requires that migrating DCs find, interact with, and properly transfer antigen to the resident DCs. The importance of cellular migration and interactions in immune responses is therefore left as an exercise for the reader.

In vivo imaging of immune responses

Fundamentally, to determine how leukocytes behave and interact within intact, living lymph nodes requires imaging *in situ*; histologic studies of fixed lymph node sections can not reveal lymphocyte dynamics. The first studies to image intact lymph nodes used explanted lymph nodes, perfused with warmed, oxygenated medium; images were acquired using both standard confocal microscopy (Stoll et al., 2002) and two-photon microscopy (Miller et al., 2002). Both of these techniques provide the optical sectioning necessary to acquire four-dimensional imaging data, but the differences in how this is achieved leads to differences in the physiology and viability of the imaged preparations.

Confocal fluorescence microscopy uses a pinhole to block emitted light that originates out of the focal plane; the aperture of the pinhole determines the thickness of the focal plane (Pawley, 2006). Multiphoton microscopy takes advantage of the ability of fluorophores to reach their excited state by accepting either one photon with energy $h\nu$, two photons each with energy $h\nu/2$, three each with $h\nu/3$, and so on (Denk et al., 1990; Xu et al., 1996; Zipfel et al., 2003). For one molecule to accept two photons within ~10^{-16} sec requires an exceedingly high photon flux, which is only achieved at the focal point of the laser, limiting excitation to a femtoliter volume (Zipfel et al., 2003). As

photobleaching and phototoxicity are caused by radical side products formed from the excited fluorophore, reducing the total volume excited in this manner dramatically reduces the amount of phototoxicity (Widengren and Rigler, 1996). For in vivo imaging experiments, avoiding phototoxicity is critical; early intravital experiments studying lymphocyte motility in LNs using confocal microscopy were confounded by phototoxicity, although this was not immediately apparent (Stoll et al., 2002). The technical difficulty of building the pulsed lasers necessary to reach the photon flux required for efficient two-photon excitation limited its experimental demonstration in inorganic and organic crystals (Kaiser and Garrett, 1961, Peticolas, 1963 #599) until thirty years after it was first theoretically predicted (Göppert-Mayer, 1931). The first use of two-photon excitation in imaging was not until 1990, when the first two-photon laser scanning microscope was built (Denk et al., 1990). Since then, parallel improvements in laser and microscope technology have made multiphoton microscopy available to many more investigators (Germain et al., 2006).

Intravital microscopy is still a relatively new technique; as of this writing, the first papers imaging immune cells were published less than six years ago. When we began, there were many unresolved methodological questions. How physiological are inguinal and popliteal lymph node preparations? How accurately does an explanted LN perfused with oxygenated medium approximate an *in vivo* preparation? What volume of tissue must be imaged to yield meaningful results? On what time scale must cells be imaged – i.e. what are appropriate intervals between subsequent images, and for how long a duration must cells be imaged? How deep in the LN must one image to observe T cells and DCs? Can a confocal microscope be used to image lymphoid organs, or must a

multiphoton laser be used instead? Is the LN parenchyma isotropic – i.e. is every direction equal, or are there tendencies to favor or avoid specific directions? After several false starts and disagreements, a consensus has been reached for all of these questions (Germain et al., 2006).

The first studies to image intact lymph nodes used explanted lymph nodes, perfused with warmed, oxygenated medium; images were acquired using both standard confocal microscopy (Stoll et al., 2002) and two-photon laser scanning microscopy (TPLSM) (Miller et al., 2002). Stoll *et al.* fluorescently labeled $CD4^+$ 5C.C7 TCR transgenic T cells with 5- (and 6-) carboxyfluorescein diacetate succininyl ester (CFSE) and injected them i.v. into host animals, while DiI-labeled antigen-pulsed splenic DCs and DiD-labeled control DCs not pulsed with antigen were injected s.c. into the footpad. Draining popliteal LNs were excised and placed in a culture dish for imaging; it was observed that DCs preferentially formed conjugates with antigen-pulsed DCs. Repeated time-lapse confocal imaging at a depth of up to 80 μm showed that naïve T cells were almost stationary, and formed extremely long-lasting interactions with antigen-bearing DCs in a 1:1 ratio. After 1.5 d of antigen-exposure, T cells separated from DCs and moved at speeds of 5-7 μm/min (Stoll et al., 2002).

A second group maintained explanted LNs in 36 °C hyperoxygenated medium and used multiphoton microscopy to image up to 350 mm deep in explanted inguinal LNs (Miller et al., 2002). DCs were not directly visualized, but $CD4^+$ T cells were labeled with CFSE and B cells with 5- (and 6-)-(((4-chloromethyl)benzoyl)amino)tetramethyl-rhodamine (CMTMR). In contrast to the results obtained with confocal microscopy, (Stoll et al., 2002), it was observed that lymphocytes were relatively motile, with T cells

moving at average speeds of 10.8 μm/min and follicular B cells moving at 6.4 μm/min; T cell peak velocities reached 25 μm/min (Miller et al., 2002). Overlaying the paths of both B and T cells revealed no net directionality, and displacement from the origin was proportional to $(\text{time})^{1/2}$, indicating that they move in a random walk; this random movement is inconsistent with chemotaxis on a large distance scale. Antigenic challenge led to the formation of T cell clusters and swarms, indicating that DCs are likely interacting with more than one T cell, and that both stable and transient DC:T cell interactions occur physiologically (Miller et al., 2002). A subsequent TPLSM study also using explanted LNs also found that $CD8^+$ lymphocytes move around 10 μm/min, and that DCs can contact up to 500 different T cells per hour, showing that T cell motility lets DCs efficiently scan the T cell repertoire (Bousso and Robey, 2003). $CD8^+$ P14 T cells made long-lasting interactions with gp33-pulsed DCs, with DCs simultaneously contacting up to 10 T cells; the limiting factor for how many different T cells one DC can engage was its surface area. (Bousso and Robey, 2003). Possible reasons for the discrepancies between these studies include differences in tissue oxygenation, imaging depth, and increased phototoxicity from confocal imaging; it is likely that all of these factors contributed to reducing the speed of the lymphocytes observed by Stoll *et al.*

The first studies to image lymph nodes *in vivo* examined T cell trafficking in the absence of antigen; CFSE-labeled DO11.10 transgenic T cells were transferred i.v. into BALB/c mice, and inguinal LNs were surgically exposed and imaged using TPLSM (Miller et al., 2003). Blood vessels within the LN could be visualized by injection of 200 μl of 10 mg/mL 10 kDa tetramethylrhodamine dextran, to permit the identification of T cell zones. T cells imaged 16 – 18 h after transfer were observed to move in stop-and-go

pattern, with peak velocities of ~25 μm/min and average velocities of ~11 μm/min; Fourier analysis revealed a periodicity of T cell speed of roughly 1.6-2.4 min (Miller et al., 2003). Analysis of instantaneous velocity revealed a small population moving < 3 mm/min, which corresponded not to a small population of arrested cells but to brief pauses of many different lymphocytes (Miller et al., 2003). As observed *in vitro* (Miller et al., 2002), overlaying the paths of T cells revealed no net directionality, and T cell movement was consistent with a random walk. As chemotaxis therefore does not shape T cell migration within the T cell zone, Miller *et al.* suggest that the T cell antigenic search algorithm is a stochastic process (Miller et al., 2003).

Steady-state behavior of dendritic cells

When we began, DCs had not been imaged *in vivo* in the absence of inflammation; all previous studies imaging DCs used splenic dendritic cells labeled *ex vivo* with fluorescent dyes and re-injected subcutaneously. We decided that visualizing resident dendritic cells precluded the use of *ex vivo* labeled DCs, and that genetic strategies to label endogenous cells were required. The Venus variant of EYFP was cloned into the dendritic cell-specific CD11c promoter, and BAC transgenic mice were generated by microinjection; these mice were found to express high levels of EYFP only in dendritic cells, with low levels of EYFP expressed in some activated B and T cells.

We adapted a method for imaging the inguinal LN previously used for video-rate studies of lymphocyte rolling and extravasation in LN vasculature (von Andrian, 1996) to image DCs and lymphocytes in the LN parenchyma using multiphoton laser scanning microscopy. Our first studies were focused on resting dendritic cells, with occasional T

or B lymphocytes transferred to provide anatomical definition; to compare endogenous DCs with the migrant DC populations imaged by other groups, we transferred labeled splenic DCs.

Comparison of tolerogenic and priming T cell responses

During the course of our early work, several imaging studies of immune responses were published. Two of these studies imaged priming responses after the local delivery of antigen *in vivo* (Mempel et al., 2004; Miller et al., 2004), while one study compared *in vitro* tolerogenic and immunogenic responses to antigen delivered to dendritic cells (Hugues et al., 2004). Both of the studies looking at T cell priming found that T cells initially made short, serial contacts with DCs for the first 8 hours, before transitioning to form stable interactions; after a second phase of stable interactions, T cells recovered their motility and resumed making transient interactions with DCs. As none of these studies looked at the behavior of dendritic cells in the steady state *in vivo*, we decided to deliver antigen to dendritic cells using a method developed previously in the lab (Bonifaz et al., 2002; Hawiger et al., 2001), and image the resulting DC:T cell interactions *in vivo*.

It is possible to target antigens to the endocytic pathway of dendritic cells using antibodies to cell-surface receptors such as Dec-205, (Bonifaz et al., 2002; Bonifaz et al., 2004; Hawiger et al., 2001; Hawiger et al., 2004); peptides derived from the endocytosed proteins are efficiently presented to T cells which, in the absence of adjuvant, are tolerized by deletion (Hawiger et al., 2001), induction of $CD4^{+}CD25^{+}$ regulatory T cells (Kretschmer et al., 2005; Mahnke et al., 2003), CD5 upregulation (Hawiger et al., 2004),

or anergy induction (Skokos et al., 2007). Simultaneous CD40 ligation or stimulation with a TLR ligand leads to dendritic cell activation and the triggering of an immunogenic response to the peptides targeted to the dendritic cell.

Subsequent experiments were performed to image both tolerance and priming *in vivo* after antigen targeting to DCs. We cloned ovalbumin epitopes into the C-terminus of an anti-Dec-205 antibody to deliver them to dendritic cells, and injected them into mice in the presence or absence of anti-CD40 antibody, to yield priming or tolerizing responses, respectively. Differentially labeled fluorescent ovalbumin-specific and nontransgenic control T cells were transferred, and intravital microscopy was performed at various time points after T cell transfer.

TCR affinity for pMHC and T cell dynamics *in vivo*

Much evidence suggests that TCR affinity for MHC II:peptide complexes (pMHC) is significant in determining T cell fate in the periphery, in addition to during thymocyte selection (Alam et al., 1996; Madrenas and Germain, 1996; Sloan-Lancaster and Allen, 1995). It is possible to manipulate the TCR affinity for pMHC by taking a stimulatory pMHC and making single amino acid replacements to generate other peptides (altered peptide ligands, or APLs) that bind the same MHC molecule (Sloan-Lancaster and Allen, 1995). These APLs can cover a broad range of affinities and functional outcomes, from nonstimulatory to partial agonist to superagonist (Evavold and Allen, 1991; Madrenas and Germain, 1996; Sloan-Lancaster et al., 1993). The extent of activation induced in T cells can be used to classify these APLs, using CD69

upregulation, proliferation, and cytokine production, in order of increasing stringency (Daniels et al., 2006). To determine the role of pMHC potency in T cell responses, we used the well-characterized moth cytochrome C system. Single point mutants of this peptide have been generated, which disrupt the interaction with the AND TCR but have no effect on binding to the I-E^k MHC II molecule (Kaye et al., 1989; Madrenas et al., 1995; Rogers et al., 1998). As described above for the Ovalbumin peptide, we cloned the MCC peptide and selected APLs into the C-terminus of an anti-Dec-205 antibody to target the pepide specifically to DCs. Mice were injected with α-Dec-APLs, CFP-expressing AND T cells and GFP-expressing nontransgenic T cells were transferred, and the resulting DC-T cell interactions were visualized by intravital microscopy.

Dynamics of germinal center reactions

Humoral immunity is mediated by antibodies secreted from B cells. After being released into the periphery, B cells can undergo secondary, antigen-dependent genetic changes in specialized lymphoid structures called germinal centers (Jacob et al., 1991a; Jacob et al., 1991b). Germinal center B cells ($FasL^+$ $GL\text{-}7^+$) proliferate rapidly, with cell cycle durations of 6-8 hours (MacLennan, 1994); as the cells proliferate, they express high levels of AID, which deaminates the genes coding for the B cell receptor, introducing somatic mutations (Di Noia and Neuberger, 2002; Ramiro et al., 2003). B cells with newly mutated antigen receptors then compete with unmutated B cells and other newly mutated B cells for antigen, on the basis of their B cell receptor's affinity for the antigen. High-affinity cells outcompete lower-affinity cells, with the higher affinity

cells continuing to proliferate, and the low-affinity cells dying by apoptosis (Kelsoe, 1996; MacLennan, 1994; Rajewsky, 1996). Germinal centers are thought to be founded by three or four antigen-specific B cells (Kroese et al., 1987); it is believed that centroblasts rapidly proliferate in the dark zone, and centrocytes are selected in the light zone (Hanna, 1964; Kelsoe, 1996; MacLennan, 1994; Nossal et al., 1965; Rajewsky, 1996).

When we began, none of this had been visualized in vivo; all of the previous studies were done histologically, on fixed sections. The only live imaging of B cell responses was a study of early B cell activation, showing that activated B cells migrate directionally to the T-B interface in a CCR7-dependent manner, where they form relatively long-lasting, motile conjugates with T cells (Okada et al., 2005). B cells would occasionally contact more than one T cell simultaneously, but T cells could only polarize to contact one B cell at a time (Okada et al., 2005).

We thus decided to investigate the cellular dynamics of germinal center reactions using the same microscopy techniques we had previously established. We transferred GFP-expressing NP-specific B cells (Shih et al., 2002a; Shih et al., 2002b) and nontransgenic CFP-expressing B cells and visualized follicular dendritic cells by s.c. injection of a fluorescently-labeled anti-FDC-M1 antibody (Kosco et al., 1992; Szakal et al., 1988). Inguinal LNs were imaged as above in our previous studies of DCs and T cells, but at shallower depths, since B cell follicles and GCs are more superficial than the T cell areas.

SUMMARY

The goal of our experiments was to visualize in intact, living lymphoid tissue the physiological role of dendritic cells in tolerance and immunity; this was achieved by intravital microscopy of fluorescently-labeled DCs and lymphocytes in the inguinal lymph nodes. We generated mice that specifically expressed EYFP in their dendritic cells and observed both DC behavior in the steady state and migratory DC behavior in living LNs. We investigated how tolerogenic DC:T cell interactions compared to immunogenic interactions, and how TCR affinity for pMHC affected the dynamics of these interactions, signaling, and functional responses. We then shifted our focus from classical dendritic cells to follicular dendritic cells and from cellular to humoral immunity, and studied the dynamics of GC B cells and their interactions with FDCs during germinal center reactions.

CHAPTER 2. METHODS

Transgenic mice. EYFP-Venus (Nagai et al., 2002) was cloned into a CD11c promoter (Brocker et al., 1997). The linearized construct was injected into B6/CBA F_1 fertilized female pronuclei, and progeny positive by PCR for the transgene were backcrossed to C57Bl/6 for at least 6 generations. C57Bl/6 mice expressing ECFP on the β-actin promoter were purchased from Jackson Labs (Hadjantonakis et al., 2002). EGFP-OTII transgenic mice were products of a cross between OTII mice and mice ubiquitously expressing EGFP on the ubiquitin promoter (Kang et al., 2003; Wright et al., 2001); ECFP-OTII mice are a cross between mice expressing ECFP on the β-actin promoter (Jackson Labs) and OTII mice. For the I-E^k TCR affinity experiments, AND TCR transgenic mice expressing the Vβ3/Vα11 TCR were kindly provided by Dr Lisa Denzin and bred to B10.BR background ($H2^k$) (Croft et al., 1992; Jaiswal et al., 1996). CD11c-EYFP (Lindquist et al., 2004), ECFP (Hadjantonakis et al., 2002) and EGFP (Wright et al., 2001) expressing mice were backcrossed to B10.BR, and ECFP-AND mice were produced by inter-crossing. B6.SJL (CD45.1) mice were crossed with B10.BR to produce B10.BR CD45.1 mice. For the germinal center experiments, B1-8^{hi} BCR knock-in mice (all B cells which express the λ light chain are specific for the hapten NP) (Shih et al., 2002a; Shih et al., 2002b) were crossed with mice expressing EGFP or CD45.1. Mice were used for experiments at 5-10 weeks of age; all mice were housed in specific pathogen-free conditions and were treated in accordance with the Institutional Animal Care and Use Committee protocols of Rockefeller University and New York University Medical Center (New York, New York)

Immunofluorescence. Lymph nodes were fixed in PBS with 4% paraformaldehyde + 10% sucrose and cryoprotected in PBS + 30% sucrose before embedding in OCT and freezing. Frozen tissue was sectioned (20 or 50 μm) on a microtome and fixed in acetone; all subsequent incubations were performed in a humidified chamber. Sections were blocked in 5% BSA, 10% serum in PBS in the presence of α-CD16/CD32 (BD Biosciences), and sequentially blocked with excess streptavidin and biotin (Vector Labs). For peroxidase amplification with biotinyl tyramides (NEN), we quenched endogenous peroxidase activity with 3% H_2O_2 in PBS before the initial blocking step as per the NEN protocol. Slides were incubated with the appropriate antibodies for 30 to 90 minutes, depending on the individual antibody's affinity; slides were washed 3 times in PBS between antibody stainings. When applicable, slides were incubated with fluorochrome-conjugated streptavidin for 30 minutes, after which slides were washed three times in PBS and dipped briefly in ddH2O immediately before mounting. The antibodies used were: directly labeled α-CD3ε-Alexa 647, α-B220-Alexa 647 (CalTag), α-B220-Pacific Blue (BD Biosciences), biotinylated α-CD3ε, α-CD1b, α-CD11c, α-CD19, α-CD80, α-CD86, α-B220, α-F4/80, α-Gr-1, α-I-A^b, α-PECAM, α-rat IgM (BD Biosciences), MOMA-1 (BMA Biomedicals), α-CD11c, α-CD45.2 (EBioscience), unconjugated MECA-79 (BD Biosciences) and biotin and Alexa 647 conjugates of α-DEC-205 produced and conjugated by the RU Monoclonal Antibody Core Facility. Anti-FDC-M1 was purified from hybridomas (Kosco et al., 1992; Kosco et al., 1988; Szakal et al., 1988) and labelled in-house with Alexa 546, 594, and 647. Streptavidin-Cy3 and -Cy5 were from Jackson ImmunoResearch; TO-PRO-3 was from Molecular Probes. Sections were mounted in Fluoromount-G (Southern Biotech) and stored at 4 °C.

Confocal microscopy. Confocal images were acquired on a Zeiss LSM 510 system with 405, 488, 543, and 633 nm excitation lines; EYFP, EGFP and ECFP fluorescence were visualized directly in all images. Images with ECFP and EYFP fluorescence were captured using 458 and 514 nm excitation lines. An array of 40x or 63x images was taken with a motorized stage to capture the entire cut surface of the lymph node, and images were exported into Adobe Photoshop for final processing. Three-dimensional reconstructions were generated from Z-stacks using Imaris (Bitplane). Positions of T cells, HEVs, and the deep paracortex were measured in Volocity software. Cells were scored as being in the deep paracortex only if the entire cell was within the boundary; cells touching the boundary were excluded. The minimum distance from T cells to HEVs were calculated as in Bajenoff *et al.*(Bajenoff et al., 2003) with the following equation: $D_i = \min \sqrt{[(X_i-X_j)^2 + (y_i-y_j)^2]}$, where i and j are indices from 1…n for T cells and HEVs, respectively, and min is the minimum function. It should be noted that this yields the distance to the center of the HEV, which is greater than the distance to the basal side of the HEV endothelium. To further refine this measurement, images and T cell positions were imported into MatLab, and the distance from each T cell to the wall of the nearest HEV was measured by a custom script based upon the same formula.

Flow cytometry analysis of DCs. Single cell suspensions from lymph nodes were pre-treated with α-CD16/CD32 and stained with CD11c-APC and biotinylated antibodies specific for: CD3, CD4, CD8a, CD11b, CD19, B220, CD86, DEC-205 and MHC class II ($I\text{-}A^b$) (BD Biosciences). Living cells were gated based on forward and side-scatter on a FACSVantage SE (Becton-Dickinson) and data analyzed using FlowJo (TreeStar).

Recombinant antibody production. Anti-DEC-OVA, and Iso-OVA were constructed by cloning the C-terminal portion of Ovalbumin protein into the C-terminus of the α-DEC-205 antibody NLDC-145 or isotype control (III-10) (Hawiger et al., 2001; Hawiger et al., 2004); the control antibody α-DEC-CSP (anti-DEC-205 fused to the irrelevant peptide SYVPSAEQI) was produced by similarly cloning the sequence encoding SYVPSAEQI into the C-terminus of NLDC-145. Anti-DEC-MCC, isotype-MCC and all α-DEC-APL variants were similarly constructed by cloning the C-terminal portion of MCC (residues 81-103) and its variants into the C-terminus of the α-DEC-205 antibody NLDC-145 or isotype control (III-10). The Quickchange II Kit (Stratagene) was used to introduce single point mutations and produce the MCC variants. Recombinant antibodies were produced by transient transfection and were purified as described (Hawiger et al., 2001).

Cell transfer, labeling, and antigen delivery for imaging experiments. To demarcate B cell follicles, we transferred 1 x 10^8 B cells purified from $EGFP^+$ C57BL/6 mice by magnetic depletion with α-CD43 microbeads (Miltenyi Biotec). To image transferred dendritic cells, $CD11c^+$ DCs were purified by immunomagnetic selection from the spleens of $ECFP^+$ mice injected with cells from a Flt3L-expressing tumor and 4-6 x 10^6 cells intradermally injected with 1 ng/μl LPS (Sigma) at 4 sites surrounding the inguinal lymph node. To image the macrophages in the subcapsular sinus and blood vessels throughout the lymph node, we injected 1 mg of rhodamine-dextran (66 kDa) (Molecular Probes) in 100 μl saline subcutaneously in the base of the tail. To examine high endothelial veins in vivo, we injected 10 μg of Alexa 594-labeled MECA-79 antibody

intravenously in the retro-orbital sinus. To label follicular dendritic cells (FDCs) in vivo, we injected 25 μg of FDC-M1 antibody (purified as above) labeled with Alexa 546, 594, or 647.

To deliver Ovalbumin epitopes to DCs, we injected CD11c-EYFP mice with 2 μg i.p. of α-DEC-OVA, Iso-OVA or α-DEC-CLS either alone or together with α-CD40 (clone 1C10, 50 μg). Five hours later mice were injected i.v. with 1-2 x 10^7 purified EGFP-OTII cells and naïve $CD4^+$ ECFP-T cells (>98% purity) prepared by magnetic depletion of non-$CD4^+$ T cells (MACS $CD4^+$ T cell Kit, Miltenyi Biotec). LNs were imaged 2-18 hours after T cell transfer, as described below.

To deliver MCC epitopes to DCs, CD11c-EYFP mice were injected i.p. with 10 μg of α-DEC-MCC or the indicated α-DEC-APL variant; 5 h later, we adoptively transferred 1 x 10^7 ECFP-AND $CD4^+$ T cells and an equal number of non-transgenic $EGFP^+$ $CD4^+$ T cells. All T cells were purified by negative selection with a $CD4^+$ T cell isolation kit (Miltenyi). LNs were imaged from 1-6 hours after T cell transfer, as described below.

To image germinal centers, we first primed WT B6 mice with i.p. injections of 100 ug of Ova/alum. Between 14-28 days later, NP-specific splenic B cells were isolated from the spleens of B1-8^{hi} mice by negative selection with anti-CD43, anti-CD11c, anti-CD90 and anti-κ light chain Abs. For most experiments, 2.5 x 10^6 B1-8^{hi} cells were transferred into the primed mice, with between 10 and 30% of the B1-8^{hi} cells expressing EGFP. One day after B cell transfer, mice were injected s.c. in the footpad and thigh with 200 ug of NP-Ova. Five days post-boost, polyclonal B cells were purified from spleens of B6/SJL (CD45.1) CFP-expressing mice by negative selection with anti-CD43, anti-

CD11c and anti-CD90; 2 x 10^7 polyclonal B cells were transferred i.v., and labeled FDC-M1 antibody was injected.

***In vivo* OT-II T cell responses.** OT-II T cells (CD45.2) were labeled with carboxyfluorescein diacetate succinimidyl ester (CFSE), transferred into 4-6 week-old B6/SJL (CD45.1) mice and challenged i.p. 24 h later with 2 μg of α-DEC-OVA, 2 μg Iso-OVA, PBS, or 2 μg α-DEC-OVA plus 90 μg α–CD40. T cells were purified from peripheral LNs 3 d or 7 d later and either cultured with irradiated $CD11c^+$ cells and OVA peptide to measure proliferation or analyzed by flow cytometry on a FACSCalibur (BD Pharmingen) to measure CFSE dye dilution (gated on $V\alpha_2$ and CD45.2). To monitor early T cell activation, CD45.2 OT-II T cells were transferred into CD45.1 B6/SJL mice injected with α-DEC-OVA (with or without α-CD40) five hours previously; T cells were purified from LNs at 3, 12, or 24 h after T cell transfer and analyzed by flow cytometry to measure surface expression of CD69 and CD62L (gated on $V\alpha_2$ and CD45.2). Antibodies were from BD Pharmingen.

***In vivo* B cell experiments - Germinal Center joining and affinity.** To study the ability of B cells to join GC reactions, we first primed WT B6 mice with i.p. injections of 100 μg of Ova/alum. Two weeks later, mice were injected s.c. in the footpad and thigh with 200 μg of NP-Ova. NP-specific B cells were isolated from the spleens of $B1\text{-}8^{hi}$ mice by negative selection with anti-CD43, anti-CD11c, anti-CD90 and anti-κ light chain Abs. B cells were transferred concurrently with the boost, or 6 or 9 days later; approximately 2.5 x 10^6 $B1\text{-}8^{hi}$ cells were transferred into the primed mice. Six days

after B cell transfer, lymph nodes were harvested and processed for histological analysis as above.

To examine the effect of B cell affinity on GC joining, we first primed WT, B1-8^{lo}, or B1-8^{hi} mice with i.p. injections of 100 μg of Ova/alum. Two weeks later, mice were injected s.c. in the footpad and thigh with 200 μg of NP-Ova. Six days after the boost, NP-specific B1-8^{lo} cells were purified as above and transferred; six days after transfer, lymph nodes were harvested and processed for histological analysis as above.

***In vivo* AND T cell responses.** AND T cells (CD45.2) were labeled with CFSE, transferred into 6-8 week old B10.BR CD45.1 mice, and challenged subcutaneously 24 h later with 10 μg α-DEC-MCC, α-DEC-L98A, α-DEC-Y97K, α-DEC-T102L, Iso-MCC, or PBS. T cells were purified from peripheral lymph nodes 3 d or 7 d later and cultured with irradiated $CD11c^+$ cells and MCC peptide to measure proliferation, or were analyzed by flow cytometry on a FACSCalibur (BD Pharmingen) to measure CFSE dye dilution (gated on CD4, Vα11/Vβ3, and CD45.2). To monitor early T cell activation, $CD45.2^+$ AND $CD4^+$ T cells were transferred into $CD45.1^+$ B10.BR mice injected 5 h previously with α-DEC-MCC, α-DEC-APLs, or Iso-MCC. T cells were purified from lymph nodes at 3 and 72 h after T cell transfer and were analyzed by flow cytometry to measure surface expression of CD62L and CD25 (gated on CD4, Vα11/Vβ3, and CD45.2). Antibodies were from BD Pharmingen.

Surgery for intravital imaging of inguinal LN. To image mice on the B6 background, mice were anaesthetized with 100 mg ketamine, 15 mg xylazine and 2.5 mg

acepromazine per kg, and kept anaesthetized with hourly injections of half this dose. Mice were restrained on a stage warmer at 37 ºC (BioTherm Micro S37, Biogenics) and the abdominal skin was incised from the edge of the rib cage through the midline to the thigh. A skin flap was separated from the abdominal muscle to expose the inguinal lymph node.

To image mice on the B10/BR background (in the AND experiments), mice were anaesthetized with 450 mg/kg avertin (Tribromoethanol, Pfaltz & Bauer, Waterbury, CT), and kept anaesthetized with injections of a third of this dose every 30 min. Mice were restrained and kept normothermic as described below, and their inguinal lymph nodes were microsurgically exposed for 2-photon intravital imaging as below.

To stabilize, moisturize and maintain the lymph node at 37 ºC, we placed the skin flap on a thermoconductive base made of silicone elastomer (Sylgard 184, Dow Corning) surrounding a core of thermoconductive putty (T-putty 502, Thermagon). The connective and adipose tissue covering the lymph node was removed microsurgically, keeping blood and lymph vessels intact, and a saline-filled chamber consisting of a cover-slip glued to a nylon washer was mounted on the skin flap over the lymph node. The chamber was laterally secured by 3 insect pins piercing the skin and lodged in the silicone base. The temperature was monitored using a probe (Bioptechs) placed near the lymph node to ensure that it was at 37±1 ºC. To compensate for anesthesia-induced respiratory depression, we provided mice with 100% oxygen by mask throughout the imaging session.

Intravital microscopy. The lymph node was imaged using a Bio-Rad Radiance multiphoton microscope fitted with a Tsunami pulsed laser (Spectraphysics) and a Nikon

40x objective (water-immersed, NA 0.8), controlled by Lasersharp2000 software (Bio-Rad). To image EYFP, EGFP and ECFP, the excitation wavelength was set to 910 nm; experiments using rhodamine dextrans or Alexa 633/546-labeled anti-FDC-M1 antibody were imaged at 870 nm. Band-pass filters optimized for detecting EYFP (550/30) and ECFP (510/30) and a 530 long-pass dichroic mirror were used to detect fluorescent proteins, with EGFP bright in both channels. Blood flow was visualized with 655 nm-emitting quantum dots (Invitrogen/Quantum Dot Corp., Hayward, Ca), excited at 910 nm. To create time-lapse sequences, we typically scanned 50x300x300 μm volumes of tissue at 6 μm Z-steps and 35 second intervals.

Data analysis. Cell movement was analyzed with Volocity software (Improvision). The position of each cell was tracked in three dimensions over time, and displacement and motility parameters were calculated for each cell. These include measurements of cell velocity, cell directionality, and cell-cell contact duration, information that can only be acquired by directly visualizing the interacting cells. Both instantaneous measurements and per-cell average measurements of velocity and immobility are taken; the percent of each track during which cells are immobile is termed the arrest coefficient (Hugues et al., 2004). The motility coefficient is the slope of the linear portion of the curve obtained when mean displacement is plotted against the square root of time, and is analogous to the diffusion coefficient of a particle exhibiting Brownian motion (Mempel et al., 2004; Sumen et al., 2004). Measurements of directionality include the confinement index and turning angle. The confinement index is the ratio of the maximum displacement to the total path length, and reflects the directionality of cell movement over the entire path (Hugues et al., 2004). The turning angle between velocity vectors at subsequent

timepoints provides an instantaneous measure of directionality (Mempel et al., 2004). As a general rule, arrested cells move less directionally than freely moving cells. Cell confinement and pausing are also analyzed. Cells which move freely in a random-walk pattern exhibit a linear relationship between their displacement and the square root of time, while cells which are confined within a smaller volume plateau at a given displacement. To examine cell-cell interactions, the duration of cell-cell contacts can be measured manually; the time a cell spends paused can be analyzed as a function of distance to another cell, to determine if relationships exist.

When tracking dendritic cells (Lindquist et al., 2004), to eliminate motion artifacts caused by dendrite probing, pulse and breathing, displacements smaller than 2.5 μm were filtered out of the cell tracks by a smoothing algorithm. Despite efforts to filter high frequency movement related to probing, DC that were clearly sessile still appear to have velocities up to 2 μm/min; this velocity was therefore used as the threshold below which cells were considered sessile. Since cell speed exhibited an asymmetrical distribution, data was presented in scattergrams and compared using a non-parametric bootstrapping procedure based on 10,000 resampling iterations (Efron and . 1979). P values smaller than 0.05 were considered significant.

When tracking T and B cells (Schwickert et al., 2007; Shakhar et al., 2005), they were characterized as immobile if their average velocity was less than 2 μm/min. The arrest coefficient was calculated as the percentage of each track in which the cell moved more slowly than 2 μm/min (Hugues et al., 2004). Measurements of directionality such as turning angle and confinement index were also calculated as above. Multivariate ANOVA was conducted to assess statistical significance, and planned contrasts were

used to assess differences between individual conditions. P values smaller than 0.05 were considered significant.

In the AND experiments (Skokos et al., 2007), the analysis was as described above (Shakhar et al., 2005), while additionally taking full advantage of our nontransgenic internal control T cells. To control for variability between different imaging fields and mice regardless of the experimental conditions, the average speed of control (non-TCR-transgenic) T cells in each field was calculated and used as a reference for the speed of TCR-transgenic T cells. The mean velocity for each cell in a given field was calculated and plotted as a percentage of the mean velocity of all the nontransgenic cells in that field; this allowed us to make more accurate quantitative comparisons between imaging fields. To illustrate confinement, cell tracks were superimposed on one starting point; the resulting sphere illustrates the mean cell displacement.

In the germinal center experiments (Schwickert et al., 2007), the general analysis of lymphocyte speed and confinement was as above. We additionally calculated plots of displacement v. $(\text{time})^{1/2}$ to measure the extent to which individual cells were confined within any particular volume. We further measured the duration of B cell-FDC contacts, by counting the number of frames ($\geq$2) in which cells remained in contact. Scattergrams of individual contact time were prepared, and statistical significance was assessed by either Student's T-test or analysis of variance (ANOVA) with Bonferroni post hoc corrections.

Altered peptide ligand (APL) synthesis. Wild-type and single substitution variants of the 23 amino-acid immunogenic MCC peptide VFAGLKKANERADLIAYLKQTAK

(81-103) were synthesized by the Proteomics Resource Center, Rockefeller University. The APL synthesized were: L98A (substitution of leucine with alanine at position 98), Y97K (substitution of tyrosine with lysine at position 97) and T102L (substitution of threonine with leucine at position 102).

***In vitro* T cell responses.** $CD4^+$ T cells were purified from the spleen and lymph nodes of AND mice by negative selection with a $CD4^+$ T cell isolation kit (Miltenyi). DCs were isolated from the spleen of B10.BR mice by positive selection with a $CD11c^+$ isolation kit (Miltenyi). $CD4^+$ T cells and irradiated DCs were plated in 96-well flat-bottom plates with different doses of WT and mutant peptides. The cultures were incubated for 60 to 72 h as indicated in the figure legends and then were pulsed with (^3H) thymidine at 1 μCi/well for the final 8 h before harvesting with a 96-well channel harvester.

IFN-γ production was measured by ELISPOT. ELISPOT plates (MAHAS, Millipore) were coated with 10 μg of the anti-mouse IFN-γ mAb (clone R4-6A2, BD Pharmingen) overnight at 4°C and plates were blocked by incubation with PBS BSA 1% for at least 2 h at 37°C. Lymph node $CD4^+$ T cells were purified by negative selection with a $CD4^+$ T cell isolation kit (Miltenyi Biotech). Purified T cells were then cultured at 10^6/ml for 36-40 hours at 37 °C with 5% CO_2 in the presence of 2 μM peptide and $CD11c^+$ DCs purified by positive selection. Plates were developed with α–IFN-γ biotinylated antibody (BD Pharmingen) and spots visualized with avidin-HRP (Vector) followed by DAB as substrate (Invitrogen). Spots were counted in an ELISPOT reader (Autoimmun Diagnostika GmbH, Germany).

***In vitro* calcium measurements.** Intracellular calcium concentrations were measured using the calcium sensitive ratiometric dye Fura-2. Activated AND T cells (see below) were labeled with 2 μM of Fura-2 in serum free media for 30 minutes at room temperature, washed and incubated at 37°C for 30 minutes in serum containing media before being used. Cells were then incubated on glass supported planar bilayers containing 2 molecules/μm^2 of relevant peptide loaded I-E^k and 300 molecules/μm^2 of GPI-anchored ICAM-1. Images were acquired through a 40 x NA 1.3 NeoFluar objective at intervals of 30 seconds for a period of 20 minutes. The ratio of emission at 510 nm excited at 340 nm and 380 nm was determined with appropriate background subtraction, and cells forming contacts with the bilayer were tracked using Volocity software (Improvision). High Ca^{2+} and low Ca^{2+} values were determined at the end of each experiment by infusing media containing respectively: 1 μM ionomycin + 1 mM Ca^{2+} + 2 mM Mg^{2+}, and 3 mM Mg^{2+}+ 2 mM EGTA + 0 mM Ca^{2+}.

The Ca^{++} response of naïve AND TCR T cells to peptides presented on freshly isolated $CD11c^+$ DCs was measured *in vitro*. Naïve AND T cells and $CD11c^+$ DCs were purified from lymph nodes as described. Naïve AND T cells were labeled with 5 μM Fura-2 in media containing 1% FBS and 0.1 mg/ml Pluronic F127 for 25 minutes at room temperature. $CD11c^+$ DCs were incubated with various concentrations of L98A or T102L at 37 °C for 2 hours at a density of 10^6 DCs /well (Nunc 8 well glass bottom chambers, Fisher). 0.5 x 10^6 Fura-2 labeled naïve AND T cells were added into the well and imaged for 20 minutes and the Fura-2 ratio was determined for conjugates of T cells and DCs. A threshold Fura-2 ratio of 0.4 was used to score T cells conjugated with DCs with high cytoplasmic calcium concentrations. This threshold was determined by imaging T cells

on bilayers containing ICAM-1 under similar imaging conditions. An average ratio of 0.3 was obtained for cells on ICAM-1. Cells interacting with bilayers containing agonist peptides loaded on MHC had a range of Fura-2 ratios from 0.4 to 0.9 and hence a threshold of 0.4 was used to score high calcium values. In each condition the percentage of T cells conjugated with DCs having a Fura-2 ratio greater than 0.4 was determined.

CHAPTER 3. IMAGING DCS *IN VIVO*

CD11c-EYFP mice express EYFP specifically in their dendritic cells

To create mice with fluorescently-labeled dendritic cells, transgenic mice that express the Venus variant of EYFP (F46L/F64L/M153T/V163A/S175G) (Nagai et al., 2002) under the control of the CD11c promoter were made by pronuclear injection, and progeny positive for the transgene were backcrossed to C57/Bl6 mice (Lindquist et al., 2004). We examined intact explanted lymph nodes from two transgenic lines by two-photon microscopy to determine their suitability for deep-tissue imaging. These mice express high levels of EYFP specifically in $CD11c^{hi}$ dendritic cells, which are visible in lymph nodes up to 300 μm deep (**Figure 3.1; Movies 3.1,3.2**). To define the B cell follicle and give anatomical context within the LN, we transferred 10^8 naïve GFP-expressing B cells purified by negative immunomagnetic selection with CD43 beads. Like wild-type $CD11c^{hi}$ DCs, EYFP DCs in our transgenic mouse express heterogenous levels of maturation markers, both by FACS (**Figure 3.2**) and by immunofluorescence (**Figure 3.3**). It should be noted that some B cells and activated T cells also express CD11c, and have EYFP expression at least one log lower than the $CD11c^{hi}$ DCs (**Figure 3.2**). Plasmacytoid DCs ($CD11c^{int}$, $B220^{+}$ $CD19^{-}$ $Gr1^{+}$ do not express significant levels of EYFP (**Figure 3.2**). The $CD11c^{hi}$ $EYFP^{hi}$ dendritic cells that are bright enough to be visible in the microscope are primarily located in the T-cell area of the lymph node, and are not related anatomically to the vasculature in most LNs (**Figure 3.3**).

Blood and lymph flow are preserved during intravital imaging

To verify that the microsurgical preparation of the inguinal lymph node did not disrupt blood flow, we injected mice with 66 kDa rhodamine dextran i.v. Blood flow was clearly visible in imaged fields, and it was possible to distinguish HEVs by their width and the shadows of lymphocytes adhering to their walls (**Movie 3.3**). To verify that lymphatic drainage was intact, we injected mice with 66 kDa rhodamine dextran s.c. and imaged the efferent lymphatic vessels from the inguinal lymph node. Pulsatile flow in the lymphatic vessels was observed (**Movie 3.4**), indicating that efferent drainage is intact. Occasionally, T cell extravasation was observed (**Movie 3.5**), providing further evidence that the physiology of our imaged lymph nodes is grossly intact. Phototoxicity was occasionally observed (**Movie 3.6**); we found that DC dendrite probing correlated well with lymphocyte motility. We therefore used the behavior of DCs as an indicator of local viability when determining which imaging sequences were suitable for analysis.

Dendritic cell movement varies by microanatomical location

We used intravital microscopy to examine the inguinal LN of anesthetized mice, and saw two distinct types of cell motility: crawling - translational movement, and probing – extension and retraction of cell processes. The most superficial DCs were found in the subcapsular sinus and crawled slowly around relatively sessile macrophages, while rapidly probing with their processes. (**Figure 3.4a; Movies 3.7, 3.8**). Other DCs in the subcapsular sinus exhibited rapid, directed translational movement into the parenchyma of the lymph node and may be recent immigrants from the afferent lymph (**Movie 3.7**).

Most of the DCs in the LN parenchyma were found in extensive networks in and around the T cell area. DCs in deep paracortical networks showed significant probing movements but were largely sessile (**Figure 3.4b; Movies 3.9, 3.10**). Another population of perifollicular DCs between the B cell follicle and subcapsular sinus showed mostly probing motions and appeared well-positioned to acquire antigens from incoming lymph (**Figure 3.4c; Movies 3.11, 3.12**). DCs were relatively sparse in B cell follicles, and individual DCs showed a crawling movement, often directionally (**Figure 3.4e; Movie 3.12**).

Dendritic cells form clusters with B and T lymphocytes at the B-T interface

At the interface between the B and T cell areas we often found DCs in stable clusters that varied in size and contained round, lymphocyte-sized inclusions that lacked EYFP (**Figure 3.4d; Movies 3.13, 3.14**). DCs in clusters moved dynamically, and frequently appeared to capture freely-moving cells (**Movie 3.15**). To determine the cellular composition of these clusters, we performed immunohistology on thick LN sections and examined 3D reconstructions of confocal micrographs. Clusters were found to contain B and T lymphocytes (**Figure 3.5**). Because of the tight packing of DCs, it is impossible to count the DCs in a cluster by the EYFP signal alone, so we stained thick sections with TO-PRO-3 to visualize nuclei and examined reconstructions as above (**Figure 3.6**); clusters typically contained up to 8 DCs.

Migrant DCs join the endogenous DC network

All of the previous intravital imaging experiments on DCs used purified splenic dendritic cells, which were matured by exposure to adjuvant and injected back into mice, where they migrated to the LN. The relationship of these migrant DC to the endogenous DC residing in the LN in the steady state, however, was unclear.

Following the protocol used by Mempel *et al.* (2004), we purified splenic DCs from ECFP-expressing mice and injected them intradermally with LPS to induce maturation and CCR7 upregulation. We then followed the course of DC migration to LNs and saw that the migrant ECFP DCs distributed throughout the T-cell area of the LN (**Figure 3.7**). Over the course of ~24 h, they migrated to the LN and incorporated into the network of EYFP DCs, gradually slowing down over time. The injection of LPS caused the recruitment of dermal EYFP DCs to the LN, leading to an increase in the mean cell velocity of EYFP DCs to twice their steady-state velocity by 72 h post-injection (**Figure 3.7; Movie 3.16**). At all timepoints, however, the migrant ECFP DCs moved more rapidly than the endogenous EYFP DCs. Anecdotally, we rarely observed DCs entering the circulation through HEVs (**Movie 3.17**); we did not observe this frequently enough to judge its dependence on inflammatory or other stimuli.

Figure 3.1 Brightness and surface markers of CD11c-EYFP cells. (**a**) Two-photon fluorescence images descending along the z-axis through explanted lymph nodes from CD11c-EYFP^{hi} and CD11c-EYFP^{lo} mice, with EYFP in green and second harmonics from collagen fibers in blue; depth from the apex of the lymph node is indicated in microns. Only CD11c-EYFP^{hi} cells can be visualized deep within the lymph node. (**b**) Fluorescence micrograph of lymph node sections from WT, CD11c-EYFP^{lo}, and CD11c-EYFP^{hi} mice stained with α-CD3 (red) and α-B220 (blue); EYFP fluorescence was visualized directly as described in Methods. Scale bars are 200 μm. (**c**) Confocal micrograph of lymph node sections immunostained for CD11c in red, with EYFP fluorescence in green. Scale bars are 10 μm.

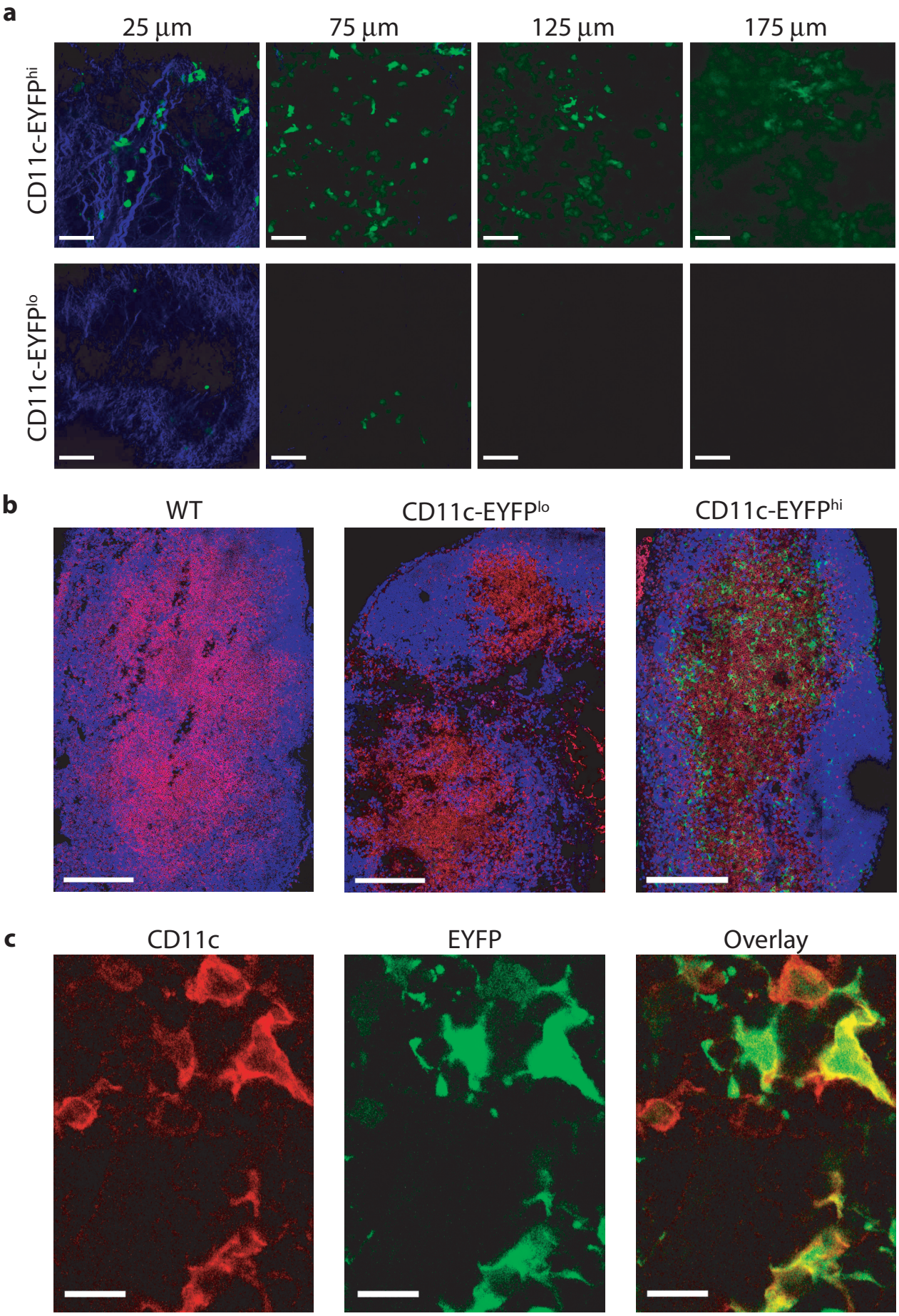
a
25 µm
75 µm
125 µm
175 µm
CD11c-EYFPhi
CD11c-EYFPlo
b
WT
CD11c-EYFPlo
CD11c-EYFPhi
c
CD11c
EYFP
Overlay

Figure 3.2 Flow cytometric analysis of EYFP cells visible by two-photon microscopy. **(a)** To determine the phenotype of visible EYFP cells, we compared EYFP fluorescence of lymph node cells from $EYFP^{hi}$ mice and $EYFP^{lo}$ mice. Since the brightest cells in $EYFP^{lo}$ mice are barely visible by two photon microscopy, we used their brightness as the threshold for gating lymph node cells from $EYFP^{hi}$ mice. **(b)** Surface marker expression of cells from $EYFP^{hi}$ mice. Only population I is visible with two-photon microscopy, and consists almost exclusively of DCs. Population II contains mainly B cells, and population III consists largely of plasmacytoid DCs.

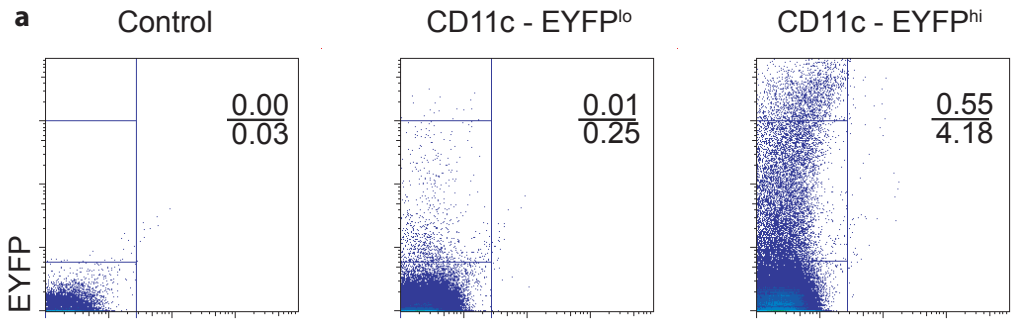
a
Control
CD11c - EYFP^lo
CD11c - EYFP^hi
0.00
0.03
0.01
0.25
0.55
4.18
EYFP

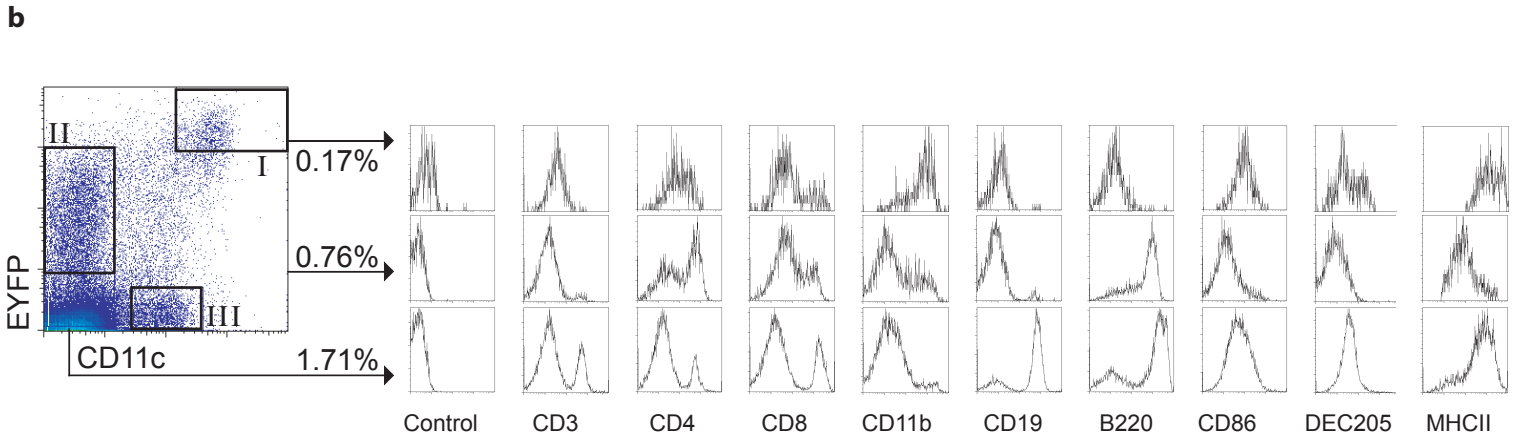
b
II
I
III
0.17%
0.76%
1.71%
EYFP
CD11c
Control
CD3
CD4
CD8
CD11b
CD19
B220
CD86
DEC205
MHCII

Figure 3.3 CD11c-EYFP mice examined by immunofluorescence. (**a-i**) Confocal micrographs of lymph node sections stained for the indicated cell surface markers in red and counterstained in blue with CD3 or B220 to provide anatomical definition within the lymph node. Squares linked to arrows indicate the area that was magnified. The scale bar represents 200 μm in low resolution panels and 100 μm in high magnification insets. The results are representative of at least three experiments.

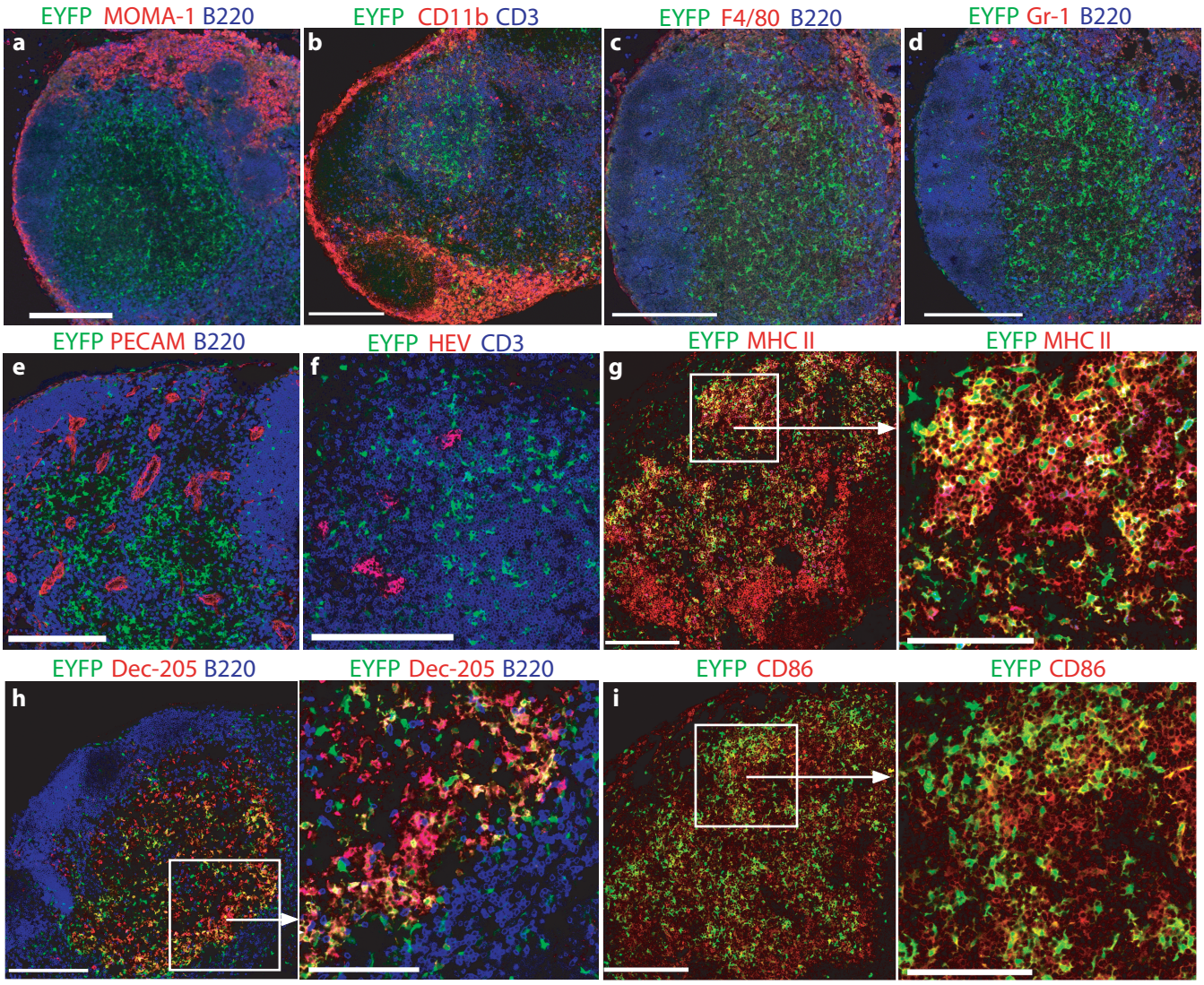
EYFP MOMA-1 B220
a
EYFP CD11b CD3
b
EYFP F4/80 B220
c
EYFP Gr-1 B220
d
EYFP PECAM B220
e
EYFP HEV CD3
f
EYFP MHC II
g
EYFP MHC II
EYFP Dec-205 B220
h
EYFP Dec-205 B220
EYFP CD86
i
EYFP CD86

Figure 3.4 Anatomic distribution and behavior of DCs within the lymph node. Inguinal lymph nodes from CD11c-EYFP mice were examined by intravital microscopy; each panel is associated with the indicated supplementary videos. EYFP fluorescence is in green; scale bars are 50 μm. (**a**) Subcapsular DCs surrounded by macrophages which have taken up Rhodamine-labeled dextran. (**b**) DCs in the T cell area of the lymph nodes, with transferred EGFP T cells false-colored red. (**c**) DCs form a network surrounding the B-cell follicles. (**d**) DC cluster at the boundary between T and B-cell areas. (**e**) Schematic diagram of the inguinal lymph node indicating the anatomic locations of the DCs shown in other panels. (**f**) DCs in a B cell follicle, with transferred EGFP B cells false-colored blue. (**g**) Crawling speed of DCs varies with anatomic location. Each point represents the average speed of one cell as calculated by the movement of the centroid; velocities less than 2 μm/min are considered sessile. Median speeds are indicated by horizontal bars. Cells tend to arrest when incorporated into cell networks, although individual fast moving cells do occur in all locations. The results summarize at least 3 imaging sessions in each location.

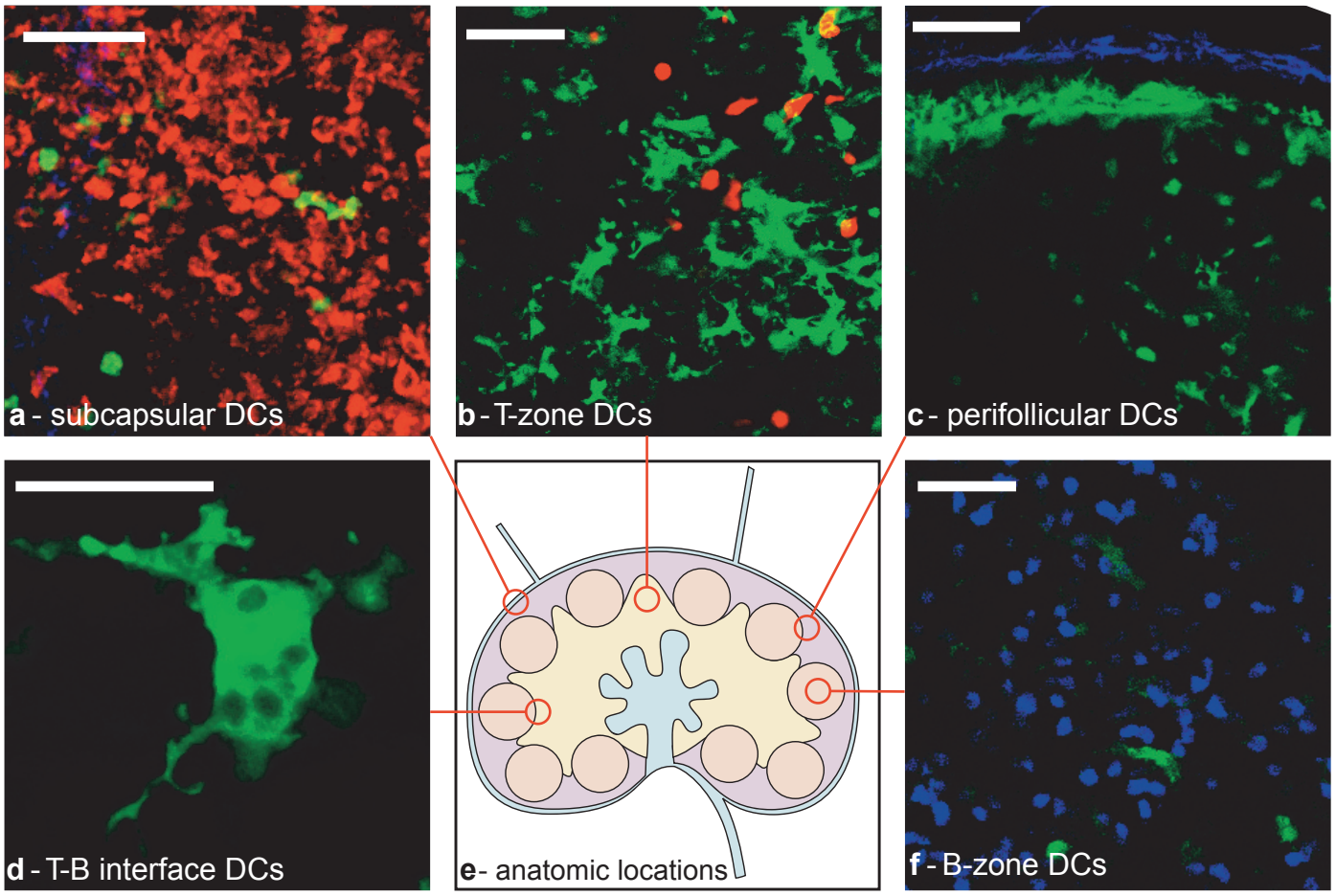
a - subcapsular DCs
b - T-zone DCs
c - perifollicular DCs
d - T-B interface DCs
e - anatomic locations
f - B-zone DCs

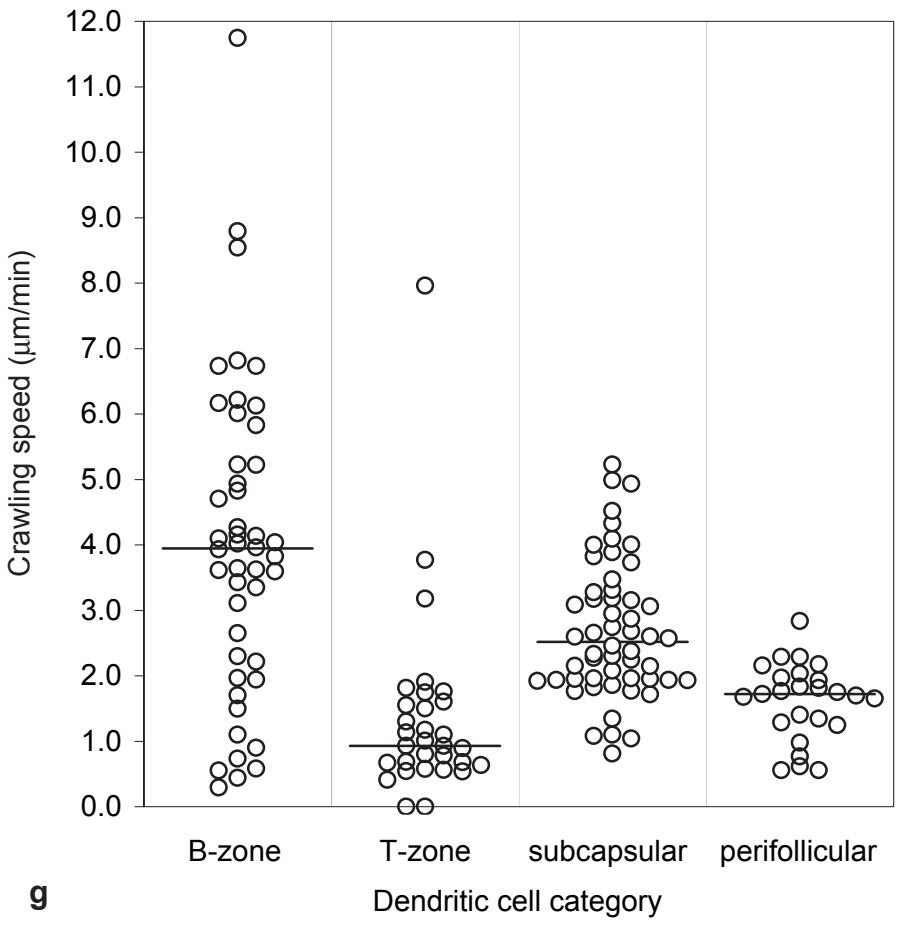
12.0
11.0
10.0
9.0
8.0
7.0
6.0
5.0
4.0
3.0
2.0
1.0
0.0
Crawling speed (µm/min)
B-zone
T-zone
subcapsular
perifollicular
Dendritic cell category

g

Figure 3.5 CD11c^{+} DCs form clusters with T and B cells in the steady state.

(a) Series of confocal images optically sectioning an inguinal lymph node, with EYFP in green, CD3 in red and B220 in blue (see also Supplementary Video 12 on-line). Scale bars are 10 mm. **(b)** Low-power view fluorescence micrograph of entire lymph node section shown above, with the cluster denoted in the inset. Scale bar is 200 mm.

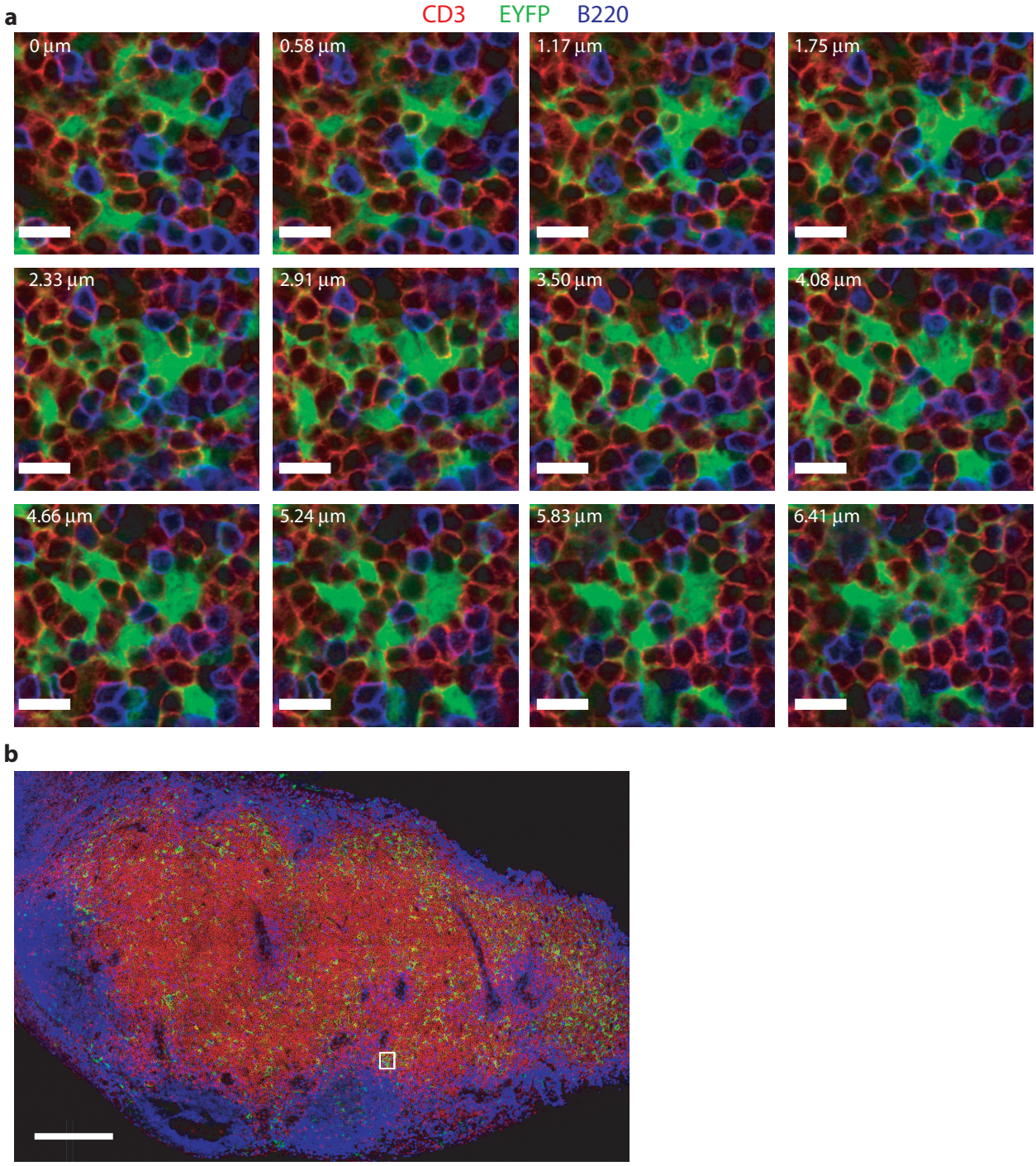
a
CD3
EYFP
B220
0 µm
0.58 µm
1.17 µm
1.75 µm
2.33 µm
2.91 µm
3.50 µm
4.08 µm
4.66 µm
5.24 µm
5.83 µm
6.41 µm
b

Figure 3.6 DC clusters include more than one DC. Series of confocal images optically sectioning an inguinal lymph node, with EYFP in green, DNA in red (TO-PRO 3), and CD3 and CD19 in blue. Nuclei from DCs in a single cluster are indicated with arrows. Note that DCs (A–H) exhibit no CD3 or CD19 staining.

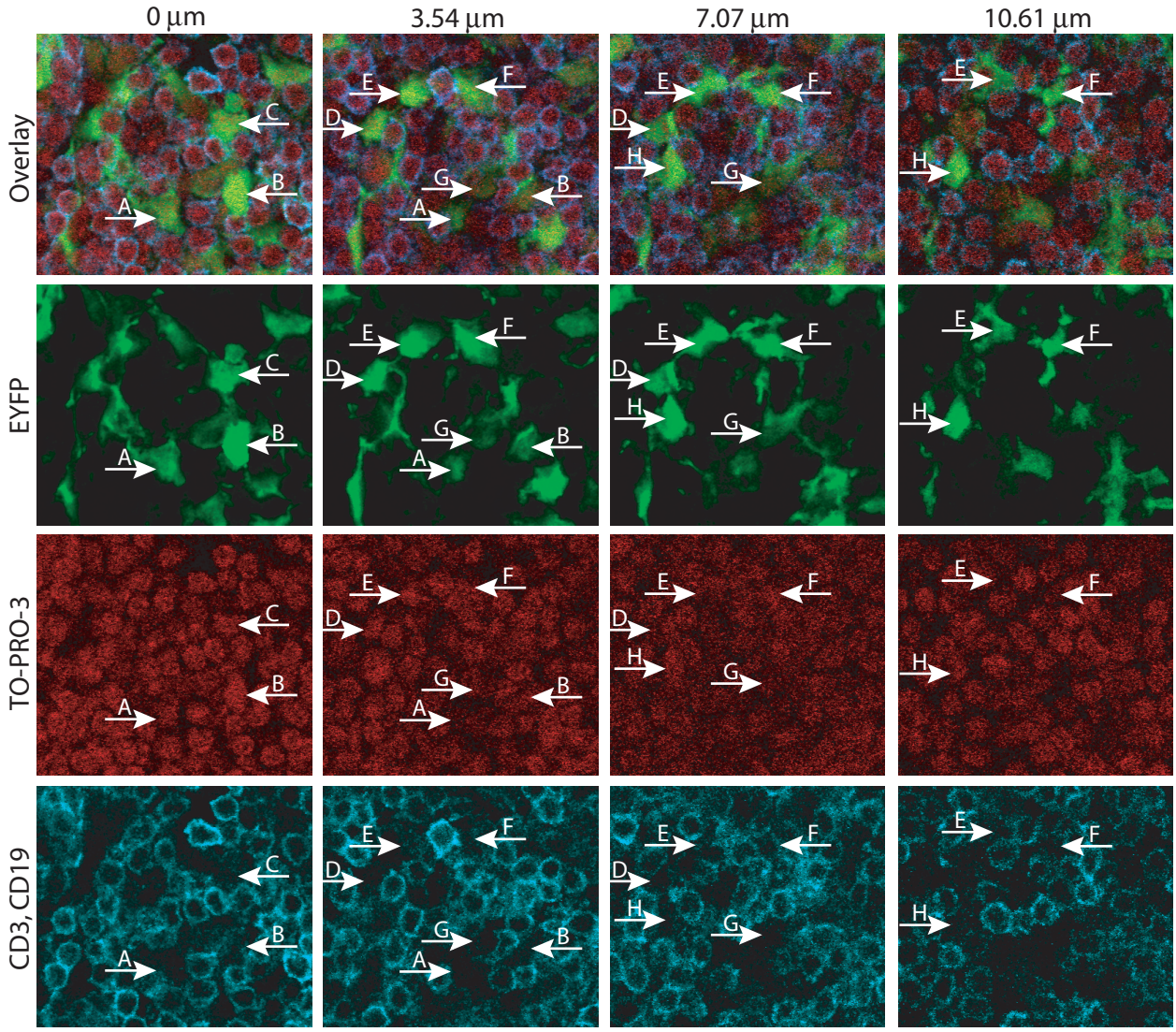
0 µm
3.54 µm
7.07 µm
10.61 µm
Overlay
EYFP
TO-PRO-3
CD3, CD19
A
B
C
D
E
F
G
H

Figure 3.7 Transferred ECFP DCs gradually incorporate into the endogenous DC network. Splenic DCs were purified by immunomagnetic selection from the spleens of ECFP mice injected s.c. with a Flt3L-secreting tumor, and 4-6 x 10^6 cells were intradermally injected with LPS into the flank of CD11c-EYFP mice. Inguinal LNs were examined by immunofluorescence and intravital microscopy at the indicated time points. (**a**) Confocal micrograph of inguinal LNs immunostained for HEVs with MECA-79 antibody. Scale bar is 200 μm in low resolution panels and 100 μm in high magnification insets; optical thickness is 10 μm in the ECFP channel and 1.2 μm in all other channels. (**b**) Plots of displacement versus $(\text{time})^{1/2}$, used to calculate the motility coefficient of transferred (filled circles) and endogenous (open circles) cells. Inguinal LNs were imaged by multiphoton microscopy, and cells were tracked as above; the motility of transferred DCs gradually decreases as the cells incorporate into the endogenous DC network. (**c**) Scattergram of the average velocities of individual transferred and endogenous DCs at the indicated time points. Panels (**b**) and (**c**) summarize at least 4 imaging fields examined in each time point.

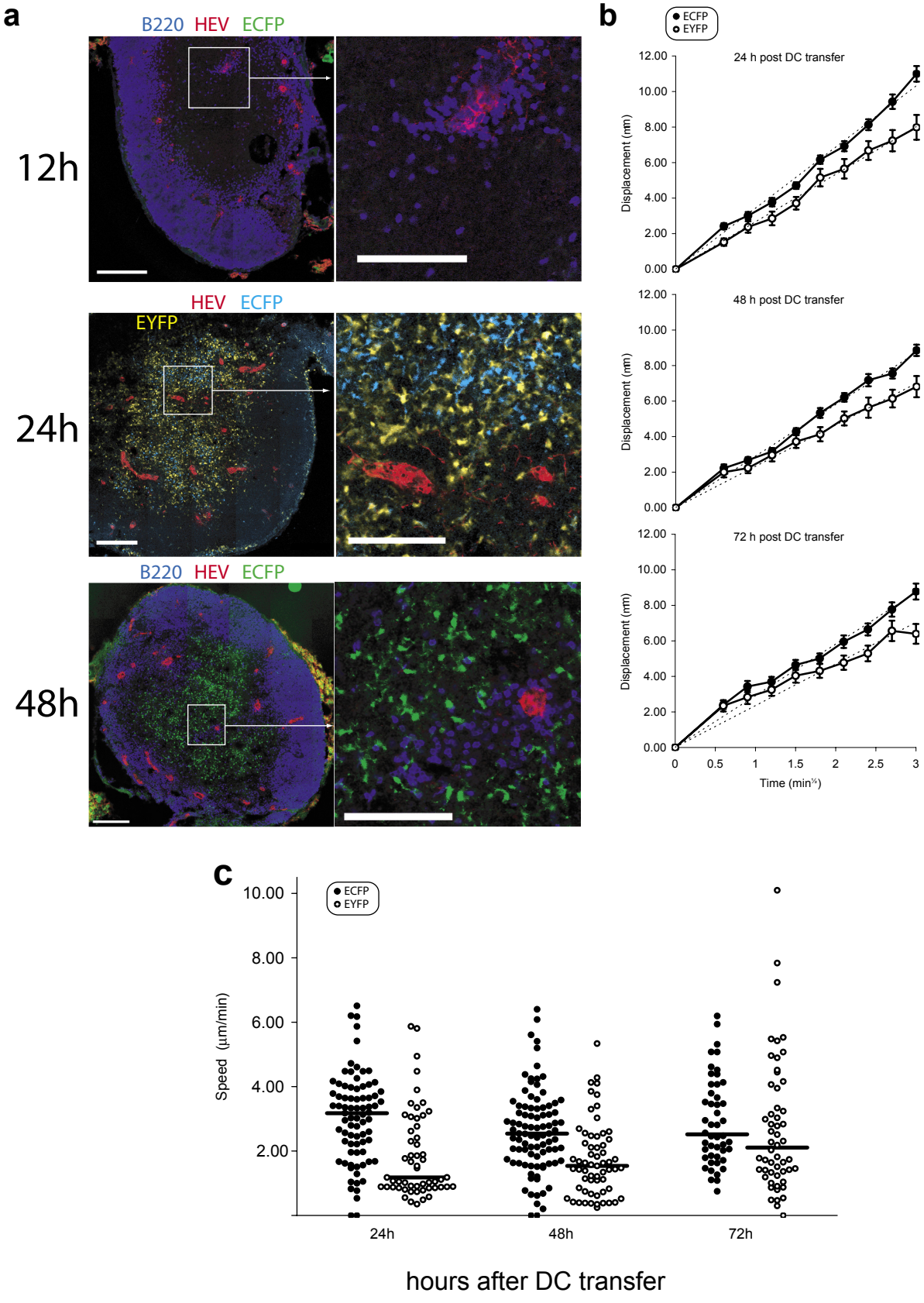
a
B220 HEV ECFP
12h
HEV ECFP
EYFP
24h
B220 HEV ECFP
48h
b
ECFP
EYFP
24 h post DC transfer
48 h post DC transfer
72 h post DC transfer
Displacement (mm)
Time (min½)
c
Speed (µm/min)
24h
48h
72h
hours after DC transfer

CHAPTER 4. DC:T CELL INTERACTIONS UNDER TOLERIZING AND IMMUNIZING CONDITIONS

Several groups have visualized DC:T cell interactions using purified, *in vitro* labeled, adjuvant-matured splenic dendritic cells and transgenic T cells (Bousso and Robey, 2003; Mempel et al., 2004; Miller et al., 2004a; Miller et al., 2004b; Miller et al., 2003; Stoll et al., 2002), but these methodologies limit the applicability of the results to DCs that mature in the periphery, precluding direct comparison with steady-state DC:T cell interactions. We took advantage of a method previously used in the lab to deliver antigen specifically to DCs (Bonifaz et al., 2002; Hawiger et al., 2001). Simultaneous CD40 ligation or stimulation with a TLR ligand leads to dendritic cell activation and the triggering of an immunogenic response to the peptides targeted to the dendritic cell (Bonifaz et al., 2002; Hawiger et al., 2001).

Specific antigens are targeted to dendritic cells by using a previously described recombinant anti-Dec-205 antibody with a C-terminal region containing an antigenic peptide as well as sequences that direct proper proteolytic processing and presentation (Hawiger et al., 2001); we cloned Ovalbumin peptide into the C-terminal region of this antibody, injected it into mice, and examined T cell activation after dendritic cell targeting. Naïve OT-II T cells were transferred i.v. into WT mice, and injected with antigen 24 h later. Antigen delivery by α-Dec-Ova activates tolerized and primed OTII T cells to a similar extent, as measured by upregulation of early activation markers, proliferation, and response to antigen at three days (**Figure 4.1**). By seven days after

antigen delivery, OT-II T cells are deleted in the absence of a priming stimulus; the few cells that remain do not proliferate in response to peptide rechallenge (**Figure 4.1**).

Tolerance and priming are characterized by similar retention near HEVs

We analyzed the distribution of specific and non-specific T cells throughout the LN, by transferring GFP-expressing OT-II or non-TCR-transgenic cells into WT mice, delivering α-Dec-Ova, and examining frozen LN sections histologically. We quantified the distribution by dividing the LN into superficial and deep regions, and counting the number of T cells in each region, as well as by measuring the position of all T cells and HEVs and calculating the distance from each T cell to the nearest HEV. Both primed and tolerized cells were retained specifically near HEVs at 3 h after transfer, while non-specific T cells were present throughout the T cell area (**Figure 4.2**). By 24 h after transfer, both tolerized and primed cells had distributed evenly throughout the LN.

Imaging tolerance and immunity

To image the induction of T cell tolerance, fluorescently-labeled T cells are transferred into CD11c-EYFP^{+} mice and the cellular interactions in the inguinal lymph node are visualized by intravital microscopy (**Figure 4.3**). As described above, to target antigen specifically to DCs, we injected mice with α-Dec-Ova (Hawiger et al., 2001). Fluorescently-labeled T cells are purified from mice ubiquitously expressing ECFP (Hadjantonakis et al., 2002) or EGFP (Kang et al., 2003; Wright et al., 2001); fluorescent antigen-specific T cells are generated by crossing these mice with OT-II TCR transgenics.

Mice are injected with two types of T cell, both antigen-specific (EGFP-OTII) and non-specific ECFP-expressing $CD4^+$ T cells, to provide an internal control in each imaging field. After image acquisition, movement parameters described below are analyzed quantitatively in order to determine how the cells are interacting.

Analysis of cell motility parameters

The position of each cell was tracked in three dimensions over time, and displacement and motility parameters were calculated for each cell. These include measurements of cell velocity, cell directionality, and cell-cell contact duration, information that can only be acquired by directly visualizing the interacting cells. Both instantaneous measurements and per-cell average measurements of velocity and immobility are taken; the percent of each track during which cells are immobile is termed the arrest coefficient (Hugues et al., 2004). "Immobile" was defined as average or instantaneous velocity less than 2 μm/min, as dendritic cells that appeared to be entirely stationary had measured velocities of up to 2 μm/min. The motility coefficient is the slope of the linear portion of the curve obtained when mean displacement is plotted against the square root of time, and is analogous to the diffusion coefficient of a particle exhibiting Brownian motion (Mempel et al., 2004; Sumen et al., 2004). Measurements of directionality include the confinement index and turning angle. The confinement index is the ratio of the maximum displacement to the total path length, and reflects the directionality of cell movement over the entire path (Hugues et al., 2004). The turning angle between velocity vectors at subsequent timepoints provides an instantaneous

measure of directionality (Mempel et al., 2004). As a general rule, arrested cells move less directionally than freely moving cells; naïve T cells tend to move in relatively straight lines.

Cell confinement and pausing are also analyzed. Cells which move freely in a random-walk pattern exhibit a linear relationship between their displacement and the square root of time, while cells that move directionally have a displacement directly proportional to time (Sumen et al., 2004). Cells that are confined within a smaller volume reach a displacement plateau, indicating that their movement is limited. To examine cell-cell interactions, the duration of cell-cell contacts can be measured manually; the time a cell spends paused can be analyzed as a function of distance to another cell, to determine if relationships exist.

Tolerized T cells rapidly undergo an antigen-specific arrest

At the first time point examined, 1-6 h after transfer, we observed that tolerized OT-II cells arrested, while control nontransgenic T cells did not (**Figure 4.4; Movie 4.1**). The tolerized T cells moved at an average velocity of 4.4 μm/min, while control non-transgenic T cells moved at 9.4 μm/min (**Figure 4.4**, $p < 0.001$). As compared with nontransgenic T cells, more of the specific T cells were arrested for the duration of the imaging period, and specific cells had a higher arrest coefficient, 47% v. 20%, $p < 0.0001$; **Figure 4.5**). Consistent with their relative immobility, specific cells moved less directionally, as shown by their higher turning angle (82° v. 61°, $p < 0.0001$) and lower confinement index (41% v. 56%, $p < 0.0001$; **Figure 4.6**. As controls, we injected mice with isotype control-targeted Ova (III/10-Ova) and irrelevant peptide α-Dec-CSP

antibodies and imaged the T cell response; antigen-specific OTII T cells did not arrest, and moved indistinguishably from nontransgenic T cells.

At the second time point examined, between 6-12 h, specific T cells remained significantly slower than non-specific T cells, but were moving faster than in the first 1-6 h (5.94 μm/min v. 7.5 μm/min, $p < 0.001$; **Figure 4.4; Movie 4.2**). Antigen-specific T cells were more immobile (12% v. 6%, $p < 0.05$; **Figure 4.5**), with a larger arrest coefficient (32% v. 13%, $p < 0.0001$; **Figure 4.5**) and moved less directionally, with a lower confinement index (53% v 66%; **Figure 4.6**). At the third time point examined, from 12-18 h, specific T cells were still significantly slower (7.0 v. 8.8 μm/min, p. 0.0001; **Figure 4.4; Movie 4.3**) and more immobile (12% v. 3%, $p < 0.002$); **Figure 4.5**), but had no significant differences in the directionality of their movement (**Figure 4.6**). To determine if the differences seen between the various imaging intervals was significant, we performed two-way analysis of variance (ANOVA). The ANOVA indicated that the difference in speeds between the antigen-specific OT-II cells and the nontransgenic control cells was significantly greater at 1-6 h than at either 6-12 h or 12-18 h ($p < 0.0001$ for both). Additionally, the difference between 6-12 h and 12–18 h was not significant, suggesting that the tolerized T cells are recovering mobility by 6-12 h.

Priming yields an antigen-specific arrest similar to that observed in tolerance

To visualize the immune response under pro-inflammatory conditions, we delivered antigen to DCs in the presence of an α-CD40 antibody as an adjuvant, and transferred T cells and imaged as above. We observed that primed cells, like tolerized cells, arrested antigen-specifically shortly after their exit into LNs (**Figure 4.7; Movie**

4.4). In the first time period imaged, from 1-6 h after T cell transfer, specific T cells moved at an average speed of 5.2 μm/min, slower than that of the control T cells (8.8 μm/min; **Figure 4.7**). The specific cells were more immobile (31% v. 10%, $p < 0.0001$; **Figure 4.8**), and had a higher arrest coefficient (40% v. 21%, $P < 0.0001$; **Figure 4.8**), and moved less directionally (**Figure 4.9**). In the second time period imaged, from 6 – 12 h after T cell transfer, specific T cells remained slower than non-specific cells (4.4 v. 8.0 μm/min, $p < 0.0001$; **Figure 4.7; Movie 4.5**), and had a higher arrest coefficient (46% v. 27%, $p < 0.001$; **Figure 4.8**), but were no longer significantly more immobile (**Figure 4.8**). Measures of directionality were also mixed – OT-II T cells showed a smaller confinement index (40% v. 49%, $P < 0.02$; **Figure 4.8**), but no significant difference in turning angle. In the third time period imaged, from 12–18 h, the primed T cells moved slightly more slowly (6.1 v. 7.5 μm/min, $p < 0.005$; **Figure 4.7; Movie 4.6**) and had slightly higher arrest coefficients (35% v. 28%, $p < 0.05$; **Figure 4.7**), but all other movement parameters were indistinguishable. Two-way ANOVA showed that the speed difference between OT-II cells and nontransgenic T cells was significantly smaller in 12-18 h than at 1-6 h ($p < 0.003$) and at 6-12 h ($p < 0.006$), while there was no difference between 1-6 h and 6-12 h.

We observed that in both tolerance and immunity, naïve T cells arrested antigen-specifically shortly after leaving HEVs (**Figure 4.2; Movies 4.1, 4.4**). Tolerized T cells recovered marginally faster than primed T cells, but both had recovered significantly by 12-18 h (**Figures 4.4, 4.7; Movies 4.3, 4.6**). The pattern of an early arrest followed by restoration of mobility is also observed if the non-specific T cells are used as internal controls, and T cell speed is normalized to that of the control cells in each imaging field

(**Figure 4.10**); this permits more reproducible comparison between separate imaging fields from independent experiments.

We occasionally observed discrete T cell swarms or clusters forming around DCs, (**Movie 4.7**), but did not always observe arrested T cells in contact with $EYFP^+$ DCs (**Movie 4.8**), perhaps because some DC processes are too thin to visualize. Although infrequently observed, these clusters were seen under both conditions of tolerance and immunity.

Figure 4.1. OT-II T cell activation and tolerance induced by α-DEC-OVA.
Transferred OT-II T cells (CD45.2) divide in response to antigen presented by DCs in vivo by day 3 and are deleted in the absence of α-CD40 by day 7. **(a)** Similar activation of OT-II T cells after delivery of α-DEC-OVA with and without α-CD40. Histograms show surface expression of the indicated marker gated on $CD45.2^+$ TCR $V\alpha2^+$ cells 3, 12, and 24 hours after challenge (see Methods). **(b)** Plots show CFSE dye dilution of gated populations of $CD4^+$ $CD45.2^+$ T cells 3 and 7 days after challenge with 2 μg of α-DEC-OVA with or without α-CD40 or with PBS. Percentages of $CFSE^{hi/lo}$ TCR $V\alpha2^+$ cells out of $CD4^+$ T cells are indicated. **(c)** Numbers of surviving OT-II cells 3 or 7 days after challenge as in **(b)**; percentages of $CD45.2^+$ TCR $V\alpha2^+$ cells among $CD4^+$ T cells are indicated. Antigen-specific T cells were deleted unless CD40 was engaged. **(d)** OT-II cells are only transiently activated by in vivo delivery of α-DEC-OVA to DCs. $CD4^+$ cells were purified from peripheral LNs 3 or 7 days after challenge as in **(b)** and cultured with irradiated $CD11c^+$ cells in the presence or absence of OVA peptide; proliferation index denotes the ratio of thymidine incorporation in antigen-challenged to unchallenged cells, corrected for background proliferation.

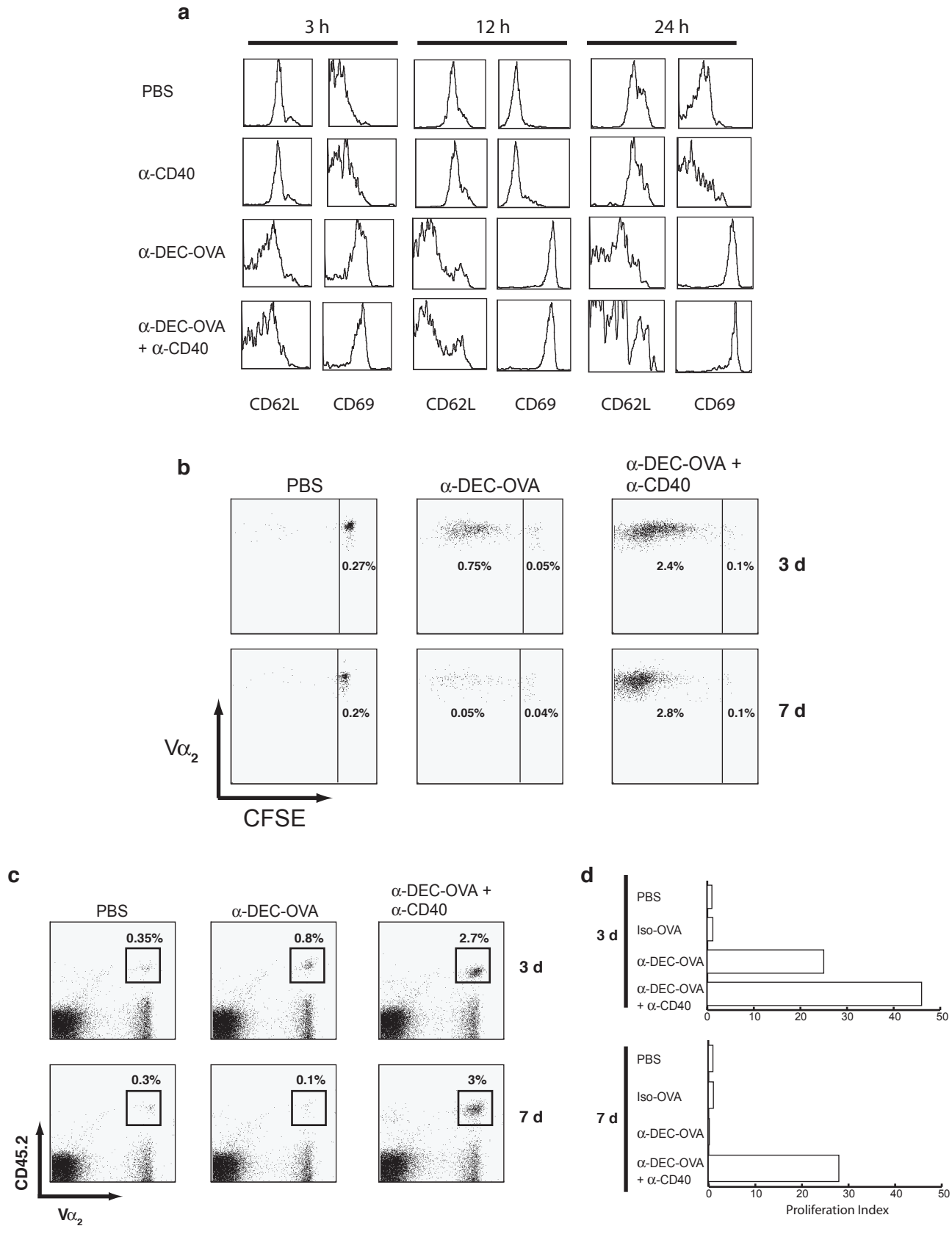
a
3 h
12 h
24 h
PBS
α-CD40
α-DEC-OVA
α-DEC-OVA + α-CD40
CD62L
CD69
b
PBS
α-DEC-OVA
α-DEC-OVA + α-CD40
0.27%
0.75%
0.05%
2.4%
0.1%
3 d
0.2%
0.05%
0.04%
2.8%
0.1%
7 d
Vα2
CFSE
c
PBS
α-DEC-OVA
α-DEC-OVA + α-CD40
0.35%
0.8%
2.7%
3 d
0.3%
0.1%
3%
7 d
CD45.2
Vα2
d
3 d
PBS
Iso-OVA
α-DEC-OVA
α-DEC-OVA + α-CD40
0
10
20
30
40
50
7 d
PBS
Iso-OVA
α-DEC-OVA
α-DEC-OVA + α-CD40
0
10
20
30
40
50
Proliferation Index

Figure 4.2. During early stages of priming and tolerance, antigen-specific T cells are located closer to HEVs in the superficial paracortex than non-specific T cells. (a) Confocal micrographs of LN frozen sections immunostained for MECA-79 (red) and B220 (blue); EGFP fluorescence from transferred T cells (green) was visualized directly. EGFP-expressing OTII or non-TCR transgenic T cells were transferred into C57BL/6 mice five hours after injection of α-DEC-OVA with or without α-CD40. Insets show high-magnification view of T cells near HEVs (left panels) or in the deep paracortex (right panels); the deep paracortex is outlined in yellow. Optical sections were 1.2 μm in both MECA-79 and B220 channels and 5 mm in the EGFP channel. **(b)** The percentage of T cells in the deep paracortex was calculated as in Bajenoff *et al*., (2003). Three hours after cell transfer, there were more non-specific T cells found in the deep paracortex than antigen-specific T cells; at 24 h after cell transfer, specific and non-specific T cells were more equally represented in the deep paracortex. **(c)** The distance from T cells to the nearest HEV was calculated as in Bajenoff *et al*. Three hours after cell transfer, antigen-specific cells were closer than non-specific cells to HEVs. Error bars denote standard error of the mean. Asterisks indicate significant differences; see text for p values.

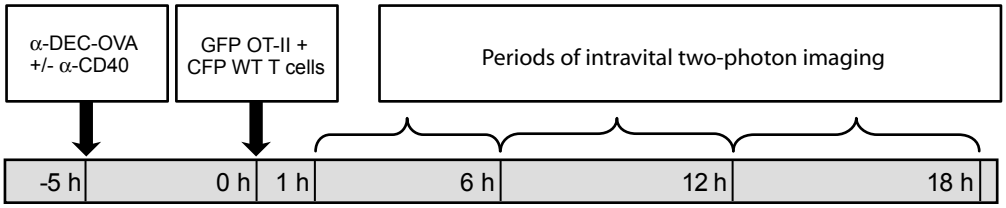
α-DEC-OVA
+/- α-CD40
GFP OT-II +
CFP WT T cells
Periods of intravital two-photon imaging
-5 h
0 h
1 h
6 h
12 h
18 h

Figure 4.3. Experimental timeline for imaging T cell tolerance and priming. CD11c-EYFP mice were injected with α-DEC-OVA with or without α-CD40 5 h prior to transfer of EGFP-OTII cells and wild-type ECFP-T cells; inguinal LNs were imaged intravitally at the indicated periods. For histologic examination, WT C57/B6 mice were injected with α-DEC-OVA with or without α-CD40 5 h prior to transfer of EGFP-OTII T cells or EGFP T cells; LNs were harvested for histology at 3 or 24 h.

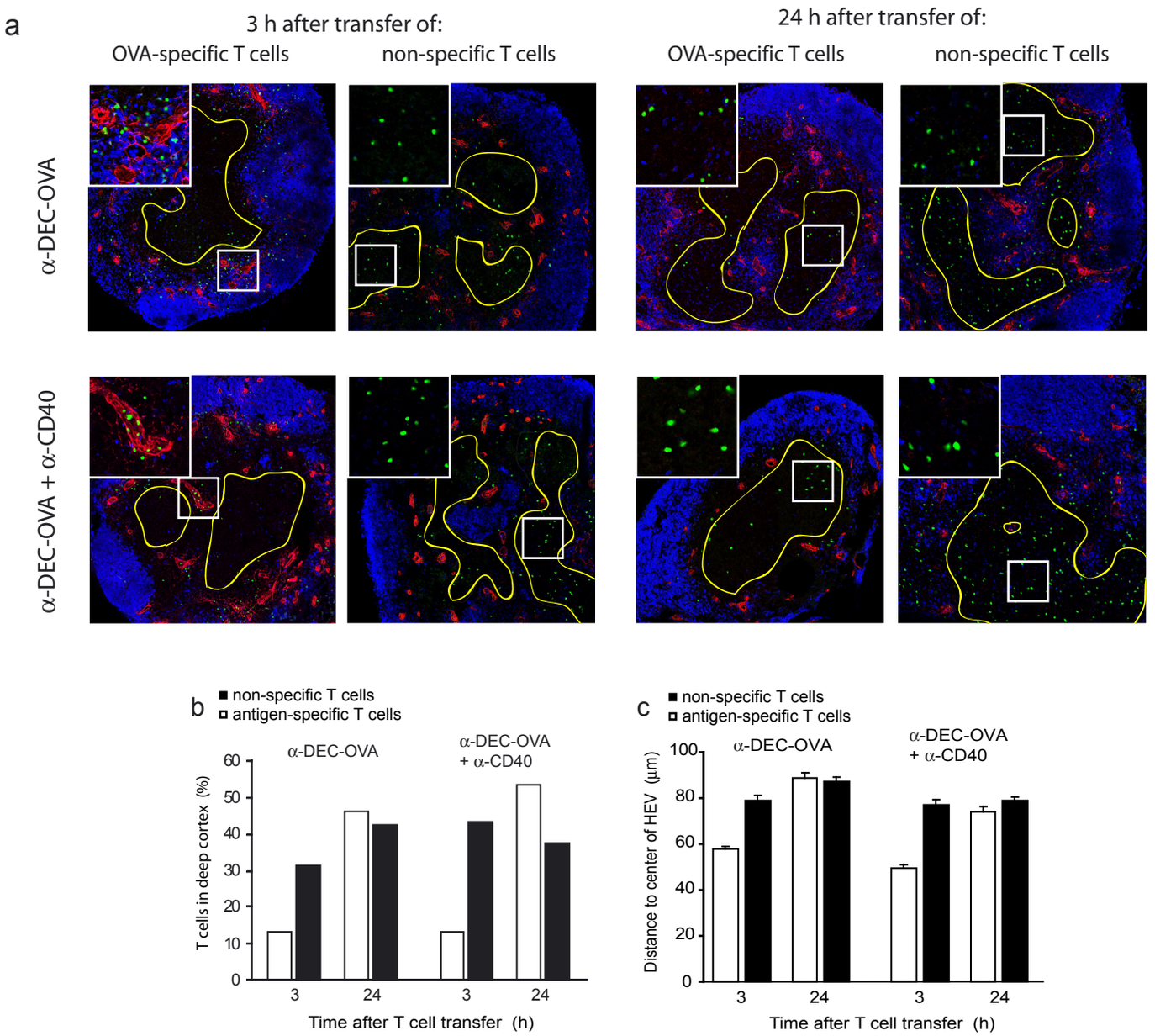
a
3 h after transfer of:
24 h after transfer of:
OVA-specific T cells
non-specific T cells
OVA-specific T cells
non-specific T cells
α-DEC-OVA
α-DEC-OVA + α-CD40
b
non-specific T cells
antigen-specific T cells
α-DEC-OVA
α-DEC-OVA + α-CD40
T cells in deep cortex (%)
0
10
20
30
40
50
60
3
24
3
24
Time after T cell transfer (h)
c
non-specific T cells
antigen-specific T cells
α-DEC-OVA
α-DEC-OVA + α-CD40
Distance to center of HEV (μm)
0
20
40
60
80
100
3
24
3
24
Time after T cell transfer (h)

Figure 4.4. T cell velocity under tolerizing conditions. Mice were injected with antibodies and T cells, inguinal LNs were imaged, and specific and non-specific T cells were tracked as above. Antigen-specific EGFP-OTII cells move slowly at 1-5 hours, with a mean cell velocity of 4.4 μm/min, while non-specific T cells maintain their normal velocity of ~9 μm/min. Error bars denote standard error of the mean. Asterisks indicate significant differences; see text for p values.

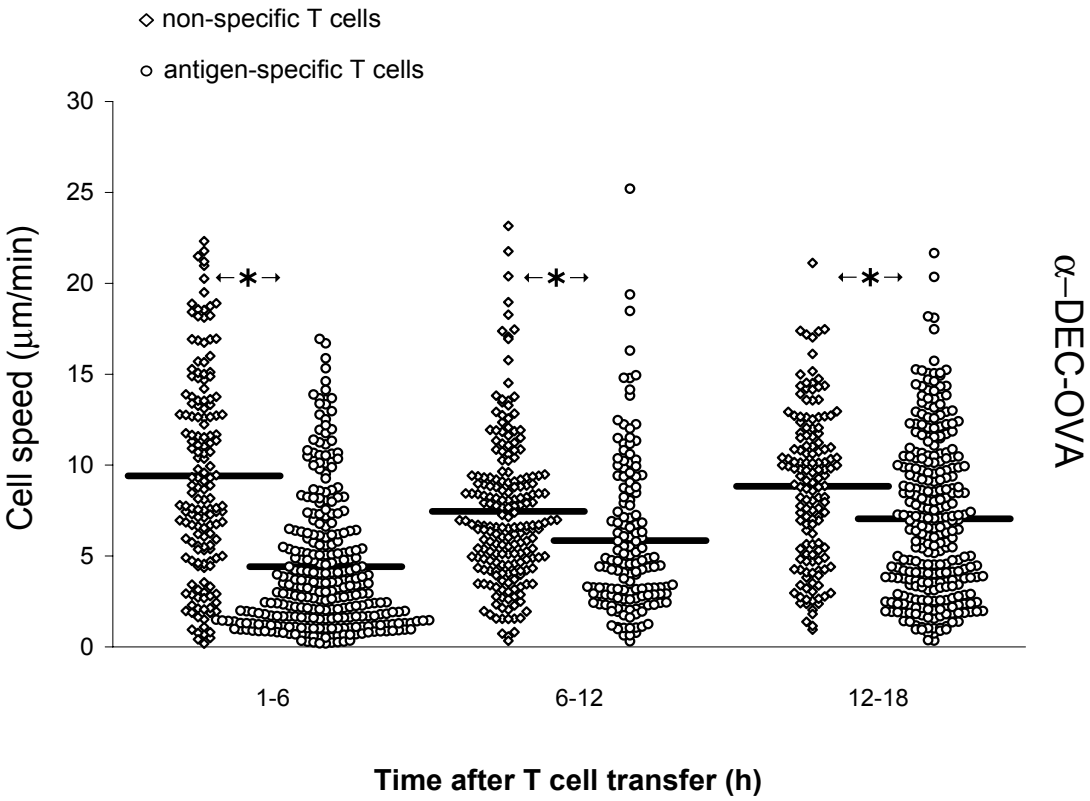
◇ non-specific T cells
○ antigen-specific T cells
Cell speed (µm/min)
30
25
20
15
10
5
0
1-6
6-12
12-18
Time after T cell transfer (h)
α–DEC-OVA

Figure 4.5. T cell arrest under tolerizing conditions. (a) Percent of immobile cells. More antigen-specific EGFP-OTII cells than non-specific T cells are immobile (mean velocity <2 μm/min) at 1-6 hours. **(b)** Arrest coefficient of specific and non-specific T cells. The arrest coefficient is the percentage of each track that a cell is immobile (instantaneous velocity <2 μm/min). From 1-6 hours after T cell transfer, tolerized EGFP-OTII cells are arrested for an average of 40-50% of each track, as compared to 20% for non-specific T cells. Error bars denote standard error of the mean. Asterisks indicate significant differences; see text for p values.

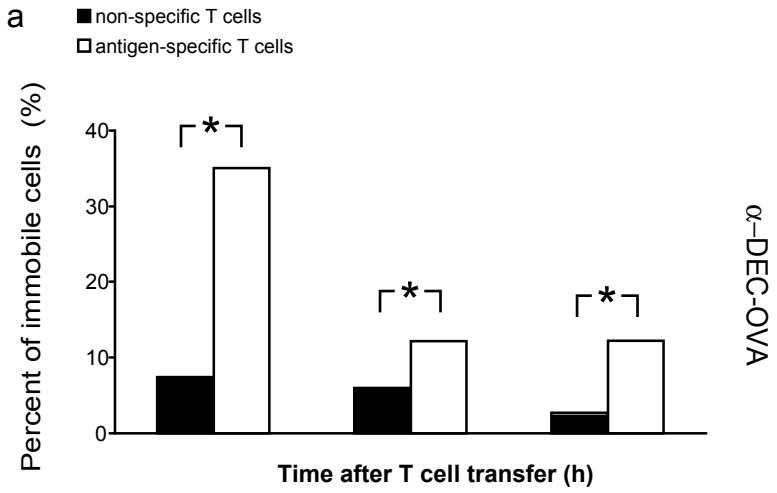
a
non-specific T cells
antigen-specific T cells
Percent of immobile cells (%)
40
30
20
10
0
*
*
*
α–DEC-OVA
Time after T cell transfer (h)

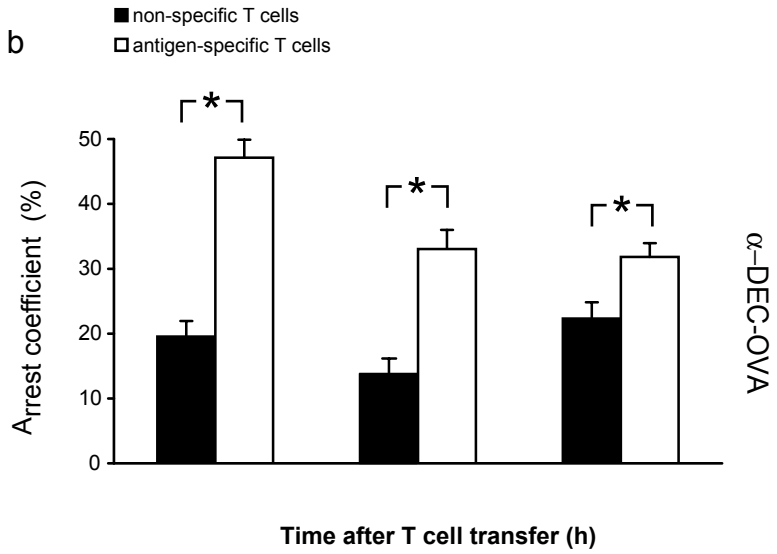
b
non-specific T cells
antigen-specific T cells
Arrest coefficient (%)
50
40
30
20
10
0
*
*
*
α–DEC-OVA
Time after T cell transfer (h)

Figure 4.6: T cell directionality under tolerizing conditions. (a) Turning angle of specific and non-specific T cells. Lower turning angles indicate more linear cell movement. **(b)** Confinement index of specific and non-specific T cells. Confinement index is the ratio of the maximum cell displacement to the path length; a higher confinement index indicates more linear movement. At time points when antigen-specific cells move more slowly than non-specific cells, the nonspecific cells move more linearly by both measures of directionality. Error bars denote standard error of the mean. Asterisks indicate significant differences; see text for p values.

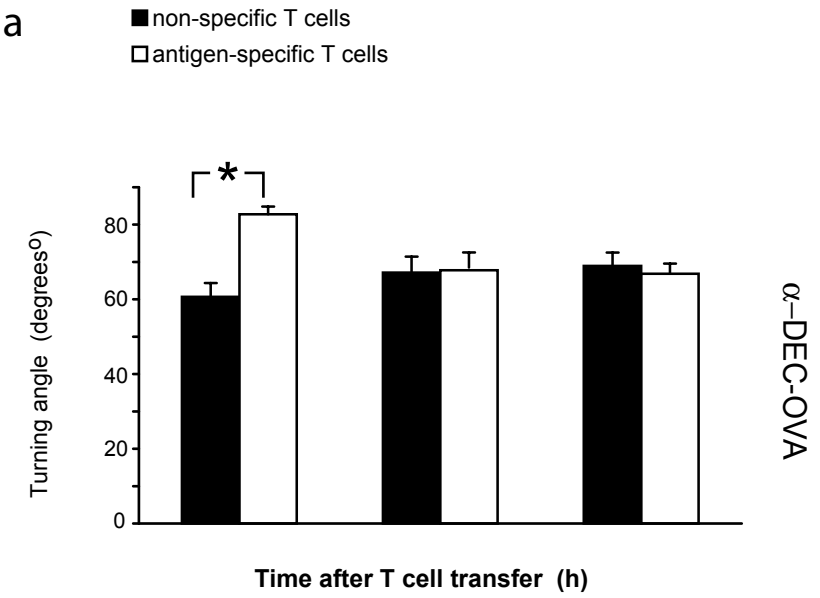
a
non-specific T cells
antigen-specific T cells
Turning angle (degrees°)
0
20
40
60
80
*
Time after T cell transfer (h)
α–DEC-OVA

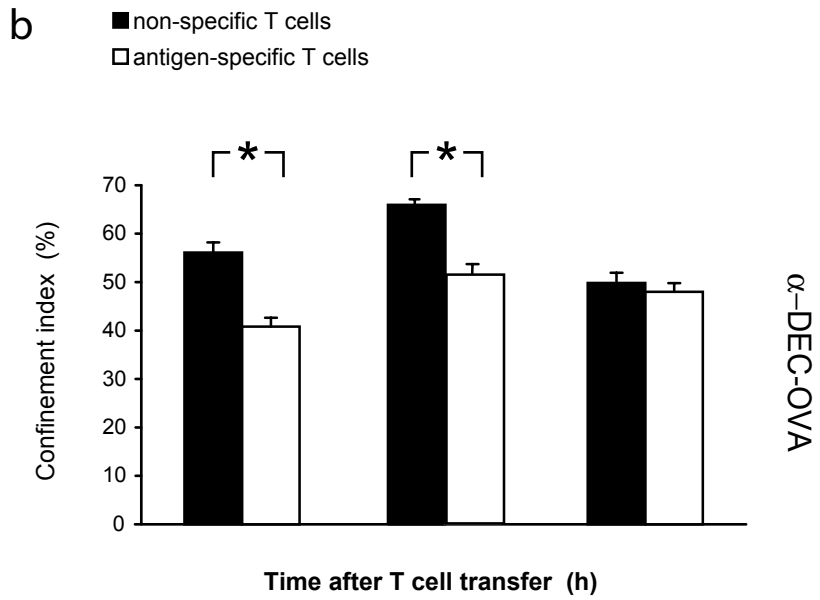
b
non-specific T cells
antigen-specific T cells
Confinement index (%)
0
10
20
30
40
50
60
70
*
*
Time after T cell transfer (h)
α–DEC-OVA

Figure 4.7. T cell velocity under priming conditions. Mice were injected with antibodies and T cells, inguinal LNs were imaged, and specific and non-specific T cells were tracked as above. Primed antigen-specific EGFP-OTII cells move slowly at 1-5 hours, with a mean cell velocity of 5.2 μm/min, while non-specific T cells maintain their normal velocity of ~9 μm/min. Error bars denote standard error of the mean. Asterisks indicate significant differences; see text for p values.

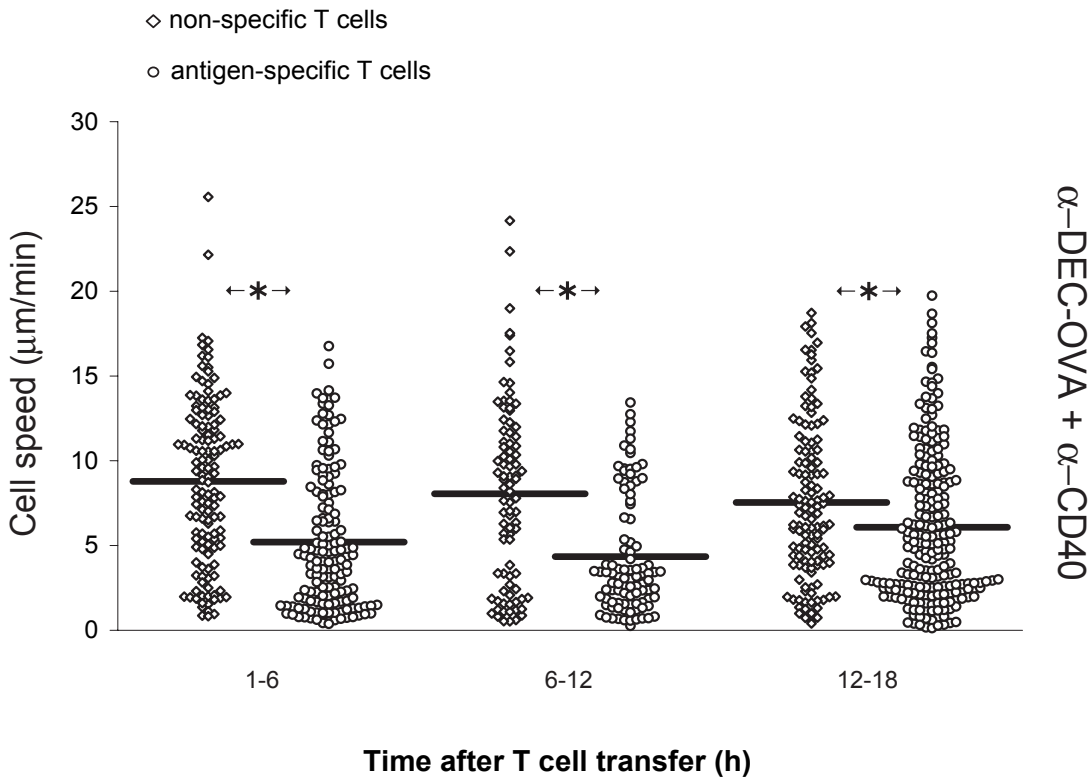
◇ non-specific T cells
○ antigen-specific T cells
Cell speed (µm/min)
30
25
20
15
10
5
0
←*→
←*→
←*→
1-6
6-12
12-18
Time after T cell transfer (h)
α–DEC-OVA + α–CD40

Figure 4.8. T cell arrest under priming conditions. (a) Percent of immobile cells. More antigen-specific EGFP-OTII cells than non-specific T cells are immobile (mean velocity < 2 μm/min) at 1-6 hours. **(b)** Arrest coefficient of specific and non-specific T cells. The arrest coefficient is the percentage of each track that a cell is immobile (instantaneous velocity < 2 μm/min). From 1-6 hours after T cell transfer, primed EGFP-OTII cells are arrested for an average of 40-50% of each track, as compared to 20% for non-specific T cells. Error bars denote standard error of the mean. Asterisks indicate significant differences; see text for p values.

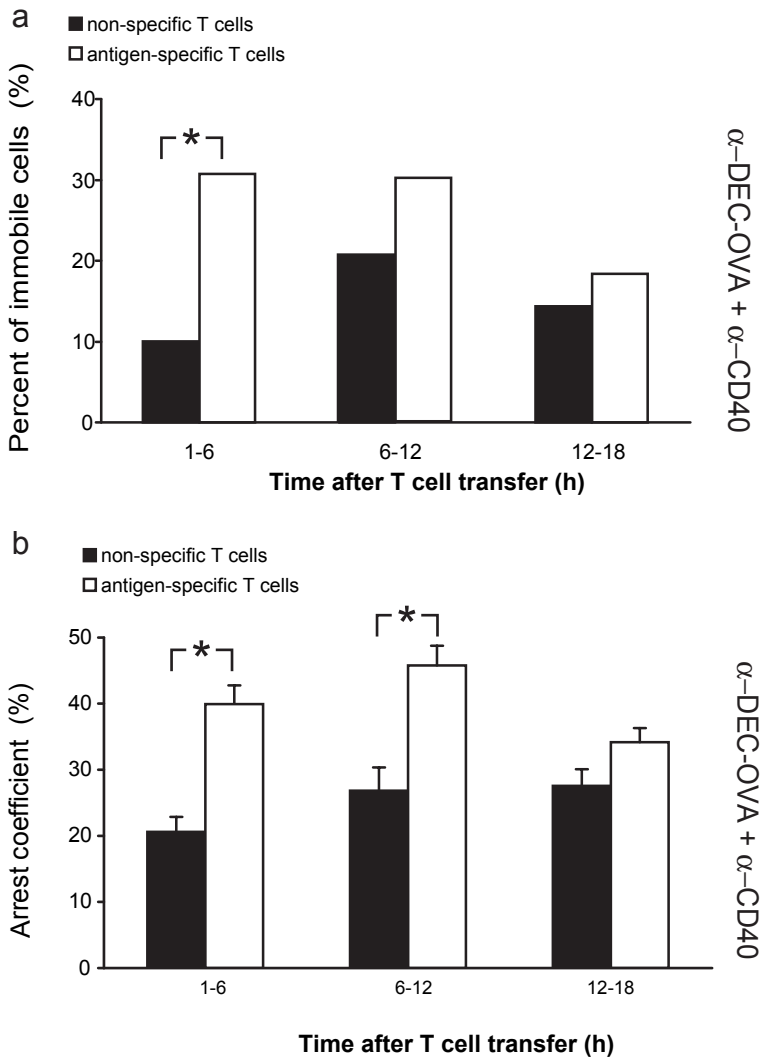
a
non-specific T cells
antigen-specific T cells
Percent of immobile cells (%)
40
30
20
10
0
*
1-6
6-12
12-18
Time after T cell transfer (h)
α–DEC-OVA + α–CD40
b
non-specific T cells
antigen-specific T cells
Arrest coefficient (%)
50
40
30
20
10
0
*
*
1-6
6-12
12-18
Time after T cell transfer (h)
α–DEC-OVA + α–CD40

Figure 4.9: T cell directionality under priming conditions. (a) Turning angle of specific and non-specific T cells. Lower turning angles indicate more linear cell movement. **(b)** Confinement index of specific and non-specific T cells. Confinement index is the ratio of the maximum cell displacement to the path length; a higher confinement index indicates more linear movement. At time points when antigen-specific cells move more slowly than non-specific cells, the nonspecific cells move more linearly by both measures of directionality. Error bars denote standard error of the mean. Asterisks indicate significant differences; see text for p values.

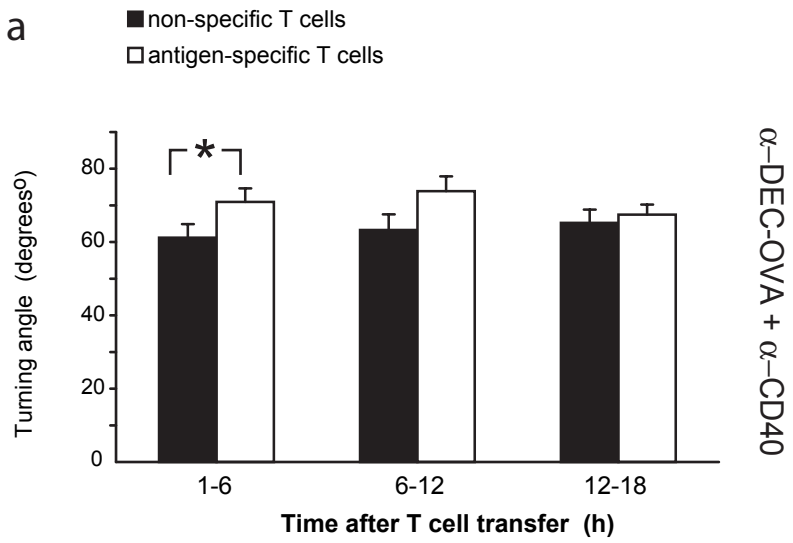
a
non-specific T cells
antigen-specific T cells
Turning angle (degrees°)
80
60
40
20
0
*
1-6
6-12
12-18
Time after T cell transfer (h)
α–DEC-OVA + α–CD40

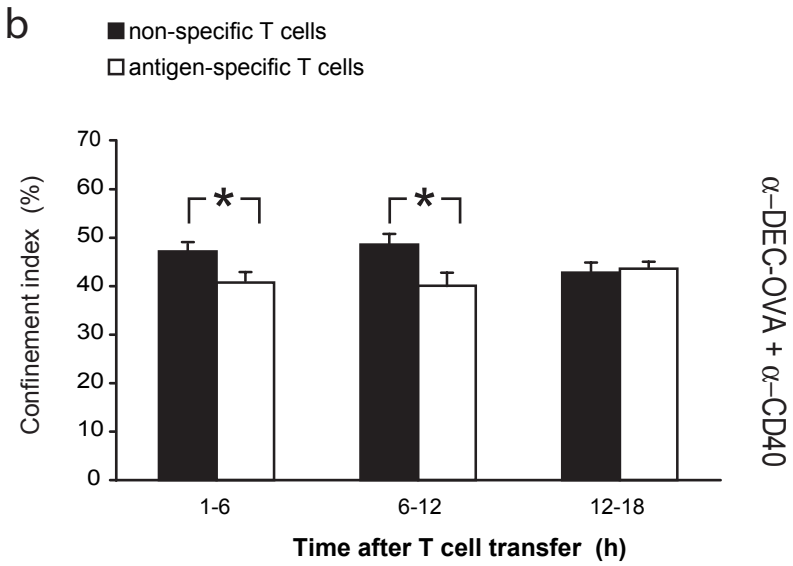
b
non-specific T cells
antigen-specific T cells
Confinement index (%)
70
60
50
40
30
20
10
0
*
*
1-6
6-12
12-18
Time after T cell transfer (h)
α–DEC-OVA + α–CD40

Figure 4.10: Speeds of antigen-specific cells normalized to speed of control cells in the same imaging field, under tolerizing and priming conditions. Cells were transferred, imaged, and tracked as above, and the median speed of the non-specific cells was determined for each imaging field; fields with fewer than three non-specific cells were excluded. Antigen-specific cell speeds were expressed as a percentage of the median non-specific speed in the same field. Results are similar to those obtained for mean cell velocity. Asterisks indicate significant differences; see text for p values.

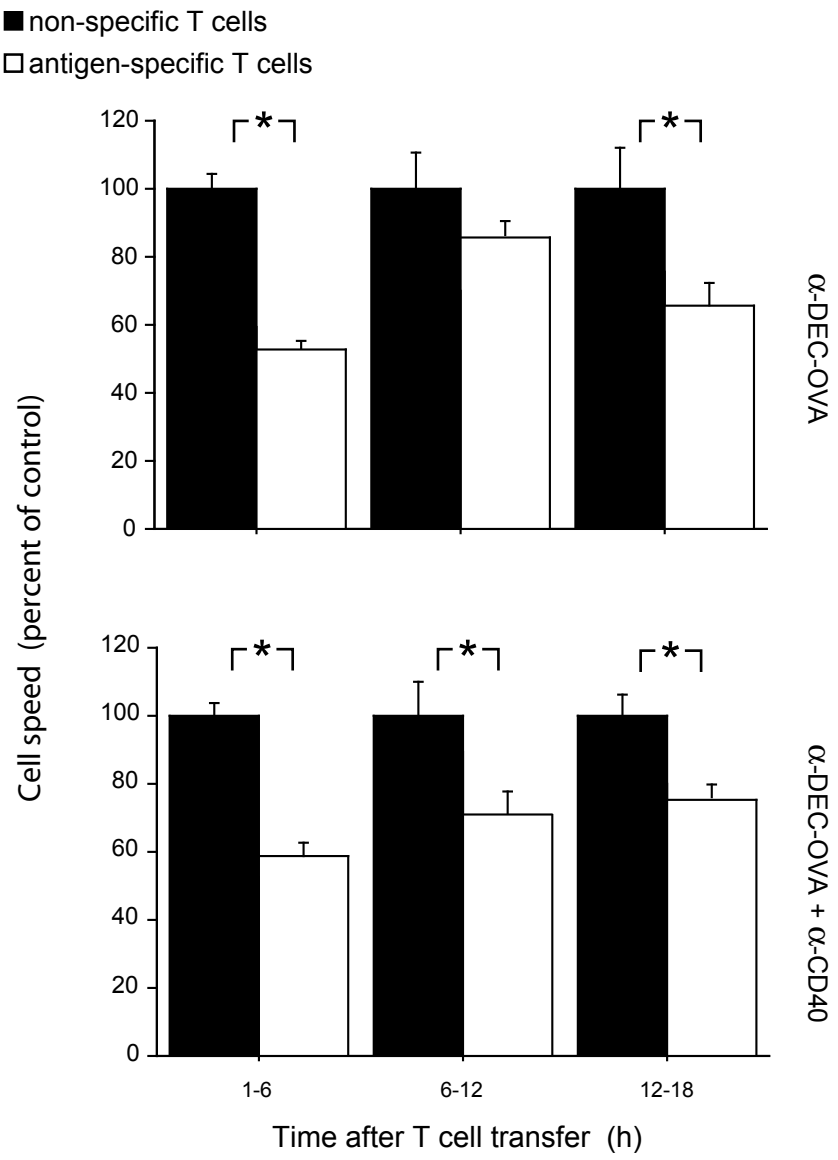
non-specific T cells
antigen-specific T cells
Cell speed (percent of control)
120
100
80
60
40
20
0
*
*
α-DEC-OVA
*
*
*
α-DEC-OVA + α-CD40
1-6
6-12
12-18
Time after T cell transfer (h)

CHAPTER 5. pMHC POTENCY IN DC:T CELL INTERACTIONS

Much evidence suggests that TCR affinity for MHC II:peptide complexes (pMHC) is significant in determining T cell fate in the periphery, not only during thymocyte selection. To determine the role of TCR affinity in T cell responses, we used the well-characterized moth cytochrome C system. Single point mutants of this peptide have been generated, which disrupt the interaction with the AND TCR but have no effect on binding to the I-E^k MHC II molecule (Kaye et al., 1989; Madrenas et al., 1995; Rogers et al., 1998). As described above for the Ovalbumin peptide, we cloned the MCC peptide and selected altered peptide ligands (APLs) into the C-terminus of an anti-Dec-205 antibody to target the peptide specifically to DCs. Mice were injected with Dec-APLs, CFP-expressing AND T cells and GFP-expressing nontransgenic T cells were transferred, and the resulting DC-T cell interactions were visualized by intravital microscopy.

pMHC potency correlates with activation and proliferation *in vitro*

Before performing any imaging studies, we first examined the effect of TCR affinity for pMHC on T cell functional responses *in vitro*. Naïve T cells from AND mice were cultured with irradiated DCs and graduated doses of soluble MCC or APL peptides; L98A was found to be 10 to 50-fold more potent than WT MCC, Y97K was 1000-fold less potent, and T102L showed no detectable response (**Figure 5.1**). To confirm that the APLs were targeted to DCs and presented, we injected mice with Dec-APLs, purified APCs, and assayed antigen presentation to T cells *in vitro*. DCs from targeted mice induced strong T cell proliferative responses, while B cells and $CD11c^-CD19^-$ cells from

these mice did not induce T cell proliferation (**Figure 5.2**); this indicates that the Dec-APLs are targeted to DCs and presented on I-E^k to T cells.

pMHC potency correlates with activation and proliferation *in vivo*

Before performing any imaging studies, we first examined the effect of TCR affinity for pMHC on T cell functional responses *in vivo*. We injected mice with Dec-APLs and measured T cell activation and proliferation. Injection of the isotype control antibody III/10-targeted Ova, unmodified α-Dec, or the irrelevant peptide α-Dec-Ova had no effect on T cell activation or proliferation, while injection of α-Dec-MCC and all the APLs induced upregulation of CD69 and downregulation of CD62L on AND T cells, but not on polyclonal control T cells (**Figure 5.3**). T cell proliferation *in vivo* at 3 days after transfer was similar to the *in vitro* proliferation measured above, with L98A yielding more proliferation than MCC, yielding more than Y97K; no proliferation was observed for T102L at day 3 (**Figure 5.3**). TCR affinity for pMHC therefore correlates well with T cell proliferation *in vivo*.

In contrast to tolerance induction in the ovalbumin/OTII system (Figure 16), AND T cells were not deleted by day 7 (**Figure 5.3**). We therefore isolated transferred T cells after 7 d of antigen exposure *in vivo* and rechallenged them *in vitro* with MCC and splenic DCs, to determine if the cells were anergized. At 7 days after challenge, all T cells from α-Dec-APL-treated mice were unresponsive to restimulation with MCC peptide; only T cells from mice treated with PBS or MCC plus CFA proliferated in response to antigen rechallenge (Figure 27).

To confirm that the anergy observed on day 7 persisted in response to *in vivo* rechallenge, we injected mice with α-Dec-APLs, PBS, or MCC plus CFA and rechallenged them on day 7 with MCC plus CFA. Only T cells from mice treated with PBS or MCC plus CFA proliferated in response to this *in vivo* rechallenge; T cells from mice treated with α-Dec-MCC or α-Dec-APLs did not proliferate or secrete IFN-γ (**Figure 5.4**). Summarizing, we found that high-potency ligands (L98A) induce CD69 activation, IFN-γ secretion, and proliferation, medium-potency ligands induce CD69 upregulation and low levels of proliferation and IFN-γ secretion, and low-potency ligands induce only CD69 upregulation. Even low-potency agonists unable of inducing T cell proliferation are capable of anergizing T cells; T cell anergy induction therefore does not require proliferation.

pMHC potency correlates with early antigen-specific T cell arrest

We next examined the effect of varying TCR affinity for pMHC on the *in vivo* dynamics of DC:T cell interactions in inguinal lymph nodes of living mice. To visualize dendritic cells, we used CD11c-EYFP mice as recipients, as above (Lindquist et al., 2004); antigen-specific AND T cells expressed ECFP, while non-transgenic control T cells expressed EGFP. We injected CD11c-EYFP mice with α-Dec-L98A, α-Dec-Y97K, α-Dec-T102L, or PBS and transferred T cells 5 h later; inguinal LNs were imaged intravitally from 0.5 to 6 h or 6-12 h after T cell transfer.

We observed that pMHC potency correlated with early T cell arrest in response to antigen. As observed for OT-II T cells in α-Dec-Ova-treated mice, T cells arrested antigen-specifically upon exposure to high-potency antigen (α-Dec-L98A), slowing to a

mean velocity less than half that of nontransgenic control T cells (**Figure 5.5; Movie 5.1**; $p < 0.001$). Treatment with medium- and low-potency APLs, however, had no detectable effect on T cell speed (**Figure 5.5; Movies 5.2, 5.3**). In addition to arresting, T cells from mice injected with α-Dec-L98A had significantly lower displacement rates and were confined in significantly smaller volumes than were nonspecific T cells (**Figure 5.5**; $p < 0.001$). Strikingly, no difference in any of the other movement parameters was observed for the medium and low-potency APLs α-Dec-Y97K and α-Dec-T102L (**Figure 5.5**), even though they had already begun to respond by upregulating CD69 and downregulating CD62L (**Figure 5.3**).

To determine if the medium- and low-potency antigens had any effect on T cell behavior at later time points, we also imaged inguinal LNs from mice injected with α-Dec-APLs at 6-12 h after T cell transfer. In mice injected with α-Dec-L98A, we found that antigen-specific T cells had recovered their mobility and moved with the same average velocity as control cells; other movement parameters were also no different than for control T cells (**Figure 5.5**). Interestingly, antigen-specific T cells from mice treated with medium and low-affinity α-Dec-Y97K and α-Dec-T102L remained unaffected by antigen exposure, moving indistinguishably from control T cells (**Figure 5.5**).

As it is known that activated T cells are sequestered in LNs for a short period after activation, we examined T cell trapping in LNs as a function of TCR affinity for pMHC. We injected mice with α-Dec-APLs, transferred equal numbers of AND and WT nontransgenic T cells, and examined the ratio of AND to WT T cells in blood at 24, 48, and 72 h post T cell transfer. We observed that all APLs induced significant trapping of AND T cells and not control cells for 48-72 h post injection, with the ratio of AND cells

to control cells returning to unity at 3 d for Y97K and T102L and by 4 d for L98A (**Figure 5.5**).

pMHC potency correlates with Ca^{2+} flux *in vitro*

It is known that TCR signaling rapidly leads to an increase in intracellular calcium (Negulescu et al., 1996), and it was recently shown that elevated intracellular Ca^{2+} is necessary and sufficient to stop thymocyte migration in explanted thymic slices (Bhakta et al., 2005). We therefore investigated the role of calcium signaling in pMHC-driven T cell arrest. We first performed *in vitro* studies, measuring the Ca^{2+} flux in preactivated T cell blasts in response to GPI-anchored I-E^k:MCC variants incorporated into lipid bilayers. Activated T cells moved rapidly and had a low basal Ca^{2+} concentration on bilayers incorporating only ICAM-1 or ICAM-1 plus irrelevant I-E^k-pMHC (**Figure 5.6; Movie 5.4**). Activated T cells on bilayers with I-E^k-L98A elicited a strong Ca^{2+} flux and had a significantly decreased mobility (**Movie 5.5**), while T cells on bilayers with the medium-affinity agonist I-E^k-Y98K exhibited only a minimal increase in Ca^{2+} over controls (**Movie 5.6**), and cells incubated with low-affinity I-E^k-T102L were indistinguishable from control cells in terms of Ca^{2+} flux or mobility (**Figure 5.6; Movie 5.7**).

To rule out the possibility that the lack of signaling induced by low-potency APLs was due to the absence of costimulatory molecules normally present on DCs but absent from the lipid bilayers, we measured Ca^{2+} flux in naïve T cells interacting with $CD11c^+$ DCs isolated from the LNs of α-Dec-APL targeted mice. Consistent with the results observed on lipid bilayers, only the high-affinity agonist L98A was able to induce

significant Ca^{2+} signaling (**Figure 5.7**). We therefore conclude that TCR affinity for pMHC is correlated with the extent of Ca^{2+} flux *in vitro* and with T cell stopping upon exposure to antigen.

pMHC potency correlates with Ca^{2+} flux *in vivo*

To determine if these conclusions held true *in vivo*, we labeled naïve AND T cells with the Ca^{2+}-sensitive dye Fluo-4-AM and visualized Ca^{2+} responses in inguinal LNs of living mice using confocal microscopy. To exclude any spurious Ca^{2+} flux, we included only cells that had clearly extravasated from HEVs. Additionally, we defined a "sustained" Ca^{2+} response as an increase 1.5 times over the average response in control T cells; on the basis of *in vitro* calibration, we estimate that an increase of 1.5-fold in fluorescence corresponds to 1.8-fold increase in intracellular Ca^{2+}, which is sufficient to cause T cell stopping *in vitro* (Negulescu et al., 1996).

In mice injected with irrelevant peptides, we observed that only 5% of AND T cells showed sustained Ca^{2+} increases, while injection of α-Dec-L98A led to a sustained Ca^{2+} flux in 30% of AND T cells (**Figure 5.8; Movies 5.8, 5.11**, $p < 0.0001$). In contrast, injection of α-Dec-Y97K or α-Dec-T102L both led to sustained Ca^{2+} flux in only 2% of AND T cells, not significantly different from the controls (**Figure 5.8; Movies 5.9, 5.10**). Additionally, the high-affinity ligand L98A induced higher levels of Ca^{2+} flux than did the medium and low-affinity ligands Y97K and T102L (**Figure 5.8**). Only α-Dec-L98A induced a significant decrease in T cell speed (as was observed in the T cell response to ovalbumin (**Figure 4.4**)), with α-Dec-Y97K and α-Dec-T102L having no effect. We

therefore conclude that *in vivo* Ca^{2+} flux is induced by high-potency pMHC ligands and leads to T cell arrest.

Figure 5.1. Differential activation of $CD4^+$ AND T cells by APLs. (**a,b**) Naive $CD4^+$ T cells from AND mice (3 x 10^5 / well) were cultured with irradiated DCs (3 x 10^4 / well) and varying doses of soluble peptides in triplicate. (**a**) Proliferation measured by (^{3}H) thymidine incorporation between 60 and 72 h with data representing the mean c.p.m. from triplicate cultures. (**b**) IFN-γ production measured by Elispot assay under the same conditions.

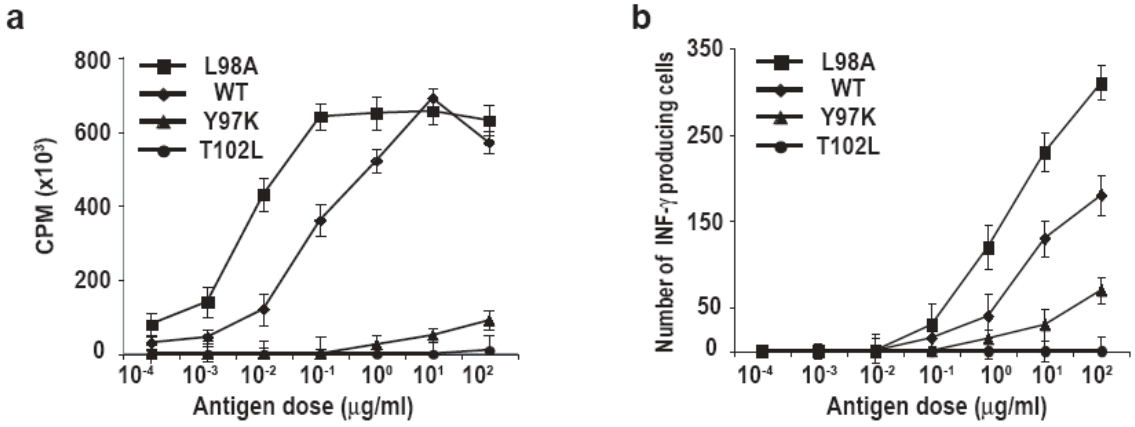
a
800
600
400
200
0
CPM (x10³)
L98A
WT
Y97K
T102L
10⁻⁴
10⁻³
10⁻²
10⁻¹
10⁰
10¹
10²
Antigen dose (μg/ml)
b
350
250
150
50
0
Number of INF-γ producing cells
L98A
WT
Y97K
T102L
10⁻⁴
10⁻³
10⁻²
10⁻¹
10⁰
10¹
10²
Antigen dose (μg/ml)

Figure 5.2. Anti-DEC delivers antigen to DCs *in vivo*. B10.BR wild type mice were injected subcutaneously in the footpads with 10 μg of α-DEC-MCC, α-DEC, Iso-MCC, α-DEC or PBS as indicated. $CD11c^+$, $CD19^+$, and $CD11c^-CD19^-$ cells were isolated from draining LNs 24 h after antibody injection and assayed for antigen processing and presentation to purified AND T cells *in vitro*. T cell proliferation was measured by (^3H) thymidine incorporation, and is expressed as a proliferation index relative to PBS control. The results are means of triplicate cultures from one of three similar experiments. Similar results were obtained using α-DEC-APLs.

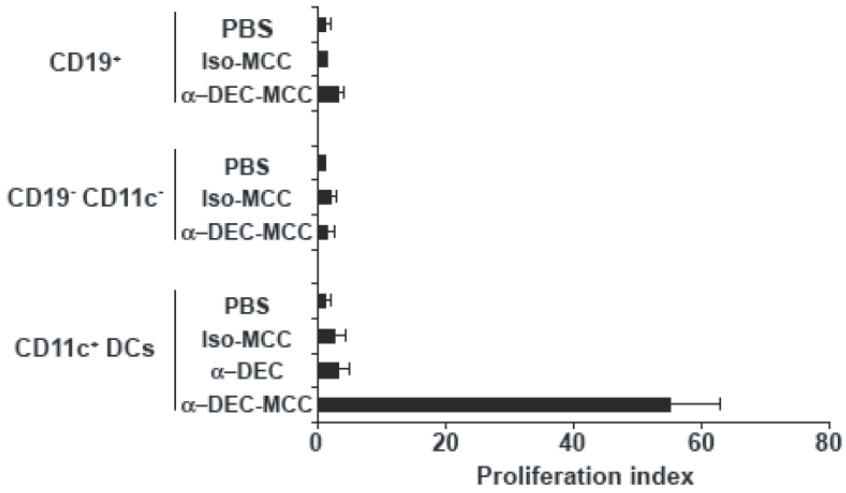
CD19+
PBS
Iso-MCC
α–DEC-MCC
CD19- CD11c-
PBS
Iso-MCC
α–DEC-MCC
CD11c+ DCs
PBS
Iso-MCC
α–DEC
α–DEC-MCC
0
20
40
60
80
Proliferation index

Figure 5.3. Activation of AND T cells in vivo by α-DEC-MCC and α-DEC-APL constructs. **(a)** Flow cytometry of CD69 and CD62L surface expression on AND transgenic T cells adoptively transferred into B10.BR mice 5 h after subcutaneous footpad injection of α-DEC-MCC and α-DEC-APL constructs, α-DEC-ovalbumin (α-DEC-OVA), isotype-MCC plus α-DEC-205 (α-DEC + iso-MCC) or PBS. Cells were gated on CD45.2 and Vα11Vβ3 and analyzed at 3 and 72 h after challenge. **(b,c)** Proliferation assay of AND T cells adoptively transferred into B10.BR mice 24 h after subcutaneous footpad injection of α-DEC-MCC, α-DEC-APL constructs (α-DEC + iso-MCC), α-DEC-OVA or PBS, assayed by CFSE dilution in gated populations of $CD4^+$ and $V\alpha11^+V\beta3^+$ T cells at 3 and 7 d after antibody injection. **(c)** Percent of $CD45.2^+V\alpha11^+V\beta3^+$ cells with low (Divided) or high (Undivided) fluorescence intensity of CFSE among $CD4^+$ T cells. Data are representative of three independent experiments.

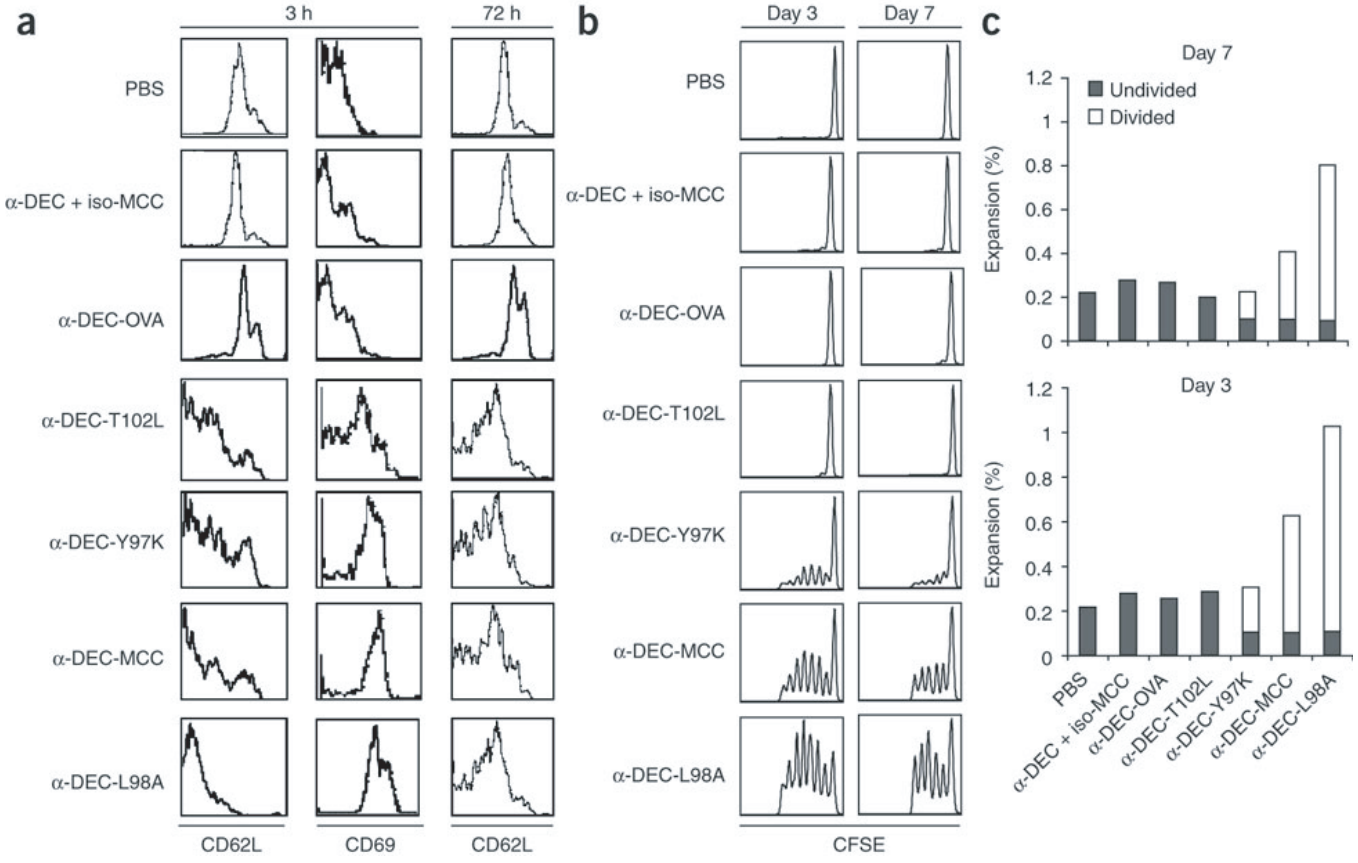
a
3 h
72 h
PBS
α-DEC + iso-MCC
α-DEC-OVA
α-DEC-T102L
α-DEC-Y97K
α-DEC-MCC
α-DEC-L98A
CD62L
CD69
CD62L
b
Day 3
Day 7
PBS
α-DEC + iso-MCC
α-DEC-OVA
α-DEC-T102L
α-DEC-Y97K
α-DEC-MCC
α-DEC-L98A
CFSE
c
Day 7
Undivided
Divided
Expansion (%)
1.2
1
0.8
0.6
0.4
0.2
0
Day 3
Expansion (%)
1.2
1
0.8
0.6
0.4
0.2
0
PBS
α-DEC + iso-MCC
α-DEC-OVA
α-DEC-T102L
α-DEC-Y97K
α-DEC-MCC
α-DEC-L98A

Figure 5.4. Proliferation is not required for the induction of T cell anergy in vivo. (a) TCR-transgenic mice were injected with 10 μg α-DEC-MCC or α-DEC-APL, 100 μg MCC in CFA, or PBS, followed by isolation and restimulation of cells with or without rechallenge of mice with MCC as described below. **(b–d)** CFSE dilution analysis of proliferation. **(b,c)** Analysis of CFSE-labeled $CD4^+$ cells isolated and restimulated with irradiated $CD11c^+$ DCs in the presence (CFA + MCC) or absence of MCC on day 3 **(b)** or day 7 **(c)** after the injection described in **a**. **(d)** Analysis of cells from mice systemically rechallenged with 100 μg MCC in CFA on day 7 after the injection described in a; 3 d later, $CD4^+$ cells were purified and restimulated as described in **b,c**. **(e–g)** Enzyme-linked immunospot assay of IFN-γ production. **(e,f)** Analysis of cells treated as described in **b,c** on day 3 **(e)** or day 7 **(f)** after antigen injection as described in **a**. **(g)** Analysis of cells from mice treated as described in **d**. Data are representative of three to four experiments.

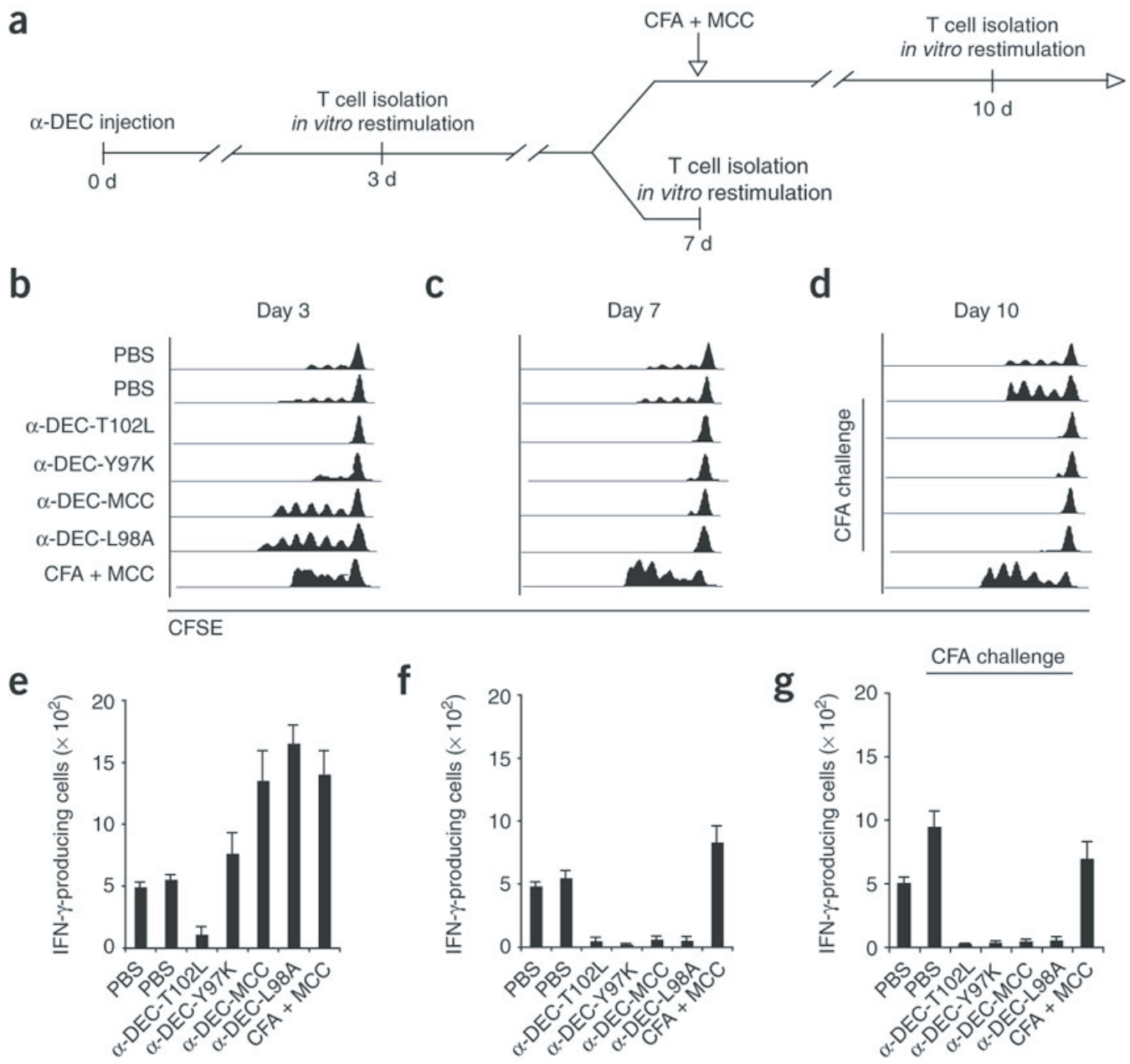
a
CFA + MCC
T cell isolation
in vitro restimulation
10 d
α-DEC injection
T cell isolation
in vitro restimulation
0 d
3 d
T cell isolation
in vitro restimulation
7 d
b
Day 3
c
Day 7
d
Day 10
PBS
PBS
α-DEC-T102L
α-DEC-Y97K
α-DEC-MCC
α-DEC-L98A
CFA + MCC
CFA challenge
CFSE
e
f
g
CFA challenge
IFN-γ-producing cells (× 10²)
0
5
10
15
20
PBS
PBS
α-DEC-T102L
α-DEC-Y97K
α-DEC-MCC
α-DEC-L98A
CFA + MCC

Figure 5.5. Potency of the pMHC complex drives early T cell deceleration. Analysis of ECFP$^+$ AND TCR-transgenic T cells (AND-CFP) or EGFP$^+$ B10.BR CD4$^+$ T cells (WT-GFP) adoptively transferred into CD11c-EYFP mice 5 h after injection with α-DEC-APL constructs or with PBS. **(a,b)** Tracks of antigen-specific and nonspecific T cells after immunization with APLs, at 1–6 h **(a)** or 6–12 h **(b)**. Axes represent 200 μm; the tracking time was 20 min. Each graph represents cells tracked at the same imaging field in one representative experiment. **(c,d)** Speeds of antigen-specific cells (filled circles) and nonspecific cells (open circles) in the lymph nodes of mice exposed to various APLs (horizontal axis). Speeds were measured along the entire cell tracks and are normalized to the average speed of nonspecific cells moving in the same field during 1–6 h **(c)** or 6–12 h **(d)**. Only the high-potency peptide L98A during the first 6 h significantly slows the antigen-specific cells ($p < 0.001$). Small horizontal bars indicate means. **(e)** Displacement rate of antigen-specific cells (filled bars) and nonspecific cells (open bars) during hours 1–6 of treatment with antigen (horizontal axes); error bar represents s.e.m.). **(f)** Confinement index of antigen specific cells (filled bars) and nonspecific cells (open bars) imaged during hours 1–6 of treatment with antigen (horizontal axes); error bar represents s.e.m.). **(g,h)** Displacement rate **(g)** and confinement index **(h)** analyzed as described above for cells during hours 6–12 of treatment with antigen. Only the high-potency peptide L98A during the first 1–6 h significantly slows the antigen-specific cells and confines them to a smaller volume (*, $P < 0.001$). Data are representative of a minimum of three to four independent experiments per condition. **(i)** Retention of activated T cells *in vivo*. Flow cytometry of surface expression of CD69 by a mixture of CFSE-labeled AND TCR-transgenic and CMRA-labeled B10.BR CD4$^+$ T cells adoptively transferred into B10.BR mice 5 h after injection with α-DEC-APLs, left panel; the ratio of AND to wild-type (WT) T cells was measured in blood collected 24, 48, 72 and 96 h later, right panel. Data are representative of a minimum of three independent experiments

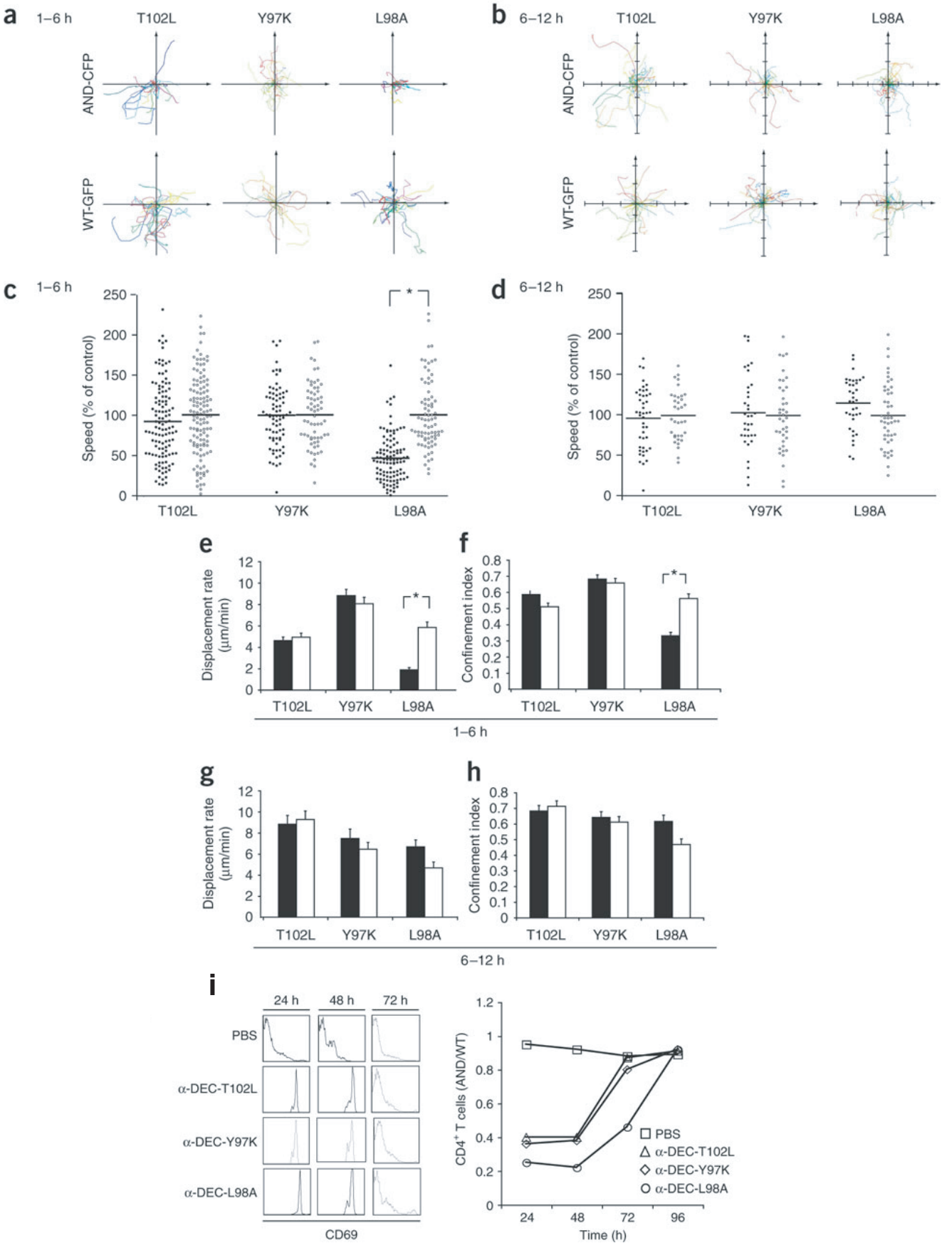
a
1–6 h
T102L
Y97K
L98A
AND-CFP
WT-GFP
b
6–12 h
T102L
Y97K
L98A
AND-CFP
WT-GFP
c
1–6 h
Speed (% of control)
250
200
150
100
50
0
*
T102L
Y97K
L98A
d
6–12 h
Speed (% of control)
250
200
150
100
50
0
T102L
Y97K
L98A
e
Displacement rate (μm/min)
12
10
8
6
4
2
0
*
T102L
Y97K
L98A
f
Confinement index
0.8
0.7
0.6
0.5
0.4
0.3
0.2
0.1
0
*
T102L
Y97K
L98A
1–6 h
g
Displacement rate (μm/min)
12
10
8
6
4
2
0
T102L
Y97K
L98A
h
Confinement index
0.8
0.7
0.6
0.5
0.4
0.3
0.2
0.1
0
T102L
Y97K
L98A
6–12 h
i
24 h
48 h
72 h
PBS
α-DEC-T102L
α-DEC-Y97K
α-DEC-L98A
CD69
CD4+ T cells (AND/WT)
1.2
1
0.8
0.6
0.4
0.2
0
PBS
α-DEC-T102L
α-DEC-Y97K
α-DEC-L98A
24
48
72
96
Time (h)

5.6 pMHC potency drives Ca^{2+} flux and arrest *in vitro* in T cell blasts. Calcium flux in Fura-2-loaded, *in vitro*–activated AND T cell blasts on bilayers containing L98A-I-E^K (red), Y97K-I-E^K (blue), T102L-I-E^K (green) or no peptide-I-E^K (black), at a density of 10 pMHC molecules per μm^2, and glycosylphosphatidylinositol–ICAM-1 (300 molecules per μm^2). The Fura-2 ratio (emission with 340 nm excitation/emission with 380 nm excitation (340/380)) was determined every 15 s after contact initiation; at the end of each measurement, the ratio in response to ionomycin plus 10 mM $CaCl_2$ (line at ratio = 1.7) and EGTA buffer containing 2 mM $MgCl_2$ and 0 mM $CaCl_2$ (line at ratio = 0.24) was determined to obtain the upper and lower limits of Ca^{2+} measurement. **(a)** Single cell traces. **(b)** Average responses. Each trace represents an average of 10–30 cells per group, with the zero time point defined by time of contact determined by interference reflection microscopy. **(c)** Speeds of the cells in **a** on the bilayer, calculated as total track length divided by time of cell in the field. Each point represents the normalized mean speed of a single cell; small horizontal bars indicate means for the entire cell population.

a

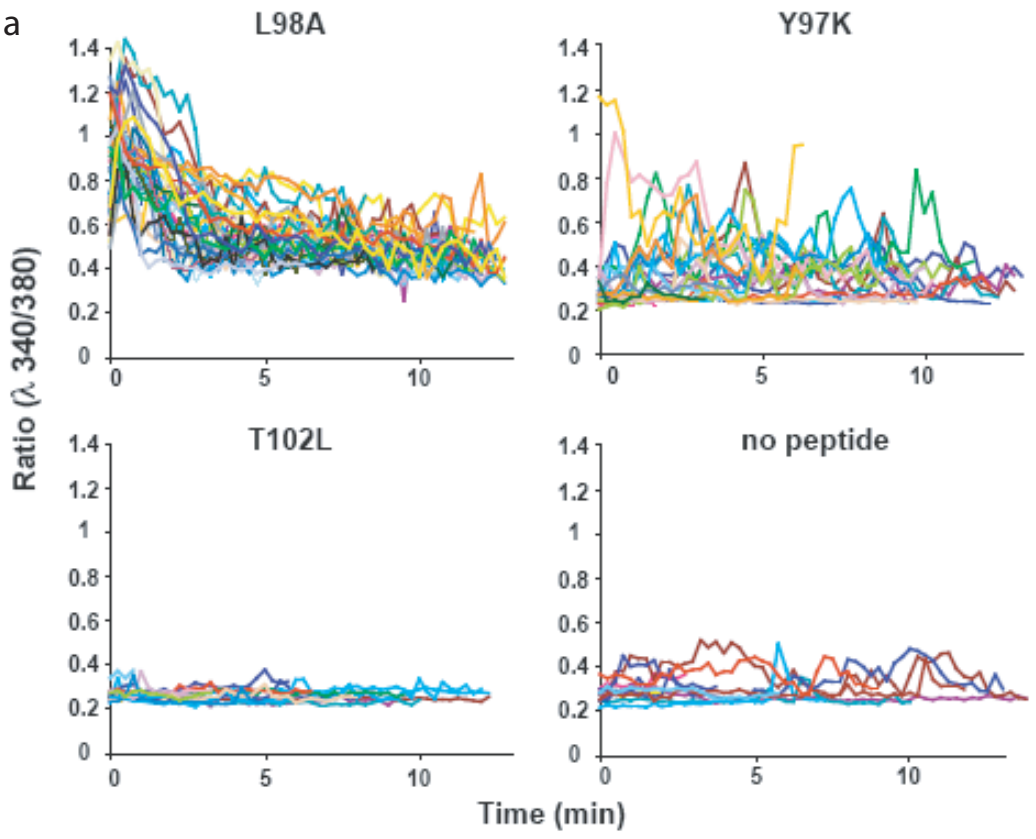
L98A
Y97K
T102L
no peptide
Ratio (λ 340/380)
Time (min)

b

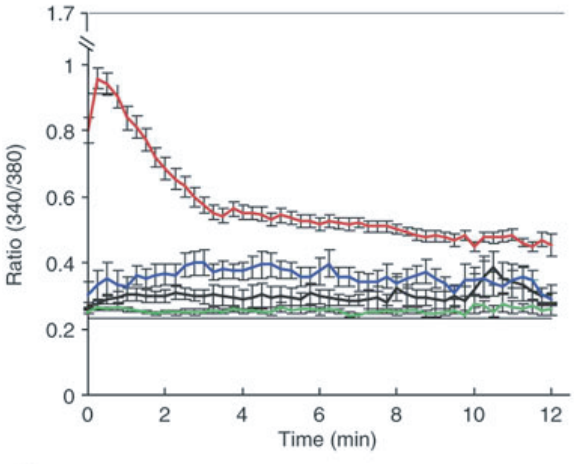
Ratio (340/380)
Time (min)

c

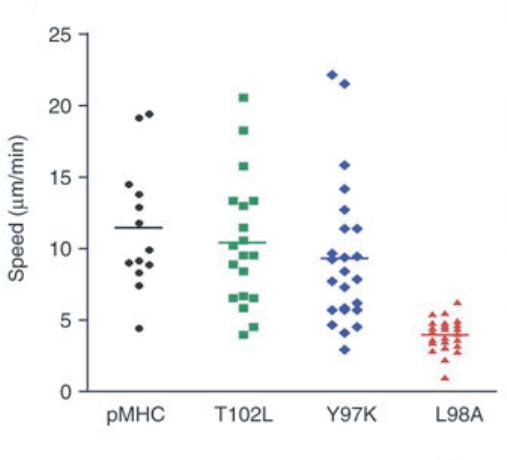
Speed (µm/min)
pMHC
T102L
Y97K
L98A

Figure 5.7. pMHC potency drives Ca^{2+} flux and arrest *in vitro* in naïve T cells. (a) Single cell Ca^{2+} flux in naïve T cells. $CD11c^{+}$ DCs were purified from lymph nodes and loaded with 100 μM of L98A, Y97K, T102L or no peptide for 2 hours at 37 °C. Fura-2 labeled naive AND T cells were incubated with peptide-loaded DCs and the Fura-2 ratio was determined as above. Shown are single cell Fura-2 ratios over the time course of imaging for the different peptides. **(b)** Ca^{2+} flux and formation of T:DC conjugates. $CD11c^{+}$ DCs were purified from lymph nodes and loaded with APLs as above, then incubated with Fura-2-labeled naive AND T cells. Figure represents percent of T cells with a high cytoplasmic Ca^{2+} concentration forming conjugates with DCs; high Ca^{2+} was defined as Fura-2 ratios above the mean ratio observed for no peptide. Numbers above bars indicate total conjugates counted.

a

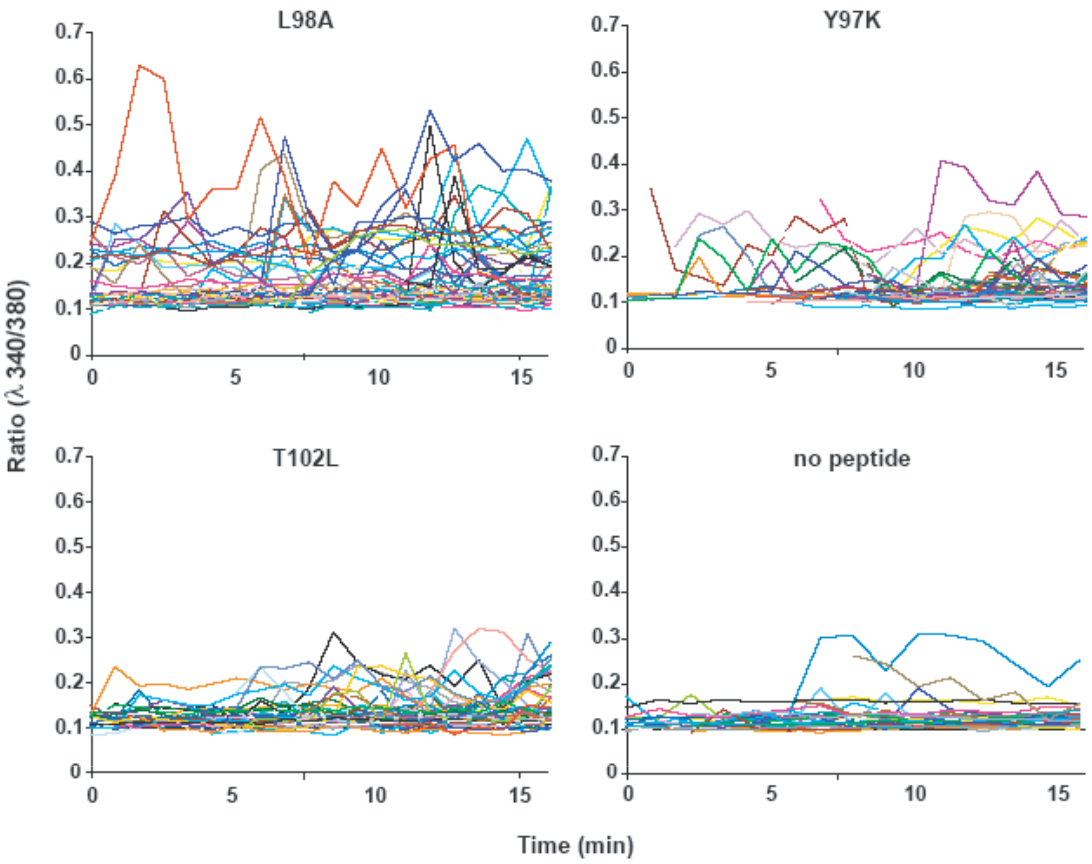
L98A
Y97K
T102L
no peptide
Ratio (λ 340/380)
Time (min)
0
5
10
15
0.1
0.2
0.3
0.4
0.5
0.6
0.7

b

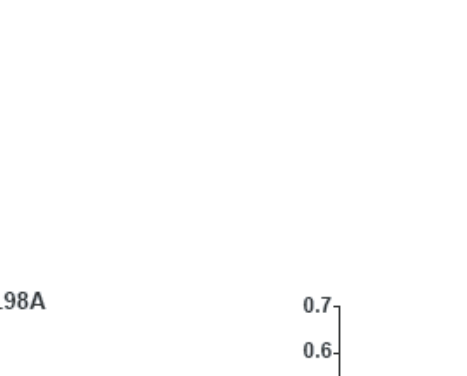
Conjugates with high Ca2+ (%)
0
10
20
30
40
50
256
370
241
384
PBS
T102L
Y97K
L98A

Figure 5.8. pMHC potency drives Ca^{2+} flux and T cell arrest *in vivo*. AND T cells, labeled with Fluo-4 calcium sensitive dye and CMRA, were adoptively transferred (15 x 10^6/mouse) into B10BR mice injected 5 h earlier with α-DEC-APLs. Calcium signaling in the inguinal lymph node was imaged *in vivo* for 2 h. **(a)** Twenty images taken at 30 seconds per frame were collapsed into one to show the path and calcium level of each cell over time. Calcium level is pseudo-colored from cool to warm colors corresponding to low to high Fluo-4 fluorescence (shown here normalized to CMRA fluorescence), see color chart. **(b)** Number of T cells with elevated Ca^{2+} level in mice treated with α-DEC-APLs relative to that in control mice treated with isotype control antibody. Asterisk indicates $p < 0.0001$. **(c)** Fluo-4-AM intensity of AND T cells in mice treated with α-DEC-L98A (red line), α-DEC-Y97K (blue line), α-DEC-T102L (green line) or isotype control antibody (black line), presented as cumulative data points. **(d)** Speed of AND T cells in the lymph nodes of mice treated with α-DEC-APLs, measured along the entire cell track and normalized to the average speed of AND T cells in mice treated with isotype control antibody (Control). Each point represents one cell track; small horizontal bars indicate means. Asterisk indicates $p < 0.0004$.

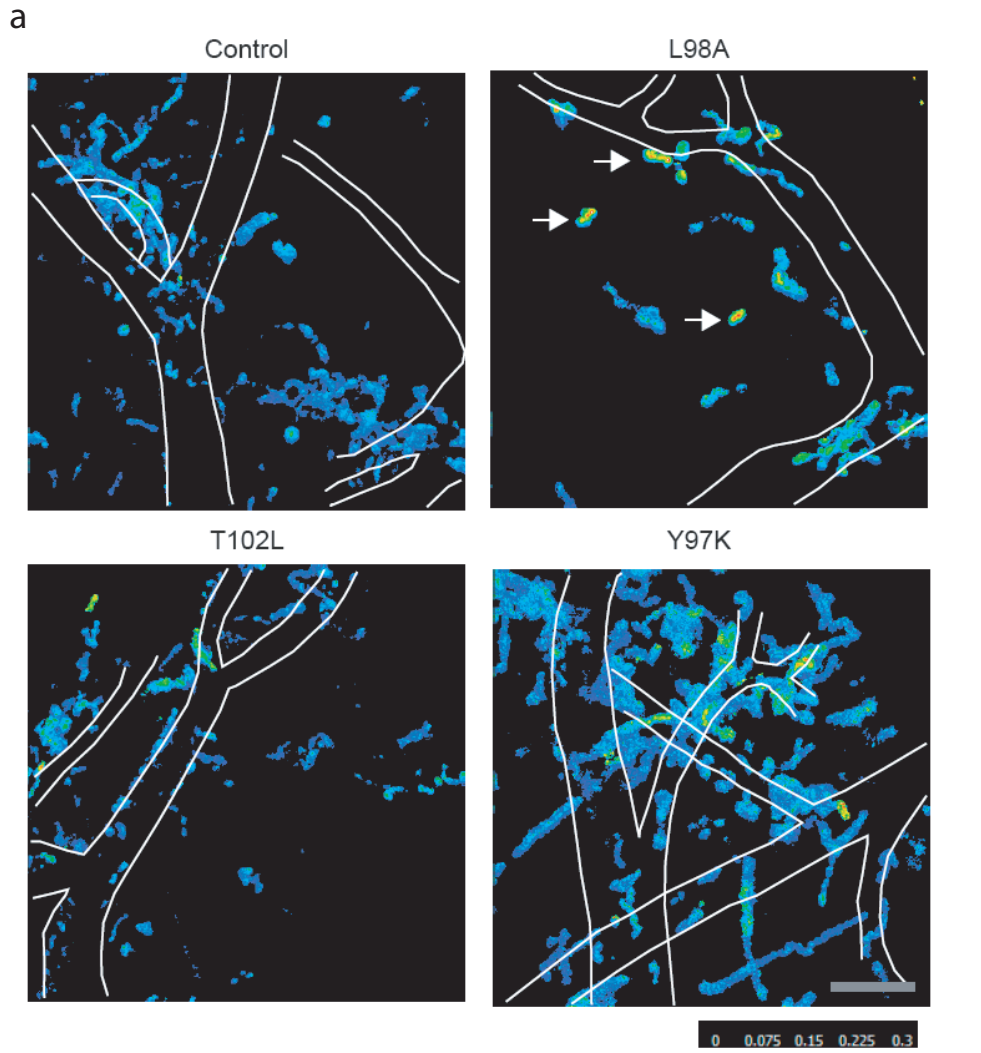
a
Control
L98A
T102L
Y97K
0 0.075 0.15 0.225 0.3

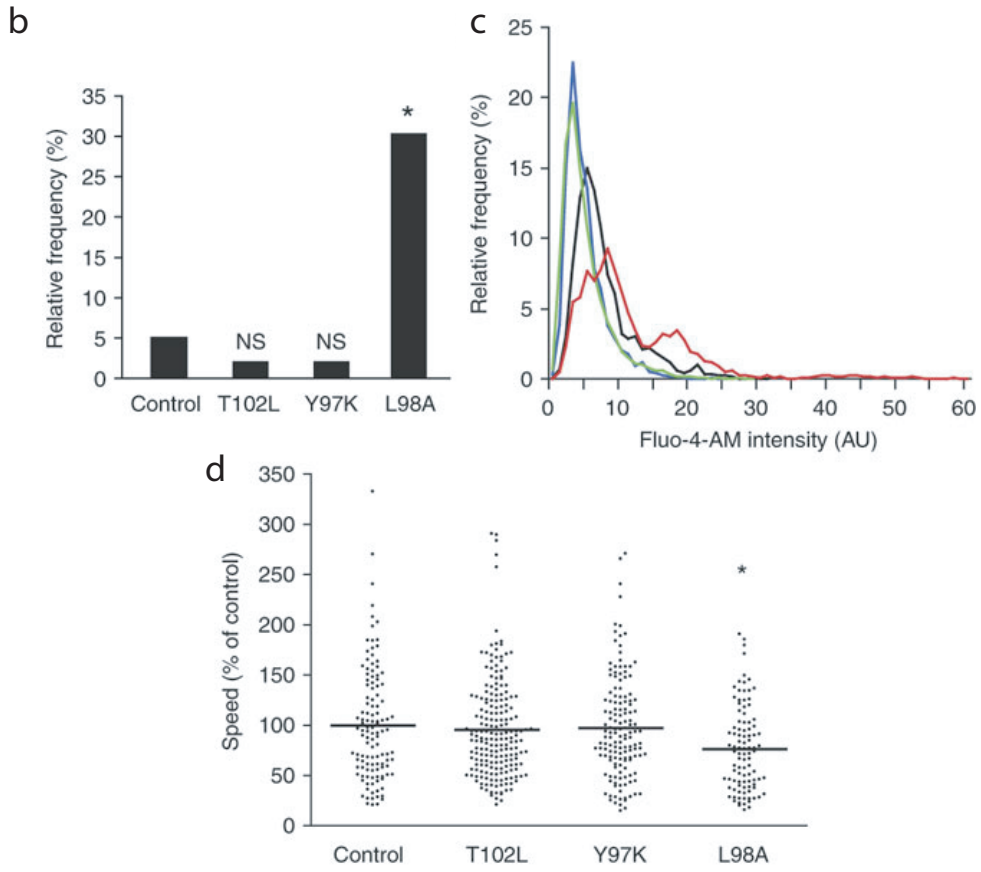
b
Relative frequency (%)
35
30
25
20
15
10
5
0
*
NS
NS
Control T102L Y97K L98A
c
Relative frequency (%)
25
20
15
10
5
0
0 10 20 30 40 50 60
Fluo-4-AM intensity (AU)
d
Speed (% of control)
350
300
250
200
150
100
50
0
*
Control T102L Y97K L98A

CHAPTER 6. IMAGING GERMINAL CENTER REACTIONS

Humoral immunity is mediated by antibodies secreted from B cells. After being released into the periphery, B cells can undergo secondary, antigen-dependent genetic changes in specialized lymphoid structures called germinal centers (Jacob et al., 1991a; Jacob et al., 1991b). Germinal center B cells (Fas^+ $GL7^+$) proliferate rapidly, with cell cycle durations of 6-8 hours (MacLennan, 1994); as the cells proliferate, they express high levels of AID, which deaminates the genes coding for the B cell receptor, introducing somatic mutations (Di Noia and Neuberger, 2002; Ramiro et al., 2003). B cells with newly mutated antigen receptors then compete with unmutated B cells and other newly mutated B cells for antigen, on the basis of their B cell receptor's affinity for the antigen. High-affinity cells outcompete lower-affinity cells, with the higher affinity cells continuing to proliferate, and the low-affinity cells dying by apoptosis.

However, none of this had been directly observed in living germinal centers – all of the previous studies used fixed sections. We thus decided to investigate the cellular dynamics of germinal center reactions using the same microscopy techniques we had previously established. Transgenic mice with antigen-specific B cells had previously been generated in the lab(Shih et al., 2002a; Shih et al., 2002b); in conjunction with κ light chain, their B cells bind to nitrophenol (NP) antigen. These B1-8^{hi} mice were bred to mice that expressed GFP ubiquitously. We transferred GFP-expressing NP-specific B cells into mice previously primed with ovalbumin, boosted the mice with NP-conjugated ovalbumin, and imaged germinal centers six days later; this transfer protocol yielded an average frequency of 0.2% NP-specific B cells in the mouse (**Figure 6.1**). FACS and

histology indicated that GC B cells (Fas^+GL7^+) were formed by day 3, and GCs were organized into dark and light zones by day 6 (**Figure 6.2**). As internal controls, nontransgenic CFP-expressing B cells were transferred 24 h prior to imaging; we visualized follicular dendritic cells by s.c. injection of a fluorescently-labeled anti-FDC-M1 antibody (**Figure 6.3**)(Kosco et al., 1992; Szakal et al., 1988). The FDC-M1 antibody largely labels follicular dendritic cells, but also reacts with $CD68^+$ tingible body macrophages; tingible body macrophages can be readily distinguished from FDCs by their large cell bodies and lack of processes (**Figure 6.3**). Inguinal LNs were imaged as above in our previous studies of DCs and T cells, but at shallower depths, since B cell follicles and GCs are more superficial than the T cell areas.

Our first observations of germinal centers revealed that GC B cells moved vigorously throughout the GC, as did nontransgenic control B cells (**Movie 6.1**). Outside the B cell follicle, we observed sessile, round cells; histologic examination indicates that these are plasma cells in the LN medulla (**Movie 6.1**). However, when every cell in the GC expressed GFP, the cells were too densely packed to follow and track individually. Therefore, we transferred a mixed population of GFP^+ and GFP^- B1-8^{hi} B cells; the best results were obtained with approximately 10-15% of the B1-8^{hi} cells expressing GFP – individual cells were easily distinguished and followed, and large numbers of cells were seen in each GC (**Movie 6.2**).

GCs are open structures in which antigen-specific B cells are retained

In the absence of antigen, we observed that both B1-8^{hi} and nontransgenic B cells moved throughout the B cell follicle and the light zone of the GC, while being largely

excluded from the dark zone (**Figure 6.4; Movie 6.3**). There was no significant difference in between the movement of control and transgenic B cells in any of the analyzed motility parameters: average velocity, displacement rate, confinement index, turning angle, arrest coefficient, maximum pause duration, or motility coefficient (**Figure 6.4**). In the absence of specific antigen, both transgenic B1-8^{hi} and nontransgenic B cells move with a mean velocity of ~8 μm/min, about 80% as rapidly as naïve T cells (typically ~10 μm/min) through both the FDC-rich light zone and the rest of the B cell follicle.

After boosting with NP-Ova, we observed that B1-8^{hi} GC B cells are largely restricted to the GC area defined by the FDC, while the size and behavior of nontransgenic B cells was unchanged (**Figure 6.4; Movie 6.2**). The NP-specific GC B cells were visibly larger than nontransgenic cells, with a two-fold increased volume; they moved more slowly, with less directionality and longer maximum pause durations (**Figure 6.4**). The motility coefficient – a measure of the volume scanned, analogous to a particle's diffusion coefficient – was reduced from 30 μm^2/min to 13 μm^2/min in the presence of specific antigen, indicating that NP-specific GC B cells are confined to a smaller volume than nontransgenic B cells or B1-8^{hi} cells in the absence of antigen. To ensure that our FDC-M1 antibody was not interfering with antigen binding by FDCs, we imaged in the absence of FDC-M1 labeling and saw no differences in any movement parameter (**Movie 6.4**).

There is no net B cell migration between GC light and dark zones

We next examined B cell migration within and between GC light zone and dark zones. The net displacement vector for B1-8^{hi} and nontransgenic B cells was less than a cell diameter after 30 min of observation, indicating that there is no significant directional bias to B cell migration. We observed that 8% of the dark zone GC B cells migrated to the LZ and 5% of light zone GC B cells migrated to the dark zone after 30 min; once corrected for the increased B cell density of the dark zone, there is no significant difference (**Figure 6.5**). This rate of inter-zone movement implies complete exchange between GC dark and light zones within 18 h, consistent with a model of GC selection that involves multiple rounds of cycling between light and dark zones.

GC B cells decelerate upon making antigen-specific contacts but do not arrest

To characterize the interactions between FDCs and B cells, contacts between FDC-M1^{+} cells and B1-8^{hi} GC B cells or nontransgenic B cells were measured by hand. On average, 30% of control B cells contacted an FDC-M1^{+} cell in each 30 min observation period; their contacts were significantly shorter than those of the B1-8^{hi} B cells (2.3 v. 3.5 min, $p < 0.001$; **Figure 6.6; Movies 6.5, 6.6**). In addition, GC B cells in contact with FDC-M1^{+} cells moved more slowly than cells not in contact with FDC-M1^{+} cells (5.6 μm/min v. 7 μm/min; **Figure 6.6**), but did not arrest. Antigen-specific GC B cells were more associated with FDCs than were control nontransgenic B cells, which seemed almost to ignore FDCs (**Movies 6.5, 6.6**).

B cells compete on the basis of affinity for antigen to join ongoing GC reactions

The fact that nontransgenic, polyclonal B cells were found within NP-boosted GCs, and that transgenic NP-specific B cells were found in Ovalbumin GCs indicates that naïve B cells are not excluded from GCs on the basis of antigenic specificity. This shows that the germinal center is an open structure, with no physical barrier preventing naïve or recirculating B cells from entering. We investigated whether B cells could join an ongoing GC reaction by transferring B1-8^{hi} GC B cells 6 or 9 days after boosting, and found that they successfully joined GCs and participated in the GC reaction (**Figure 6.7**). To examine the role of affinity in germinal-center joining, we took advantage of the B1-8^{lo} mouse, a heavy-chain knock-in with 40-fold lower affinity for NP. We transferred B1-8^{hi} B cells into WT mice, B1-8^{lo} mice, and B1-8^{hi} mice immunized with Ovalbumin and boosted with NP-Ova six days prior to transfer (**Figure 6.7**). We found that B1-8^{hi} cells efficiently joined GCs in WT (19/21) and in B1-8^{lo} mice (25/25), but not in B1-8^{hi} mice (0/18), indicating that B cells can join pre-existing GC reactions when they have an advantage in antigen-binding affinity (**Figure 6.7**). GC reactions are therefore continually scanned, with continuous competition on the basis of affinity; the implications of this with regard to B cell memory and epitope spreading are discussed in the next chapter.

Figure 6.1. Transferred B cell frequency and oligoclonal generation of GCs. (a) Flow cytometric analysis of splenocytes. 2 x10^6 B1-8^{hi}, λ^+, GFP^+ B cells, were transferred into B6.SJL immunized with Ova in alum. B cell chimerism was assed by FACS after gating on $CD19^+$ cells. Upper panel shows histogram of GFP expression. Numbers indicate percentage of total $CD19^+$ cells which are also GFP^+. Lower panel shows dot plot of GFP versus Igλ expression after gating on all $CD19^+$ cells. GFP^+ cells were Igλ expressing. Numbers indicate percentage of total $CD19^+$ cells. **(b)** Oligoclonal generation of GCs. A mixture of B1-8^{hi} B6.SJL and B1-8^{hi}, GFP^+ B6.SJL B cells (9:1 mixture, 2 x 10^7 total $CD43^-$ B cells) were transferred into OVA/alum-primed B6 hosts. Boosting was carried out by s.c. injection of NP-OVA. Lymph nodes were harvested 6 days after the boost. FACS histogram gated on $CD45.1^+$ transferred cells reveals that 10% of the transferred cells were GFP^+ cells. **(c)** Lymph node section (GFP (green), CD45.1 (red), B220 (blue)) showing GC composition. **(d)** Zoom on single GC representative for difference in GFP^+ B cells density. All transferred B cells are stained with CD45.1 (red) and GFP^+ fraction is displayed in green. When 10% of the antigen specific B cells were GFP labeled B cells, the percentage of GFP^+ B cells in GC varied and 2 out of 39 GC (5 %) did not contain any GFP^+ B cell. When a higher percentage of GFP^+ B cells were transferred, all GC contained GFP^+ B cells (data not shown). With lower percentages of labeled B cells we did not reliably see labeled cells in GCs. We conclude that under these conditions GC are established out of about 10 clones.

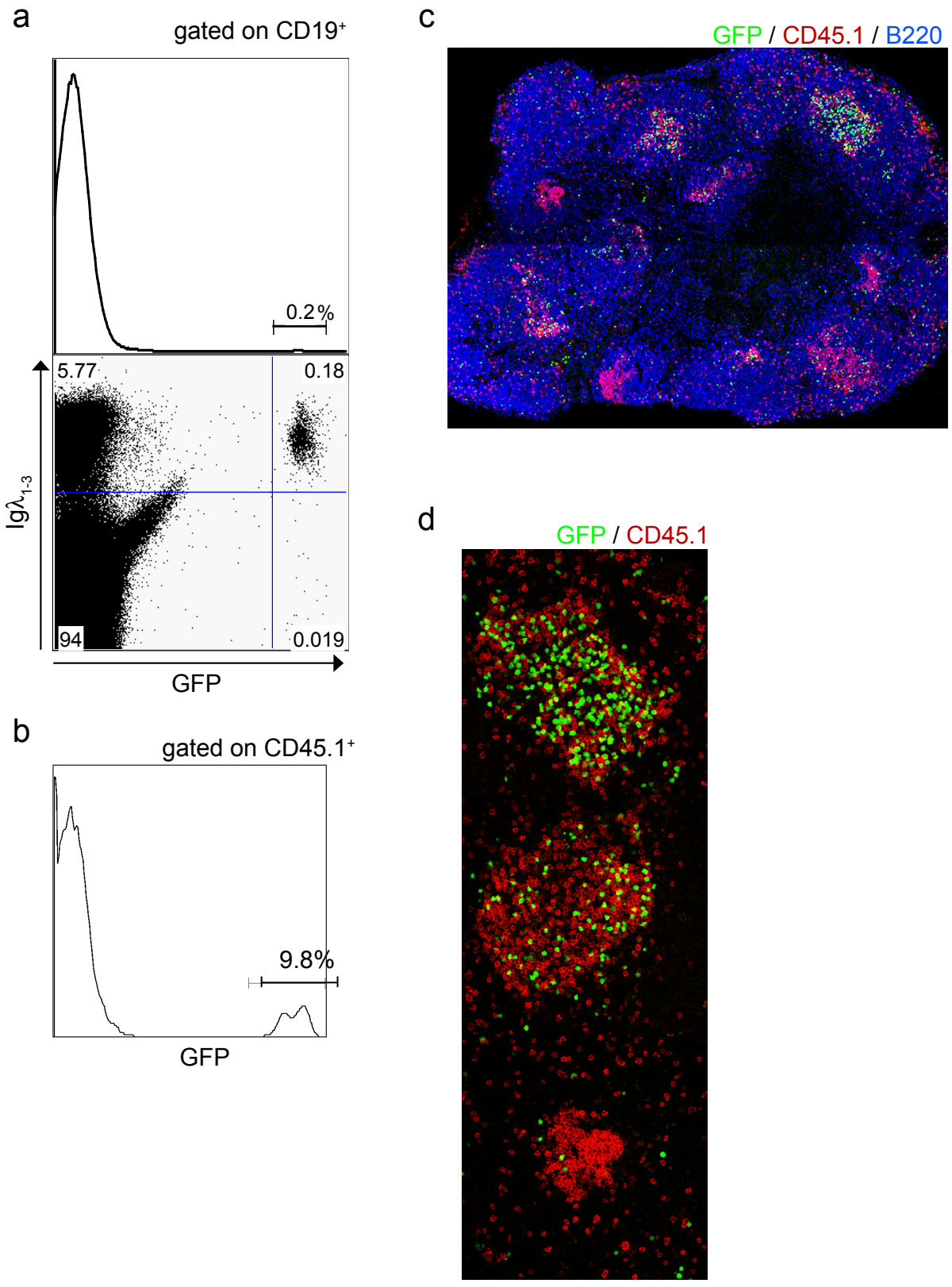
a
gated on CD19+
0.2%
5.77
0.18
94
0.019
Igλ1-3
GFP
b
gated on CD45.1+
9.8%
GFP
c
GFP / CD45.1 / B220
d
GFP / CD45.1

Figure 6.2. Flow cytometric and histological analysis of NP/B1-8^{hi} GC kinetics. (a) Flow cytometric analysis. B1-8^{hi} B6.SJL B cells were transferred into OVA/alum-primed B6 hosts. Boosting was carried out by s.c. injection of NP-OVA. Draining lymph nodes were harvested 0, 3, 6, 10, 14, 18 days after boosting. FACS profiles were gated on CD45.1 and B220 expressing live lymphocytes. Numbers in the upper right corner indicate the percentage of Fas^{+} and GL7^{+} gated cells. GL7^{+} and Fas^{+} cells developed by day 3 and were detectable up to 18 days after boosting. **(b)** Flow cytometric analysis. B1-8^{hi} B6.SJL B cells were transferred into OVA/alum-primed B6 hosts. Boosting was carried out by s.c. injection of NP-OVA. Popliteal lymph nodes were harvested 4, 6, 10, 14, and 18 days after the boost. Histological sections were stained with CD45.1 (green), IgD (blue), PNA (red). Transferred cells developed into PNA^{+} B cells and were visible in clusters as early as day 4 after boosting. After 6 days GC organized in DZ and LZ and were detected up to 18 days after boost

a

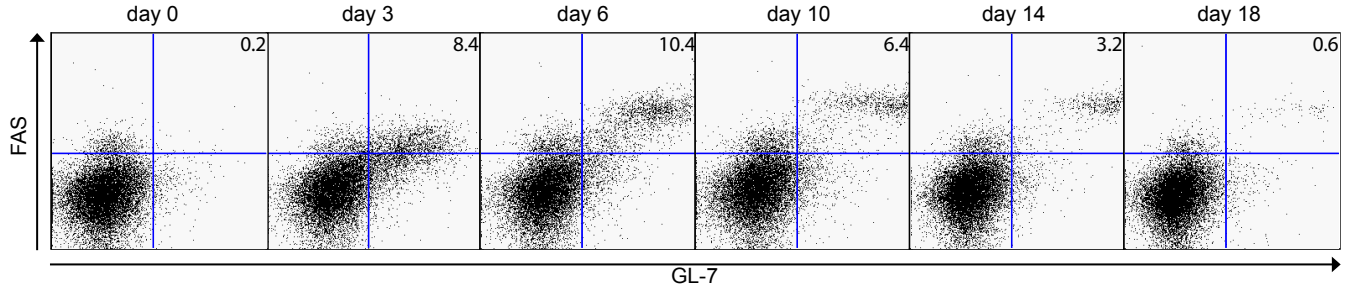
day 0
day 3
day 6
day 10
day 14
day 18
0.2
8.4
10.4
6.4
3.2
0.6
FAS
GL-7

b

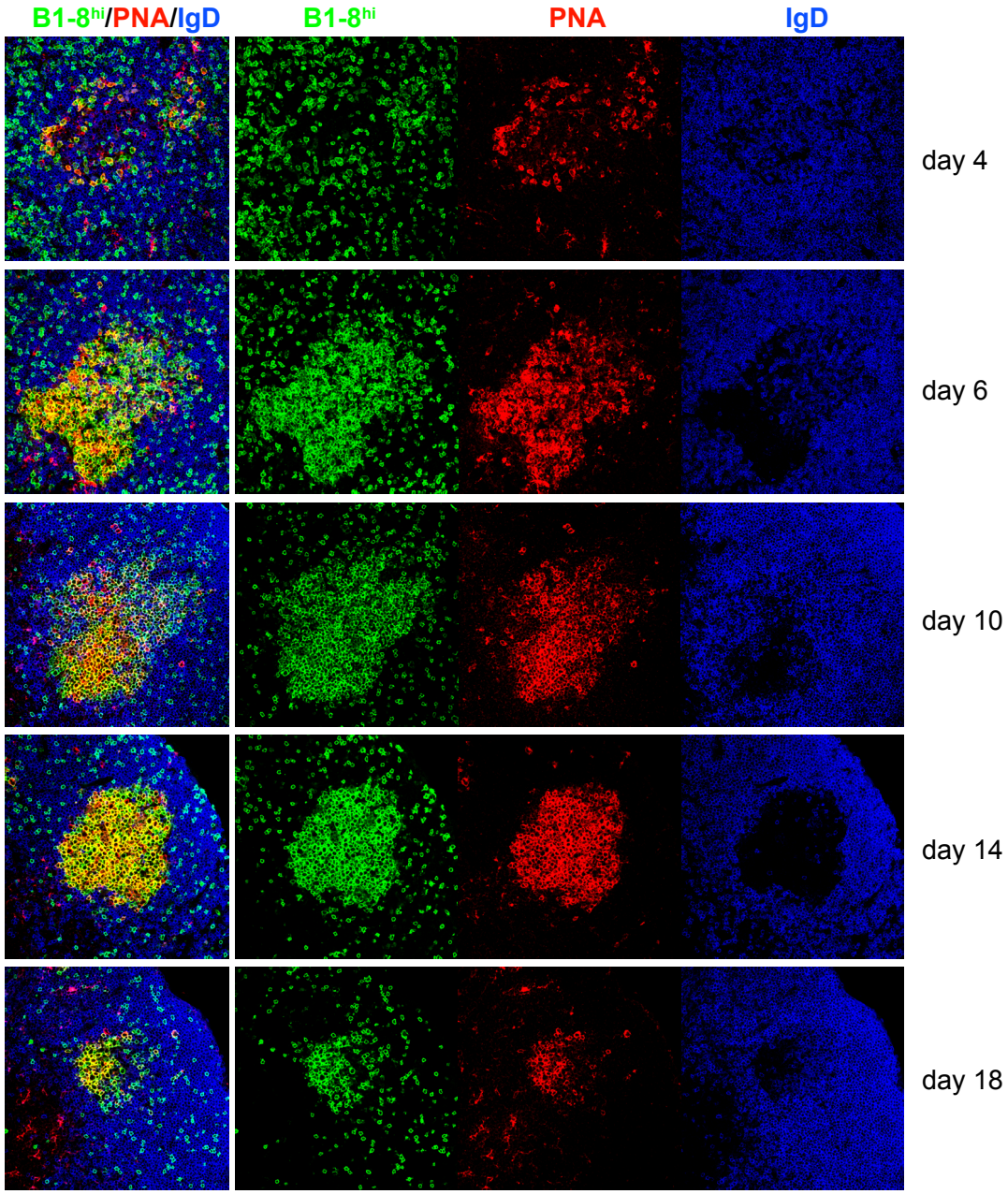
B1-8hi/PNA/IgD
B1-8hi
PNA
IgD
day 4
day 6
day 10
day 14
day 18

Figure 6.3. FDC-M1 *in vivo* staining. For *in vivo* labeling (**a**-**d**) of FDCs, FDC-M1 antibody or rat IgG2b was injected s.c.. Inguinal and popliteal lymph nodes were harvested 16 hours later. Histological sections were stained with anti-CD35 (green) and anti-IgD (blue) (**a** and **c**), or with anti-CD68 (green) and anti-IgD (blue) (**b** and **d**). FDC-M1 *in vivo* staining co-localized with CD35 immuno-fluorescent staining, but also co-localized with CD68 positive macrophages (tingible body macrophages). Isotype control doesn't stain GCs. **(e**-**f)**, Histological staining of day 6 GCs with anti-IgD (blue), anti-CD35 (**e**) or FDC-M1 (**f**) (red) and CD68 (green). TBM are visible in the DZ and LZ of the GC. FDC-M1 partially co-stains with CD68. We find a good coincidence of CD35 (a light zone marker) and FDC-M1 staining. We do see coincidence of tingible body macrophages with FDC-M1 and CD68 and these cells are found in the DZ as well as LZ but they do not interfere with the distinction between DZ and LZ because of the relative density of staining in the two regions. Furthermore, tingible body macrophages are clearly distinguished from the FDC network by their large cell bodies and relative lack of processes.

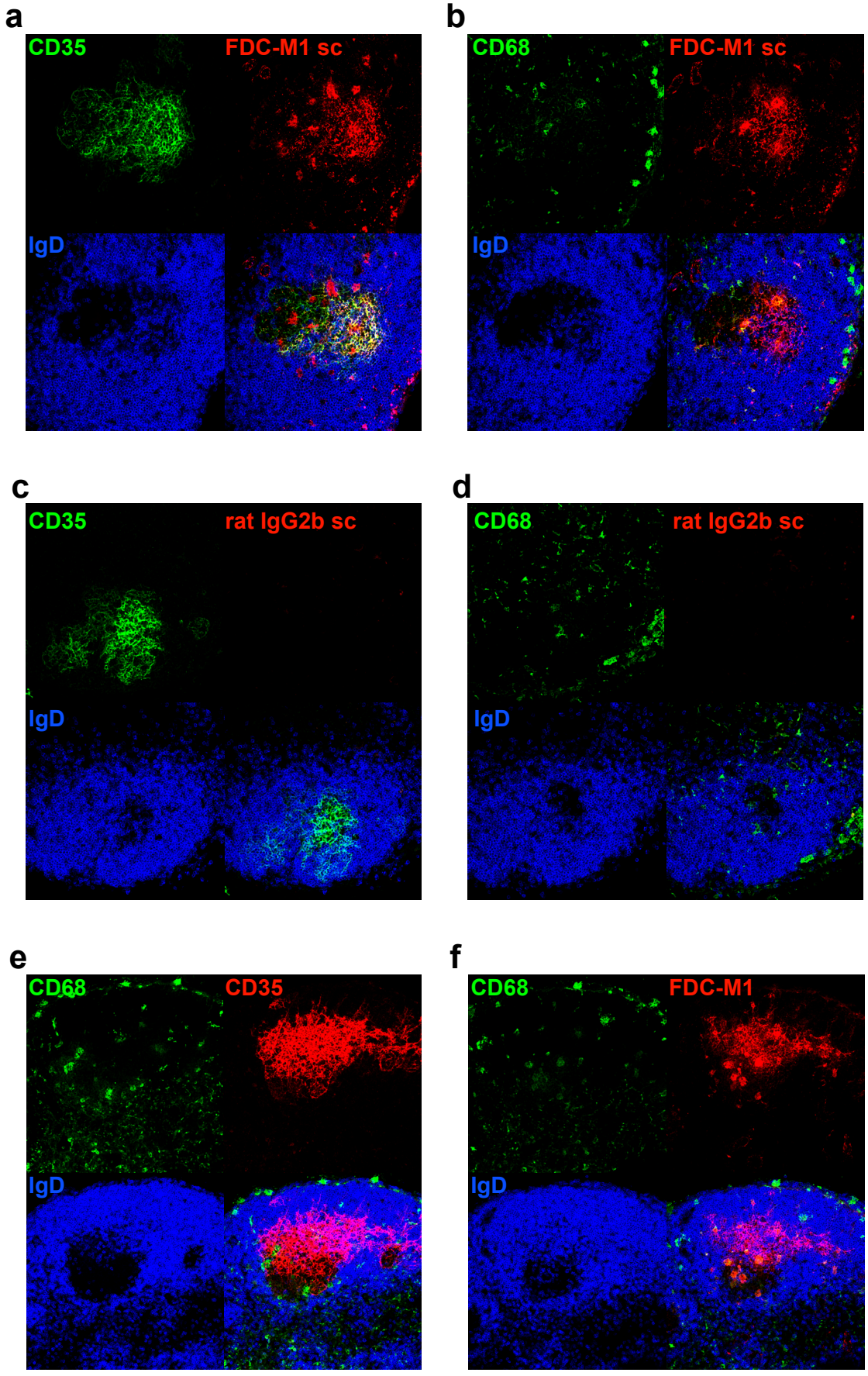
a
CD35
FDC-M1 sc
IgD
b
CD68
FDC-M1 sc
IgD
c
CD35
rat IgG2b sc
IgD
d
CD68
rat IgG2b sc
IgD
e
CD68
CD35
IgD
f
CD68
FDC-M1
IgD

Figure 6.4 Behavior of GC and naïve B cells in secondary follicles. (a) Timeline for immunization, cell transfer and imaging. **(b)** Diagram showing the region of the inguinal lymph node that was imaged *in vivo* (right, G: GC, B: B cell follicle, T: T cell zone, I: interfollicular zone, M: medulla) and dimensions of time-lapse still (left). **(c)** Time-lapse still z projection of FDC signal (red) superimposed with tracks of B1-8^{hi} (green, upper row) and control (blue, middle row) B cells. Two representative movies with (right) and without (left) antigen boost are displayed. **(d, e)** Quantitative analysis of WT and B1-8^{hi} B cells in the presence (right; WT: 534 cells, B1-8^{hi}: 311 cells) and absence (left; WT: 212 cells, B1-8^{hi}: 200 cells) of specific antigen. Analysis is based on 3 independent experiments for both conditions **(d)** Random walk analysis in the absence (left) and presence of NP-OVA (right). Displacement values are averaged for all B1-8^{hi} (green) and WT (blue) B cells. From the slope ($\Delta x/t^{1/2}$) of the linear segment (R^2=0.99) the motility coefficient ($M = \Delta x^2/6t$) was calculated, which is a measure of the volume scanned by a cell per time interval. Error bars represent standard error. **(e)** Statistical analysis of cell behavior. Each data point represents a value for a single cell and black horizontal bars represent mean values. A parametric test (ANOVA) followed by Bonferroni multiple comparison test was performed. Only cell volumes from cells within the same movies were tested for differences (unpaired two-tailed t-test). Samples that are significantly different from all other samples are marked with *** ($p<0.001$).

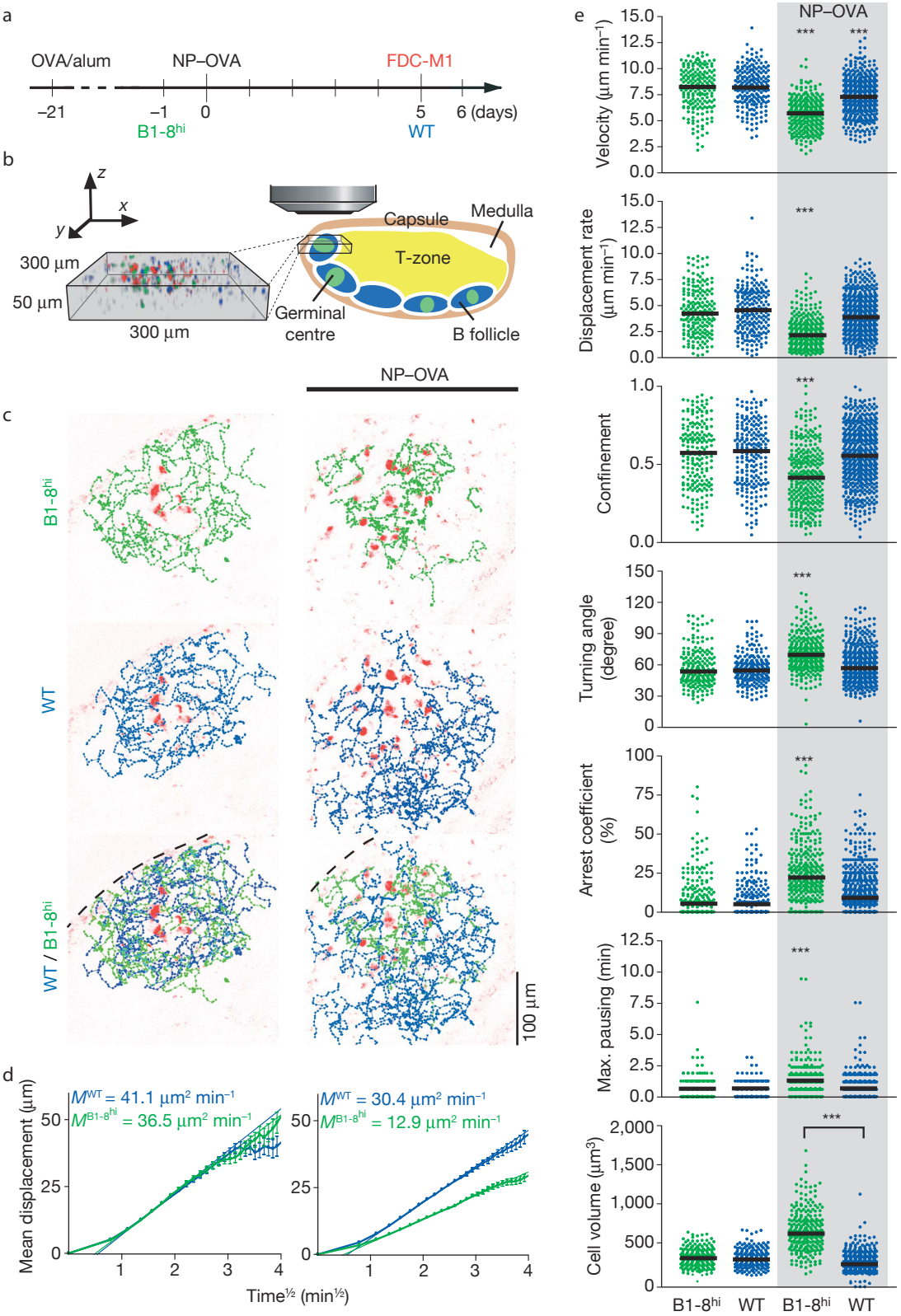
a
OVA/alum
NP–OVA
FDC-M1
–21
–1
0
5
6 (days)
B1-8hi
WT
b
z
x
y
300 µm
50 µm
300 µm
Capsule
Medulla
T-zone
Germinal centre
B follicle
c
NP–OVA
B1-8hi
WT
WT / B1-8hi
100 µm
d
Mean displacement (µm)
MWT = 41.1 µm2 min–1
MB1-8hi = 36.5 µm2 min–1
MWT = 30.4 µm2 min–1
MB1-8hi = 12.9 µm2 min–1
Time½ (min½)
e
NP–OVA
Velocity (µm min–1)
Displacement rate (µm min–1)
Confinement
Turning angle (degree)
Arrest coefficient (%)
Max. pausing (min)
Cell volume (µm3)
***
B1-8hi
WT
B1-8hi
WT

Figure 6.5. Analysis of B cell behavior in GC LZ and DZ. (a) Time-lapse still showing GC division into LZ and DZ and lymph node capsule is indicated as dashed line. **(b)**, Percentage of cells that were moving from the LZ to the DZ and the reverse within 30 minutes. 8% (n=188) moved from the DZ to the LZ and 5% (n=188) did the reverse (upper panel). To correct for the different B cell density, the number of cells migrating from DZ to LZ are shown as percentage of DZ cells (n=111) and the LZ to DZ converting cells are shown as percent of LZ cells (n=77) (lower panel). **(d)** The arrest coefficients (upper panel) and velocity (lower panel) for DZ and LZ B cells (green) are shown separately in comparison to naïve control B cells (blue) (two-tailed t-test: arrest coefficient p=0.03; velocity p= 0.08). The velocity is representative for all other migratory parameters shown in Fig.1e. Analysis represents 4 different time-lapse movies from 3 independent experiments. **(e)** Vector analysis**.** Displacement vector for all antigen-specific B cells in GCs (upper panel) and all control B cells in B cell follicle (lower panel) irrespective their initial position. The average net displacement vector is displayed in red. **(f)** The magnitude of the average net displacement are shown for 4 time lapse movies (3 independent experiments). **(g)** The angle of the average displacement vector and a vector perpendicular to the lymph node capsule are shown for 4 time lapse movies (3 independent experiments).

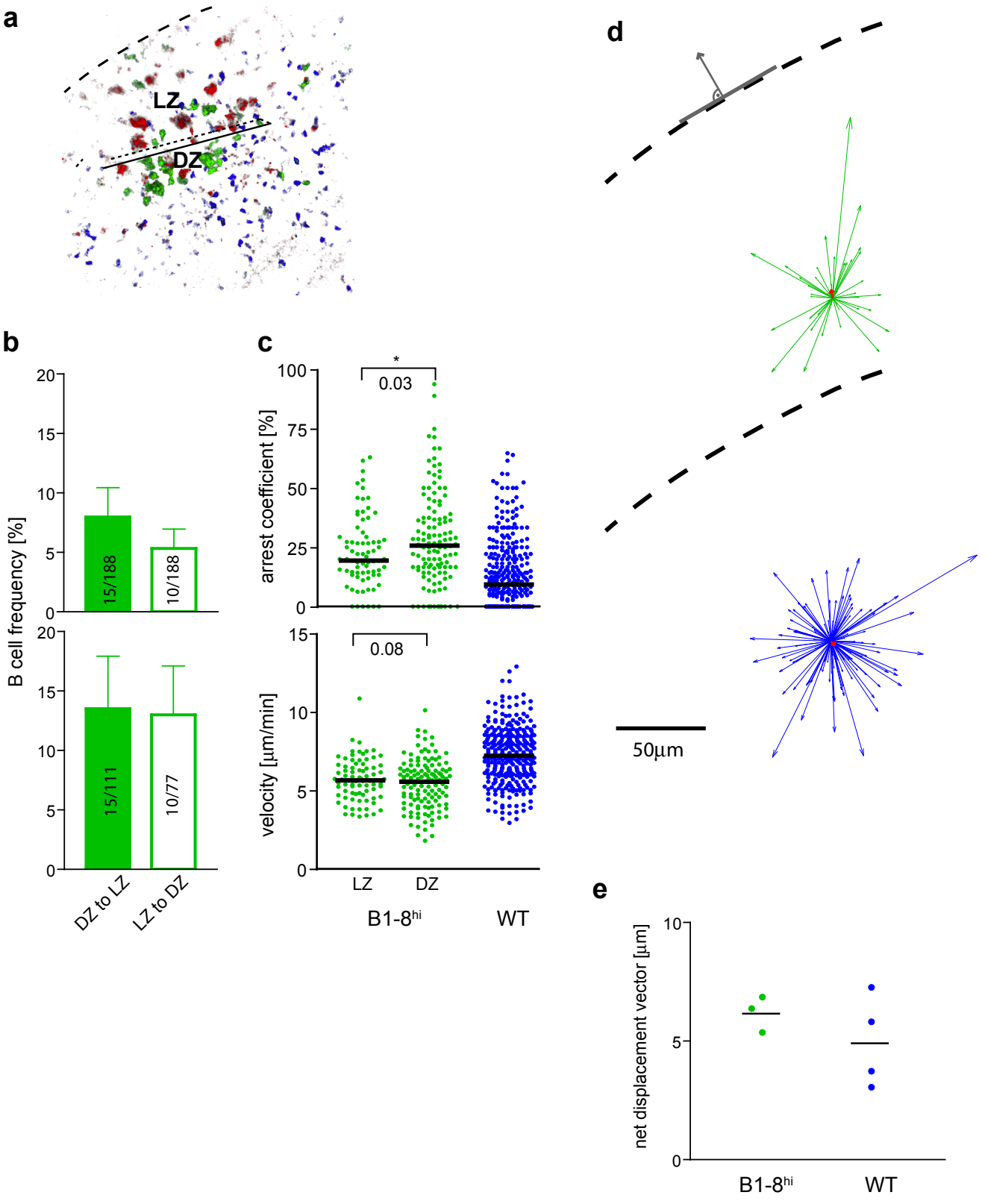
a
LZ
DZ
b
B cell frequency [%]
15/188
10/188
15/111
10/77
DZ to LZ
LZ to DZ
c
arrest coefficient [%]
*
0.03
0.08
velocity [µm/min]
LZ
DZ
B1-8hi
WT
d
50µm
e
net displacement vector [µm]
B1-8hi
WT

Figure 6.6 Analysis of contacts between B cells and FDC-M1$^+$ cells. (a) *In vivo* observation of B cell FDC contact. Time-lapse images showing contacts between FDC and GC B cell (lower row) and naïve B cell (upper row). White arrows indicates position of B cell and cell tracks are displayed in blue and green for WT and B1-8^{hi} B cell respectively. **(b)** Instantaneous velocity profile during FDC-M1$^+$ cell contact. Contact duration is indicated by grey shading. Corresponding time points of stills in (a) are indicated with black arrows. **(c)** Statistical analysis of B cell/FDC-M1$^+$ cell contacts. The contact duration between FDC-M1$^+$ and follicular (blue dots) or GC B cells (green dots) was retrieved from time-lapse movies. Each dot represents a contact ($p < 0.0001$, unpaired t-test two-tailed). **(d)** Cell velocity of follicular and GC B cells in contact with FDC-M1$^+$ cells (grey shading) or not (WT: $p = 0.26$; B1-8^{hi}: $p < 0.0001$, paired t-test). Analysis is based on two independent experiments and 3 time-lapse movies.

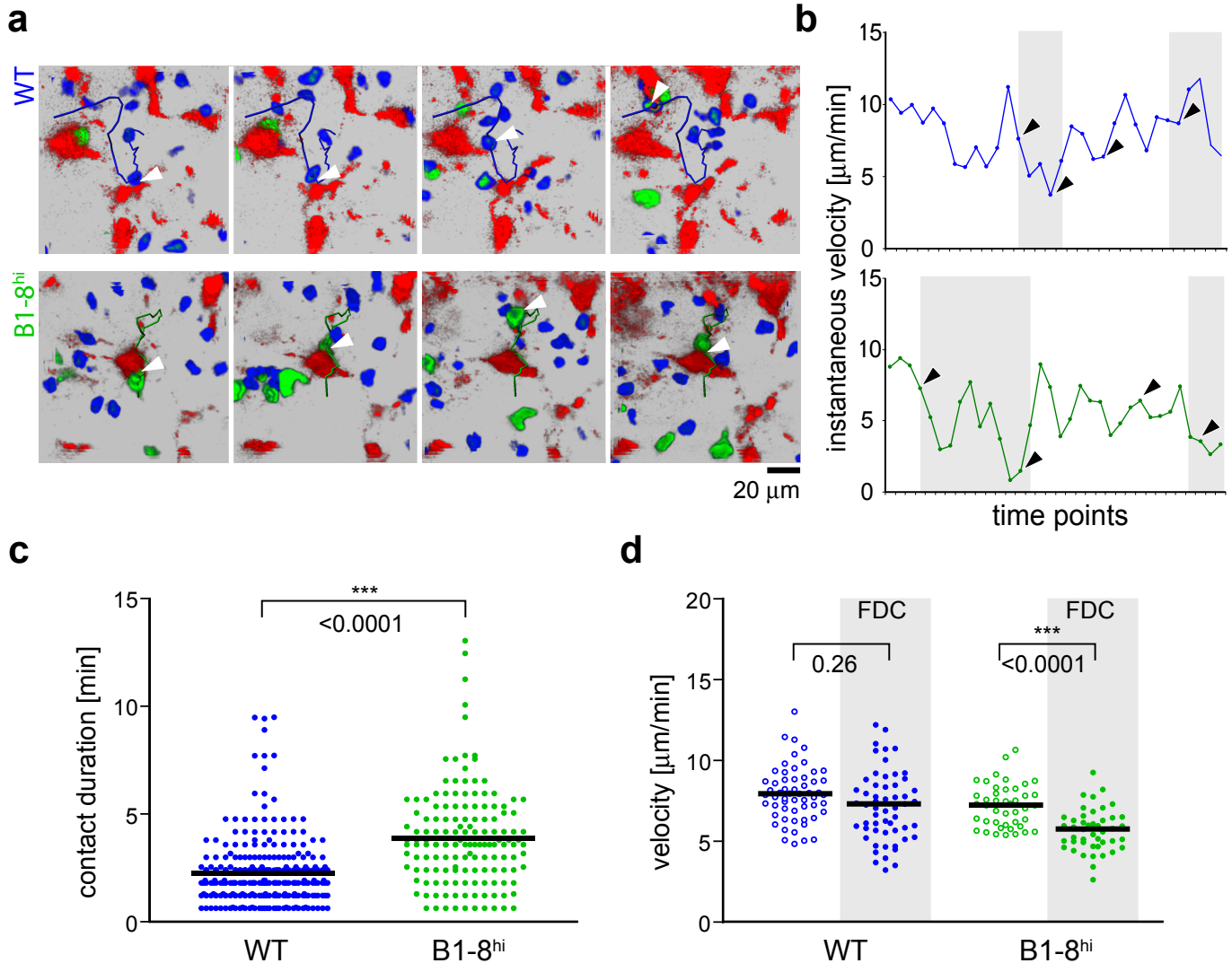
a
WT
B1-8hi
20 µm
b
instantaneous velocity [µm/min]
15
10
5
0
time points
c
contact duration [min]
***
<0.0001
WT
B1-8hi
d
velocity [µm/min]
FDC
FDC
0.26
***
<0.0001
WT
B1-8hi

Figure 6.7 B cell entry into ongoing GC reactions is affinity-dependent. (a) Timeline of immunization (top) and B cell transfer (bottom). B cells were transferred 0, 6, or 9 days after the NP-OVA boost. **(b)** Histological sections of lymph nodes harvested 6 days after B cell transfer stained with PNA (red), IgD (blue) to label GC B cells and naïve B cells respectively. Transferred B cells were GFP^+ (green). In 2 experiments, when cells were transferred with the boost (0 d), we analyzed 25 GCs of which 22 were composed entirely of transferred B cells. In four experiments, when cells were transferred 6 or 9 days after the NP-OVA boost, we analyzed 44 GCs of which 38 were mixed. **(c)** Timeline of immunization and B cell transfer. WT (B6.SJL), B1-8^{lo}, and B1-8^{hi} recipient mice were immunized with Ova and boosted with NP-Ova as in all previous experiments. B1-8^{hi} B cells were transferred into the immunized mice 6 days after the boost. **(d)** Histological sections of lymph nodes harvested 6 days after B cell transfer stained with PNA (red), IgD (blue) to label GC B cells and naïve B cells respectively. Transferred B cells were GFP^+ (green). B1-8^{hi} B cells only joined GCs in WT (B6.SJL) and B1-8^{lo} mice, and therefore joining is dependent on BCR affinity. In 3 experiments, when cells were transferred in B1-8^{lo} mice, we analyzed 25 GCs all of which were mixed. In 3 experiments, when cells were transferred in B1-8^{hi} mice, we analyzed 18 GCs all of which were composed of endogenous B cells. **(e)** Flow cytometric analysis of GC-joining B cells. OVA-immunized B6 mice were boosted with NP-OVA. B1-8^{hi} SJL B cells were either transferred together (0 days) or 6 days after the NP-OVA boost (-6 days). **(f)** Proliferation of transferred B cells was measured 1, 2, and 3 days after B cell transfer by CFSE dilution. Percentages indicate divided cells. **(g)** GL7 and Fas expression 6 days after B cell transfer (gated on $CD19^+$ and $CD45.1^+$). Percentages indicate FAS^+ and $GL7^+$ cells.

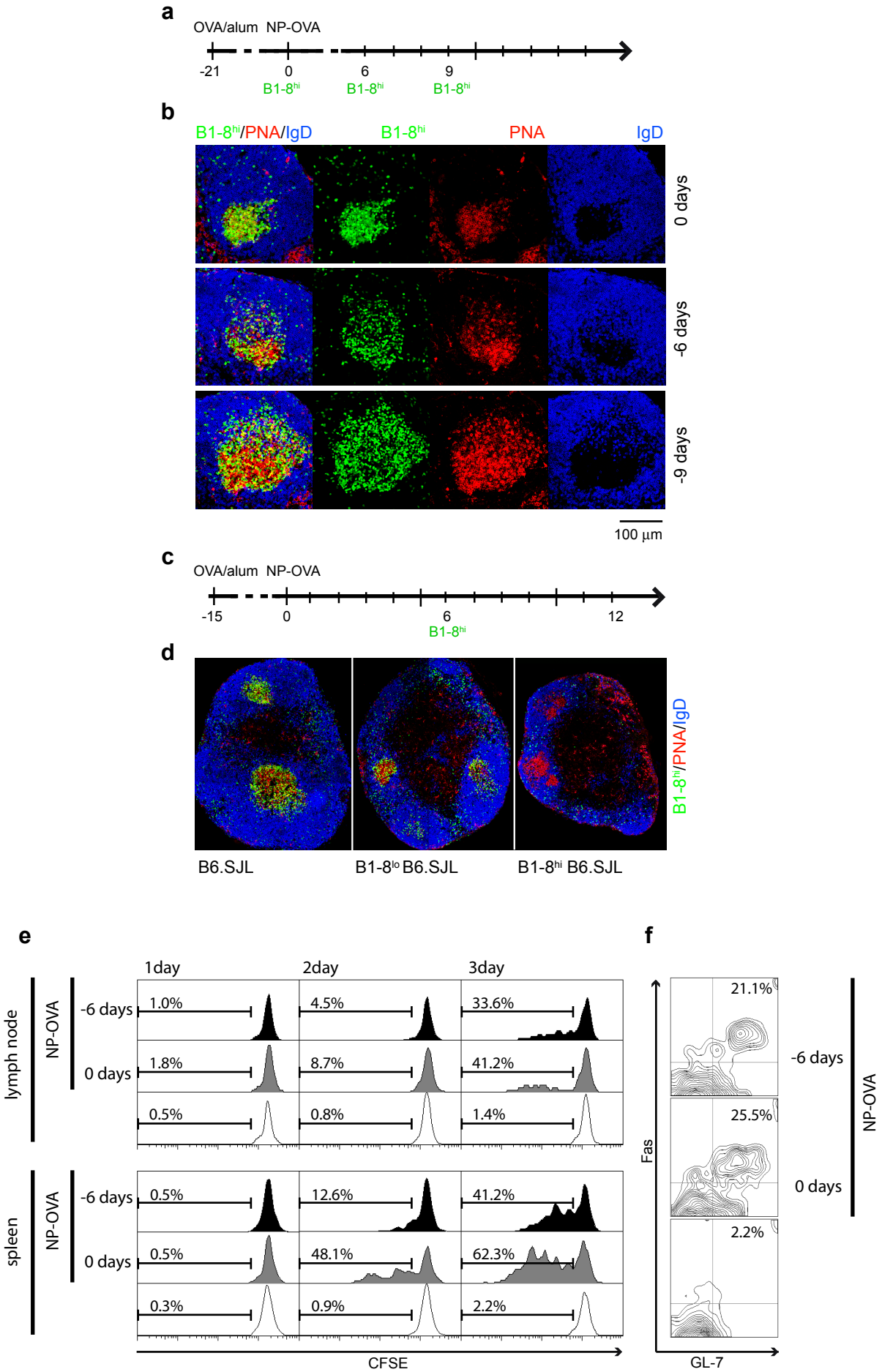
a
OVA/alum NP-OVA
-21
0
6
9
B1-8hi
B1-8hi
B1-8hi
b
B1-8hi/PNA/IgD
B1-8hi
PNA
IgD
0 days
-6 days
-9 days
100 µm
c
OVA/alum NP-OVA
-15
0
6
12
B1-8hi
d
B1-8hi/PNA/IgD
B6.SJL
B1-8lo B6.SJL
B1-8hi B6.SJL
e
1day
2day
3day
lymph node
NP-OVA
-6 days
0 days
1.0%
4.5%
33.6%
1.8%
8.7%
41.2%
0.5%
0.8%
1.4%
spleen
NP-OVA
-6 days
0 days
0.5%
12.6%
41.2%
0.5%
48.1%
62.3%
0.3%
0.9%
2.2%
CFSE
f
21.1%
25.5%
2.2%
Fas
GL-7
-6 days
0 days
NP-OVA

CHAPTER 7. DISCUSSION

T cell Antigenic Search Algorithm

For naïve T cells to promptly respond to pathogens requires that they survey antigenic space effectively; this in turn requires that antigens be rapidly delivered to the LN and the full range of antigenic pMHC be made available to T cells. We observed that DCs in the T cell area form a dense network of cells whose processes extend throughout the entire paracortex. The majority of these DCs do not show significant translational movement, instead remaining largely stationary while extending their dendrites in probing motions (**Figure 3.4; Movie 3.9**). Higher-order clusters of DCs, T cells, and B cells were seen at the interface between the B and T cell areas (**Figure 3.5, 3.6; Movie 3.13**); based on their cellular composition and location, we speculate that they are the physical correlates of T cell help. Newly emigrated DCs distribute themselves throughout the T cell area and integrate into the existing DC network; as they become more settled, their probing motions replace translational movement (**Figure 3.7; Movie 3.16**). It has been shown that the extensive movements of DC processes enable DCs to contact up to 5,000 T cells per hour (Miller et al., 2004a); this "probing" movement is dependent on the small GTPases Rac1 and Rac2, which are necessary for proper antigen presentation (Benvenuti et al., 2004). The T cell antigenic search mechanism is largely driven by T cell motility through a network of probing dendritic cells; we speculate that the higher motility of mature DCs functions to distribute dendritic cells throughout the paracortex. We further speculate that this change from "mobile" to "sessile" phenotypes is necessary

for appropriate interaction with migrating T cells and therefore for proper antigen presentation.

In the steady state, the DC network presents migrating T cells with an enormous surface area rich in self pMHC complexes required to sustain T cell longevity (Kirberg et al., 1997; Takeda et al., 1996) and to maintain self-tolerance. Both self and non-self antigen delivered to the LN via the lymph are processed simultaneously by many DCs in the network (Belz et al., 2004; Inaba et al., 1997; Inaba et al., 1998; Itano et al., 2003), maximizing the surface area for presentation of such antigens. The networked arrangement of DCs positions them efficiently to transfer antigen transfer from one APC to another by releasing exosomes or apoptotic bodies (Inaba et al., 1998; Thery et al., 1999). If antigen is distributed from one migrating cell to several resident cells, the antigen-presenting surface area expands as the local concentration of pMHC decreases, increasing the likelihood of detection by a migrating T cell.

As dendritic cells are evenly dispersed throughout the T cell area, the random walk of T cells maximizes their ability to scan antigenic space (Mempel et al., 2004; Miller et al., 2003; Miller et al., 2002). The substrate for the DC network is formed by fibroblastic reticular cells, and is induced by contacts with lymphocytes, in a TNFα and LTβ-dependent manner (Katakai et al., 2004). Interestingly, it was recently shown that T cell migration is not completely random, but that it is guided by the paracortical FRC network (Bajenoff et al., 2006). T cells migrate along the fibers, contacting them upwards of 95% of the time, and change directions only at branching points in the network; similar results were seen for B cells migrating on FDCs in B cell follicles (Bajenoff et al., 2006). This provides an interesting explanation for the periodicity in T

cell velocity observed by Miller *et al.* (Miller et al., 2003). It was observed that T cell velocity has rhythmic peaks at ~2 min intervals, which can now be explained as a T cell choosing a fiber to crawl on, crawling a distance of 15-30 μm, reaching a new branch point, and pausing to pick a new direction. While the steady-state T cell motility along this network is a random walk, additional directional cues can be imparted locally by chemokines secreted from activated DCs, to change the local attractiveness and net directionality (Castellino et al., 2006). This model is attractive as it explains baseline T cell movement while permitting additional chemotactic information to be literally layered on top; variations along these lines have been suggested by von Andrian's group (Henrickson and von Andrian, 2007; Mempel et al., 2006a). We further speculate that DC movement will be found to follow similar patterns – i.e. that migratory DCs move along the FRC network, changing directions at branch points, until they "settle down" and fix their position in the FRC network.

Initial stages of priming and tolerance induction are similar

We observed that in both tolerance and immunity, naïve T cells arrested antigen-specifically shortly after leaving HEVs (**Figure 4.10; Movies 4.1, 4.4**). Tolerized T cells recovered marginally faster than primed T cells, but both had recovered significantly by 12-18 h (**Figure 4.10; Movies 4.3, 4.6**).

This similarity in the early stages of T cell antigen recognition is in contrast to the results obtained by Hugues *et al.*, who saw stable interactions only in priming and not in tolerance (Hugues et al., 2004). Possible explanations for this discrepancy include their

use of explanted lymph nodes which lack blood and lymph circulation, and their failure to image time points less than 8 h post-T cell transfer. Their method for visualizing DCs – microinjecting the LN with a labeled anti-CD11c antibody and labeling for 3 h *ex vivo* at 37 °C – was also nonphysiological and likely to introduce artifact such as LPS contamination.

The rapid arrest we observed shortly after T cell exit from HEVs also contrasts with the dynamic early contacts observed by other groups (Mempel et al., 2004; Miller et al., 2004b). These groups reported that T cells made only transient interactions during the first 8 h post-transfer, and stable contacts only formed between 8-20 h, with T cells regaining speed and making transient contacts at later time points. It was suggested that the early transient DC:T cell interactions changed the T cell activation state, to permit the subsequent formation of stable, long-lasting contacts. We should note that we started imaging between 30 and 60 min after T cell transfer, and are therefore unable to rule out the existence of a short "phase I" of 30 minutes or less duration. Our *in vivo* calcium imaging suggests that T cells signal while decelerating, but that T cells do not stop immediately upon Ca^{2+} elevation (**Figure 5.8; Movie 5.8**), consistent with a brief phase I in which T cell formation of stable contacts is licensed on the order of 30 minutes or less. Additionally, our imaging and histology data are consistent with other reports showing that immunization with antigen in CFA results in early antigen-specific retention of T cells near HEVs (Bajenoff et al., 2003).

Possible explanations for the difference in the length of phase I observed in various studies include the use of labelled splenic DCs that must migrate from the injection site to the LN and enter the T cell area before presenting antigen. If migratory

splenic DCs are not immediately able to form stable interactions with T cells, only transient interactions will be observed until the DCs are competent to undergo stable interactions; however, as DCs were observed simultaneously making both stable and transient contacts, this may not contribute (Mempel et al., 2004). Another possible explanation is the increased density of pMHC after antigen targeting with α-Dec-205, compared to the relatively small number of DCs carrying peptide that migrate to the LN. DCs that have migrated from the periphery, carrying pMHC, are relatively rare, comprising approximately 1% of DCs in the LN. LN resident DCs, on the other hand, compose the majority of LN DCs, and after antigen delivery with α-Dec-OVA antibodies, over 50% of DCs express Ova pMHC (Bonifaz et al., 2004).

If T cells do not immediately arrest upon initiation of TCR signalling but must integrate the signal up to a threshold, T cells that are integrating these signals will first make serial contacts with DCs before forming stable interactions: while signals are being integrated, they will make serial contacts, and once this threshold is reached, stable T cell:DC conjugates will form. This is exactly what was observed and termed phases I and II, respectively (Mempel et al., 2004). We suggest that the high density of pMHC after targeting with α-Dec-Ova lets T cells rapidly accumulate enough TCR signal to reach the threshold for prolonged interactions: within 30 min of LN entry, T cells had arrested on α-Dec-Ova targeted DCs, as compared to the 8 hours required for stable contacts to form on LN migrant DCs (Mempel et al., 2004). We further suggest the general principle that the amount of pMHC available to T cells may influence the speed with which T cells arrest and form stable interactions with DCs – that is, the duration of phase I.

It is fairly evident that the number of DCs that can present a given antigen will vary depending on how that antigen has reached the LN. Soluble antigen rapidly drains to the LNs and is quickly presented by large numbers of LN DCs (Itano et al., 2003). In addition, in the steady state, self antigens from dead cells and serum proteins are continually picked up, processed, and presented by large numbers of resident DCs (Inaba et al., 1997; Inaba et al., 1998; Scheinecker et al., 2002). It should also be noted that not all pathogens are carried by DCs into the LN - any blood-borne virus or microbe, for instance, will rapidly be delivered systemically. It thus seems likely that in conditions of immunity or tolerance, T cells will encounter varying numbers of antigen-presenting DCs; we therefore suggest that the kinetics of the initial T cell-DC interaction will depend on the relative frequency of antigen-positive DCs. Further work by von Andrian's group supports our earlier speculations: they extended their earlier intravital imaging by varying the density of pMHC on DCs, and the number of DCs presenting antigen in the LN, and observed that as the number of dendritic cells presenting antigen, and the density of antigen on the DC surface increased, the duration of phase I decreased (Henrickson et al., 2008). This is consistent with our earlier hypothesis that T cells integrate TCR signals up to a certain threshold, at which point they are licensed to form stable contacts with DCs.

In conditions of both tolerance and immunity, we occasionally observed T cell swarming and clustering (**Movie 4.7**), but the relative rarity with which clusters were observed was not surprising, as large numbers of DCs present antigen after targeting with α-DEC-Ova (Bonifaz et al., 2004; Hawiger et al., 2001), and the number of T cells in each cluster is inversely proportional to the number of antigen-presenting DCs (Bousso

and Robey, 2003).

In some cases, we observed T cells arrested in not in contact with EYFP$^+$ DCs (**Movie 4.8**); we feel that the likeliest explanation is that some DC processes are too thin to be visualized by MPLSM. Other possible explanations are insufficient EYFP expression in some Dec-205$^+$ cells of the CD11c-EYFP mouse, or antigen transfer to YFP-low DCs. One further possibility is pMHC presentation by non-DCs: It was recently shown that LN stromal cells can present pMHC and activate T cells; although this remains controversial, if CD11c$^-$ cells can present Ova pMHC to T cells, it would follow that T cells could arrest on the antigen-presenting stromal cells (Lee et al., 2007). We should also note that these possibilities are not mutually exclusive.

It has been argued that delivering antigen systemically is less representative of physiological antigen presentation than is subcutaneuous inoculation with exogenously labeled DCs and LPS. This is in fact debatable – the exogenous DCs that are introduced are not identical to the dermal DCs and Langerhans cells that carry pathogens to the LN. It is not clear whether splenic DCs, proliferating rapidly due to Flt3L overstimulation, then purified and injected into the periphery have similar migratory characteristics, antigen-handling behavior, or responses to pathogens as the endogenous dermal DCs and Langerhans cells. We observed that exogenous CFP-expressing DCs gradually incorporated into the paracortical DC network and grew to behave like endogenous DCs over time (**Figure 3.7; Movie 3.16**), but we were unable to make direct comparisons with endogenous migratory cells. It seems unlikely that the kinetics of their immigration and incorporation into LN DC networks does not differ from that of splenic DCs after purification.

Significant heterogeneity in cell behavior exists across the LN; it has been observed by several groups that superficial cells generally move more slowly than deep cells (Huang et al., 2004). Our observations, however, do not reflect this finding; we speculate that it may be due to enhanced phototoxicity in shallow regions of the LN. It is thus important to compare cells within the same imaging field, to minimize non-specific effects on the motility of observed cells; ideally, speeds can be normalized to that of control cells in the same field.

Data we have not yet prepared for publication suggests that adjuvant delivery leads to a late antigen-independent slowing of T cells. When agonistic α-CD40 antibody was injected concurrently with α-DEC-Ova, both specific and non-specific cells slowed down, beginning 15-18 h after T cell transfer, and persisting for two to three days. This corresponds with the upregulation of adhesion molecules on DCs, B cells and stromal cells in lymphoid tissues reacting to inflammation (Dustin et al., 1986), as well structural changes in the lymph node as it begins to swell (Katakai et al., 2004). It is thus unclear whether this reflects a purely physical effect due to compression and increased cell number, increased "stickiness" of the DC and stromal surface as they activate in response to inflammatory cytokines, or some combination thereof. It is tempting to speculate that this late antigen-independent adjuvant-induced slowing is a correlate of "signal 2", the presence or absence of which leads to priming or tolerizing responses, respectively (Bretscher and Cohn, 1970; Janeway, 1989).

We found that the early stages of tolerance and immunity are characterized by similar early T cell arrest near HEVs, with movement recovering to normal by 18 hours. This is consistent with our findings that T cell activation, proliferation, and responses to

antigen *in vitro* were similar in the first 3 d of tolerance and priming. Additionally, this is corroborated by results showing that T cells can be rescued from deletion 3 d after antigen exposure if transferred to an antigen-free environment (Redmond et al., 2003). We suggest that the early stable DC:T cell interactions that can occur in both tolerance and immunity do not determine commitment to tolerance or immunity; we speculate that cellular fate commitment to priming or tolerance occurs later as T cells dynamically contact DCs.

pMHC potency, Ca^{2+}, and the dynamics of DC:T cell interactions

We have evaluated how TCR affinity for pMHC affects T cell functional responses and migration patterns in LNs in steady-state conditions. High-potency APL induced rapid deceleration of antigen-specific T cells, T cell proliferation, trapping within LNs, and anergy (**Figure 5.5; Movie 5.1**). Medium-potency APL did not alter T cell motility, but induced a small amount of T cell proliferation and IFN-γ production, significant T cell trapping, and a robust anergy (**Figure 5.5; Movie 5.2**). Low-potency APL did not alter T cell motility or induce T cell proliferation, but induced anergy and T cell trapping within LNs (**Figure 5.5; Movie 5.3**).

All of the APLs tested bind to I-E^k with similar affinity (Lyons et al., 1996; Rogers et al., 1998), all were delivered via α-Dec-205 antibodies, and all induced similar levels of CD69 upregulation and CD62L downregulation (**Figure 5.3**). We therefore conclude that the lack of T cell stopping in response to medium- and low-potency APLs was not due to reduced pMHC formation or an inability of T cells to detect these APLs *in vivo*; the absence of T cell arrest is due to the inability of medium- and low-affinity TCR

ligands to elevate T cell Ca^{2+} levels (**Figure 5.8**). Notably, medium- and low-affinity APLs still effectively induced LN T cell trapping and anergy (**Figure 5.4, 5.5**), demonstrating that these downstream T cell behaviors are independent of Ca^{2+} elevation or cellular dynamics.

Since some studies of T cell:DC interactions reported an early, dynamic "phase I" before the formation of stable interactions (Mempel et al., 2004; Miller et al., 2004b), we imaged between 6-12 h after T cell transfer, a time frame consistent with reports of an early dynamic phase. We found no effect of medium- and low-affinity pMHC at either early or later time points (**Figure 5.5**), demonstrating that T:DC interactions at all time points do not determine T cell fate.

Because T cell arrest is necessary for immunological synapse formation, the absence of T cell arrest in response to medium- and low-potency antigens indicates that immunological synapse formation is not required for the induction of tolerance *in vivo*. The medium-potency APLs did not generate sufficient intracellular Ca^{2+} to mediate cell stopping, but did lead to low levels of proliferation, LN trapping, and anergy. This is consistent with reports of low-avidity pMHC sufficient to induce proliferation without immunological synapse formation *in vitro* (Cemerski et al., 2007). Additionally, *in vitro* models have shown sequential transient, mobile DC:T cell interactions in cultured ECM (Gunzer et al., 2000; Gunzer et al., 2004).

Steady-state presentation of medium- and low-potency throughout the DC network leads to T cell tolerance without antigen-specific arrest on DCs, although T cells were sequestered antigen-specifically for 2-3 days in LNs. Our results show that TCR affinity for pMHC determines the dynamics of DC:T cell contacts *in vivo*, which is

independent of CD69 upregulation and CD62L downregulation. CD69 was recently shown to be a negative regulator of sphingosine-1-phosphate receptors, and CD69 upregulation prevents lymphocyte egress from LNs (Matloubian et al., 2004; Shiow et al., 2006). Thus, although T cells responding to medium- and low-affinity pMHC antigens under conditions that induce anergy do not arrest, they remain in the antigen-presenting LN and continue to scan the DC network for 48-72 h. This prolonged exposure to antigen ensures that T cells that recognize even low-affinity self-pMHC will have sufficient antigenic contact to integrate many low-level signaling events involving hundreds of T cell:DC interactions, which is especially important for self antigens with a restricted range of expression (Iezzi et al., 1998; Lindquist et al., 2004; Miller et al., 2004a).

Dynamics of germinal centers *in vivo*.

Germinal centers are physically open structures that are continually scanned by recirculating B cells; the germinal center – as is the entire B cell follicle – is more dynamic than had previously been appreciated. Strikingly, naïve B cells enter and pass through GCs relatively unimpeded, indicating that B cells can enter germinal centers without participating in germinal center reactions, and that the presence of a B cell in the germinal center in no way indicates that it is participating in the GC reactions. GC B cells are distinguishable from follicular B cells and plasmablasts by their location, morphology, and restricted motion within the GC (**Figure 6.4; Movies 6.1, 6.2**). In contrast to naïve B and T cells, which arrest after encountering high-affinity antigens

presented by DCs, GC B cells decelerate and make longer contacts with FDC-M1$^+$ cells, but rarely stop for prolonged periods of time (**Figure 6.6; Movie 6.5**) (Mempel et al., 2004; Miller et al., 2004b; Qi et al., 2006; Shakhar et al., 2005). We propose that the selection of GC B cells is governed by multiple dynamic interactions, and note that this resembles T cell anergy induction by medium- and low-affinity antigens (Skokos et al., 2007).

Affinity maturation is achieved during the germinal center reaction through repeated rounds of proliferation and selection on the basis of affinity (MacLennan, 1994). We have shown that B cells can join an ongoing GC reaction if their affinity is high enough for them to outcompete the extant cells in the GC (**Figure 6.7**). Since naïve B cells migrate for 12-18 h in a given LN follicle before exiting and recirculating to other LNs, and since 30% of follicular B cells contacted an FDC-M1$^+$ cell, even assuming some selection bias in the choice of imaged regions, essentially all follicular B cells will interact with antigen displayed on FDCs in any GC-containing follicle. As GCs last for 2-3 weeks, with B cells entering LN follicles at random and moving almost entirely along stromal cell processes, particularly FDCs (Bajenoff et al., 2006), a significant fraction of all circulating B cells will be exposed to antigen in any given GC; correspondingly, a significant fraction of B cells within a GC at any given moment will not have descended from the founder B cells. This, although initially surprising to us, is consistent with a single-cell analysis of human GCs that found numerous B cells with unmutated and unrelated antibody genes in tonsillar germinal centers (Kuppers et al., 1993). Continuous B cell scanning thus ensures that a significant fraction of the entire B-cell repertoire is exposed to antigen trapped on FDCs, permitting rare high-affinity cells not present in the

LN when the GC first developed to participate in the GC reaction. This also suggests that recirculating memory B cells may be able to join and participate in GC reactions – effectively letting any antibody response compete with the memory response to the same antigen.

The observation that both B cells and antigen can join an existing GC suggests a mechanism for intermolecular epitope spreading: a GC forms appropriately in response to a pathogenic stimulus, and a second antigen is trapped on immune complexes on FDCs in the GC. As B cells scan this GC, any cells that recognize the second antigen can be recruited into the GC reaction in a Th-dependent manner.

GC B cells are specifically retained inside the light or dark zone, with contributions from chemokine receptors CXCR4 and CXCR5 (Allen et al., 2004), and transit from one zone to the other in approximately 18 h. We observed approximately equal proportions of cells migrating from one zone to the other, indicating that cells are not proliferating in one compartment and being selected in the other (**Figure 6.5**). This is still consistent with a GC reaction composed of successive rounds of proliferation and selection, as long as proliferation and/or selection can occur in either zone.

Our results are similar to those observed in a paper that came out shortly before ours (Allen et al., 2007); Allen *et al.* observed that the GC was a dynamic structure, with GC B cells transiting between light and dark zones, and decelerating but not arresting on FDCs. Cell proliferation and apoptosis was found in both zones; imaging of T cell help revealed predominantly short interactions, leading them to propose that T cell help is one of the limiting factors for which newly mutated B cells compete (Allen et al., 2007). A third paper was published shortly after ours, and found a similar frequency of cells

transiting directly between light and dark zones, but claimed that most cells do not transit directly between light and dark zones, instead taking an indirect path via the outer zone (Hauser et al., 2007). It is difficult to directly compare frequencies among different studies, as the cells are typically imaged for only 30 minutes, with many cells moving in and out of the field, which is usually too small to capture an entire GC in all three dimensions. An alternative explanation of the observation that most cells do not constantly migrate directly from one zone to another might simply be that the cells need to spend half a generation time (~3-5 hours) in one zone before becoming licensed to transit into the other zone; cells that approach the border before they are prepared to cross it would turn away, leading to tracks that appear to enter the outer zone. As the duration that B cells spend in one zone is significantly longer than the time it takes a B cell to transit across one zone and enter the other – 100 μm zone diameter, with a median displacement rate of 2 μm /min, yields a 50 minute transit time – this indicates that the velocity of B cells is not the limiting step in DZ-LZ transit. Therefore, most GC B cells will approach the DZ/LZ border many times before they are licensed to cross it, and as the cells turn away, this will lead to cell tracks and net cell movement vectors at the DZ/LZ border in the direction of the outer zone. In any case, it should be emphasized that all studies have observed that the GC reaction is dynamic, with cells transiting either directly or indirectly between zones, and that proliferation and selection are not rigidly segregated into the DZ and LZ, respectively.

General principles in the cellular dynamics of antigen recognition

The T cell antigenic search algorithm is largely driven by random motility along the FRC fibers that underlie a network of probing dendritic cells (Bajenoff et al., 2006; Mempel et al., 2004; Miller et al., 2003). We have shown that migrating DCs distribute themselves throughout the LN before settling in a fixed location among the LN-resident DC network, and propose that the FRC fibers serve as a substrate for motility and guidance for migrating DCs as they do for T cells.

We have shown that the *in vivo* dynamics of T cell antigen recognition depend on pMHC potency; as discussed above, considerable evidence suggests that pMHC density affects the *in vivo* cellular dynamics as well, which may explain some of the differences observed (Mempel et al., 2004; Miller et al., 2004b; Shakhar et al., 2005). We propose that T cell antigen recognition integrates both pMHC density and pMHC potency in reaching the thresholds for stable conjugate formation, Ca^{2+} signaling, and proliferation, but not T cell fate determination, which is independent of pMHC density or potency. Further work by the von Andrian group supports our hypothesis that T cell signaling integrates pMHC potency and pMHC density in forming stable contacts (Henrickson et al., 2008).

Our results have shown that prolonged interactions are not necessary for T cell fate determination or for continued GC B cell proliferation during GC reactions. This is additionally consistent with the observations that prolonged Treg:DC or Treg:CTL interactions are infrequently observed in Treg-mediated suppression (Mempel et al., 2006b; Tang et al., 2006), T cell help during GC reactions (Allen et al., 2007), or $CD8^+$ T cell killing (Purbhoo et al., 2004). Although prolonged interactions are observed in the T

cell response to high-affinity antigens (Mempel et al., 2004; Miller et al., 2004b; Shakhar et al., 2005; Skokos et al., 2007) and to T cell help early in the B cell response (Okada et al., 2005), there appear to be relatively few cell:cell interactions characterized by stable contact formation *in vivo*. As stable contact formation is necessary for immunological synapse formation, this suggests that immunological synapses are dispensable for most cell:cell interactions; the transmission of immunological information *in vivo* seems to occur largely through relatively short-lived interactions. Our close collaborator Mike Dustin recently introduced the term “kinapse” to describe a mobile cell:cell contact that permits the exchange of information (Dustin, 2008). As more methods for imaging functional responses and signaling become available, it will be possible to study in more detail how signaling at the kinapse leads to changes in cellular behavior and function.

APPENDIX: MOVIE LEGENDS

Movie 3.1. Anatomic location of EYFP$^+$ DCs within the LN. Z-stack of two-photon images taken at depths of 0-300 μm through a B cell follicle in the LN of a living mouse. EYFP DCs are green, adoptively transferred EGFP B cells are false-colored cyan. Four populations of DCs are visible. Bright extended subcapsular DCs (arrows); dimmer DCs in a network surrounding the follicle; scattered compact DCs in the follicles (circles) and an extensive network of DCs in the T cell zone of the paracortex.

Movie 3.2. Reconstruction of EYFP$^+$ DCs within the LN. Three-dimensional reconstruction of the different DC populations around a B cell follicle based on the data presented in **Movie 3.1**. Colors are as in **Movie 3.1**.

Movie 3.3. Blood flow remains intact during intravital imaging. This and all movies below, unless noted otherwise, are maximum intensity projections of a 50 μm-thick volume, accelerated ~300-fold over real time; time elapsed is indicated in minutes: seconds. Blood vessels were visualized with i.v. injection of 66 kDa TRITC-dextran. The HEVs (crossing from top left to bottom right), can be distinguished from arterioles (crossing in the perpendicular direction) based on their irregular epithelium and the shadows of lymphocytes slowly rolling along it. YFP cellular debris is seen on the middle left. A mixture of slowly moving and sessile CD11c-YFP cells is seen scattered in the general area of the HEVs, but not immediately juxtaposed to them. Also seen are CFP lymphocytes (cyan), which exhibit a tighter morphology than DCs and can reach higher maximum speeds.

Movie 3.4. Lymph flow remains intact during intravital imaging. Lymphatic vessels were visualized with subcutaneous injection of 66 kDa TRITC-dextran; afferent lymphatics were imaged in one XY plane every 400 ms. Regular pulsatile motion is seen, and the shadows of lymphocytes in the vessel can be observed.

Movie 3.5. T cell extravasation in the lymph node of a living mouse. T cells (blue, cyan) are visible moving throughout the vasculature (red), visualized by i.v. injection of 655 nm-emitting quantum dots. Many vessels are partially in contact with dendritic cells (yellow). A single T cell is visible extravasating in the lower right quadrant, indicated by an arrow - it appears in the middle of the HEV at 8:11, remains relatively stationary for ten minutes and moves to the left and up over the next ten minutes.

Movie 3.6. Phototoxicity interferes with dendrite probing and cell migration. Even before phototoxicity is manifested in cell morphology, it leads to cellular immobility. Lymphocytes (red) stop moving and DCs (green) stop the probing motions of their dendrites. The use of both dendrite movement and non-specific T cells as internal controls permits sensitive detection of damage to the imaging field. In the upper right corner of the field, which was not affected, both T cell crawling and dendrite probing is visible.

Movie 3.7. Subcapsular sinus DCs and macrophages. Subcapsular sinus EYFP DCs (green) navigating among the less mobile macrophages, visualized by their phagocytosis of subcutaneously injected 66 kDa rhodamine-dextran (red). Note some DCS move rapidly and directionally.

Movie 3.8. Subcapsular DCs probing movement. At higher resolution, the probing movement of subcapsular DCs can be better appreciated. Note the characteristic ruffle shaped extensions of these cells. Dimmer, less motile perifollicular DCs are seen in the background.

Movie 3.9. T cell zone DCs form an extensive network. EYFP DCs (green) form a network throughout the T cell zone of the LN. Note that the DCs exhibit extensive probing movements but show little crawling.

Movie 3.10. T cell zone DC network dynamics. A time sequence depicting a two-dimensional projection of a 50 μm volume in the interface of the T cell and B cell zones. The T cell zone is located below and to the left of the B cell follicle. The behavior of CD11c-EYFP DCs (green) in the network was followed. The great majority of the cells are laterally stable, exhibiting only probing movement, but occasionally a cell could be seen repositioning within the network (red circles). Adoptively transferred EGFP B cells are false-colored cyan.

Movie 3.11. Perifollicular DCs in relation to the LN capsule. A 3-dimensional reconstruction of a lymph node, showing the spatial relation of the perifollicular network of EYFP DCs (green) to the fibrous capsule (blue, second harmonics signal from collagen).

Movie 3.12. Different movement patterns of follicular and perifollicular DCs. Different behaviors of EYFP DCs (green) and ECFP B cells (cyan) in a B cell follicle (top right) and the perifollicular network (bottom left). Whereas some crawling movement is observed in the follicle, the DCs in the perifollicular network appear more dendritic and mainly probe with their processes.

Movie 3.13. DC clusters observed at the T-B interface. DC clusters (EYFP, green) are seen in the T-B interface zone. Note cells appearing to join and dissociate from clusters.

Movie 3.14. Z-stack through DC clusters in Movie 3.13. A higher resolution Z-stack (45 μm deep, at 1 μm intervals) descending through DC clusters in the T-B interface area seen in **Movie 13**. Each cluster is made up of numerous tightly apposed DCs enveloping lymphocytes.

Movie 3.15. The behavior of DC clusters in the T-B interface zone. Cluster position was stable for the duration and remained the same when the area was imaged again 4 hours later. DCs can be seen joining (blue circles) or leaving (red circles) the cluster. The

shadows of lymphocytes can be seen drawn into the clusters enveloped in DC processes (yellow circles).

Movie 3.16. Resident LN DCs vs. transferred mature DCs of splenic origin. Transferred $ECFP^+$ DCs (cyan), immunomagnetically purified from the spleen of a mouse treated with a FLT3-L-secreting tumor are seen here moving among resident CD11c-EYFP cells (yellow). The sequence was recorded at a depth of 180-230 μm 48 h after cell transfer. In this particular field, transferred cells crawled slightly faster than residents. Most of the movement consists of process probing, with cells occasionally flowing their soma and nucleus into one of the processes. To emphasize cell morphology and dynamic probing of migrant DCs, the CFP channel is shown alone on the right.

Movie 3.17. DC Intravasation into HEV. $EYFP^+$ DCs (green) are visible near blood vessels (red), visualized by injection of 655 nm-emitting quantum dots; $ECFP^+$ (blue) and $EGFP^+$ (cyan) lymphocytes move around the T cell area. In the upper right corner, a YFP-expressing DC enters the HEV in the first ten minutes, gradually detaches from the wall, and is swept away at 19:24.

Movie 4.1. Tolerizing interactions 1-6 h after T cell transfer. Antigen-specific T cells (orange) move more slowly than non-specific T cells (red), and are more frequently arrested on dendritic cells (green). Tracks of specific EGFP-OT-II cells are cyan, and tracks of nonspecific ECFP-T cells are purple.

Movie 4.2. Tolerizing interactions 6-12 h after T cell transfer. Antigen-specific T cells (orange) move more slowly than non-specific T cells (red), and are more frequently arrested on dendritic cells (green). Tracks of specific EGFP-OT-II cells are cyan, and tracks of nonspecific ECFP-T cells are purple. Antigen-specific T cells are less arrested than at 1-6 h.

Movie 4.3. Tolerizing interactions 12-18 h after T cell transfer. Antigen-specific T cells (orange) and non-specific T cells (red) interact with DCs (green) as they move throughout the T cell area. Tracks of specific EGFP-OT-II cells are cyan, and tracks of nonspecific ECFP-T cells are purple. Antigen-specific T cells have largely recovered in speed, but still move slightly slower than nonspecific T cells.

Movie 4.4. Priming interactions 1-6 h after T cell transfer. Antigen-specific T cells (orange) move more slowly than nonspecific T cells (red) and are more frequently arrested on DCs (green). Tracks of specific EGFP-OT-II cells are cyan, and tracks of nonspecific ECFP-T cells are purple.

Movie 4.5. Priming interactions 6-12 h after T cell transfer. Antigen-specific T cells (orange) move more slowly than nonspecific T cells (red) and are more frequently arrested on DCs (green). Tracks of specific EGFP-OT-II cells are cyan, and tracks of nonspecific ECFP-T cells are purple. EGFP-OT-II cells are equally arrested at 6-12 h as they are at 1-6 h after transfer.

Movie 4.6. Priming interactions 12-18 h after T cell transfer. Antigen-specific T cells (orange) move more slowly than nonspecific T cells (red) and are more frequently

arrested on DCs (green). Tracks of specific EGFP-OT-II cells are cyan, and tracks of nonspecific ECFP-T cells are purple. EGFP-OT-II cells have partially recovered in speed, but are still more arrested than the nonspecific ECFP-T cells.

Movie 4.7. T cell swarming. This phenomenon is relatively rare with antigen targeted to DEC-205, as compared to cell-bound antigen delivered by a small fraction of APCs in the lymph node. The swarm seen here is composed of antigen-specific EGFP-OT-II T cells (orange) and not wild-type ECFP T cells (red).

Movie 4.8. T cell arrest on fluorescent and non-fluorescent dendritic cells. T cell arrest on EYFP- cells was often observed. This may reflect DCs that express relatively low levels of EYFP or processes of $EYFP^+$ DCs too thin to be visualized by multiphoton microscopy. The rightmost T cell is seen contacting an $EYFP^+$ DC, then detaching and arresting nearby, possibly on the surface of a non-fluorescent APC.

Movie 5.1. T cells arrest upon recognizing the high-potency pMHC L98A. Two-photon visualization of T cell motility in a representative lymph node of a CD11c-EYFP mouse injected 6-9 hours earlier with the high-potency construct α-Dec-L98A. Shown is a maximum intensity projection of a 50 μm-thick volume. Antigen-specific AND T cells which express ECFP (pseudo-colored red) move more slowly than non-specific T cells (EGFP, pseudo-colored orange), and are more frequently decelerated on dendritic cells (EYFP, pseudo-colored green). The sequence is repeated with tracks of specific ECFP-AND cells indicated in cyan, and tracks of nonspecific EGFP-T cells shown in magenta. Time elapsed is in minutes: seconds.

Movie 5.2. T cells do not arrest upon recognizing the medium-potency pMHC Y97K. A representative lymph node of a mouse similarly treated with the medium-potency α-Dec-Y97K, visualized as in **Movie 5.1**. Antigen-specific T cells move as fast as non-specific T cells, and interact similarly with dendritic cells.

Movie 5.3. T cells do not arrest upon recognizing the low-potency pMHC T102L.A representative lymph node of a mouse similarly treated with the low-potency α-Dec-T102L, visualized as in **Movie 5.1**. Antigen-specific T cells move as fast as non-specific T cells, and interact similarly with dendritic cells.

Movie 5.4. *In vitro* Ca^{2+} flux in response to unloaded GPI–I-E^k. Calcium signaling and migration on glass supported bilayers. In vitro activated AND T cells were labeled with Fura-2 and were imaged every 15 seconds. The images on the left are pseudo-colored ratio images representing Fura-2 ratios, such that purple corresponds to a ratio of 0.2 and red corresponds to a ratio of 1.0. The images on the right are generated using Interference Reflection Microscopy and the dark areas represent cells making contact with the bilayer substrate. The bilayer in this sequence contains 50 molecules/ μm^2 of unloaded GPI–I-E^k and 300 molecules / μm^2 of GPI–ICAM-1. Only the cells making contacts are quantified. Scale bar equals 10 μm.

Movie 5.5. *In vitro* Ca^{2+} flux in response to L98A. Calcium signaling and migration on glass supported bilayers. In vitro activated AND T cells were labeled with Fura-2 and were imaged every 15 seconds. The images on the left are pseudo-colored ratio images representing Fura-2 ratios, such that purple corresponds to a ratio of 0.2 and red corresponds to a ratio of 1.0. The images on the right are generated using Interference Reflection Microscopy (IRM) and the dark areas represent cells making contact with the bilayer substrate. The bilayer in this sequence contains 10 molecules/ μm^2 of L98A loaded GPI–I-E^k and 300 molecules / μm^2 of GPI–ICAM-1. High calcium fluxes are observed as soon as cells make contact, and calcium levels are sustained for long periods of time. Only the cells making contact are quantified. Scale bar equals 10 μm.

Movie 5.6. *In vitro* Ca^{2+} flux in response to Y97K. Calcium signaling and migration on glass supported bilayers. This movie was acquired using similar conditions as in **Movie 5.5**, except that the bilayer contains 10 molecules/ μm^2 of Y97K loaded GPI–I-E^k and 300 molecules / μm^2 of GPI–ICAM-1. Only the cells making IRMs are quantified. Scale bar equals 10 μm.

Movie 5.7. *In vitro* Ca^{2+} flux in response to T102L. Calcium signaling and migration on glass supported bilayers. This movie was acquired using similar conditions as in **Movie 5.5**, except that the bilayer contains 10 molecules/ μm^2 of T102L loaded GPI–I-E^k and 300 molecules / μm^2 of GPI–ICAM-1. Only the cells making contacts are quantified. Scale bar equals 10 μm.

Movie 5.8. In vivo Ca^{2+} flux in response to α-Dec-L98A. Confocal visualization of Ca^{2+} response in a representative lymph node of a B10BR mouse injected 5 hours earlier with the high-potency construct α-Dec-L98A. Intravital images were acquired between 0 and 2 h after cell transfer. Shown is a maximum intensity projection of a 20 μm-thick volume. Blood flow is visualized by Alexa-647 70 Kd dextran administration (pseudo-colored blue). Antigen-specific AND T cells labeled with CMRA (red). Cells were co-labeled with Fluo-4, a calcium sensitive dye (green). Increases in Fluo-4 fluorescence indicate high Ca^{2+} levels. Shown here, high Fluo-4 fluorescence intensity occurs as AND

T cells exit the blood vessel, appears as yellow/orange when overlapping with the cytoplasmic dye.

Movie 5.9. In vivo Ca^{2+} flux in response to α-Dec-Y97K. Confocal visualization of Ca^{2+} response in a representative lymph node of a B10BR mouse injected 5 h earlier with the medium-potency construct α-Dec-Y97K. As described in **Movie 5.8**.

Movie 5.10. In vivo Ca^{2+} flux in response to α-Dec-T102L. Confocal visualization of Ca^{2+} response in a representative lymph node of a B10BR mouse injected 5 h earlier with the low-potency construct α-Dec-T102L. As described in **Movie 5.8**.

Movie 5.11. In vivo Ca^{2+} flux in untreated control. Confocal visualization of Ca^{2+} response in a representative lymph node of a B10BR mouse used as untreated control. As described in **Movie 5.8**.

Movie 6.1. Overview of a germinal center. Intravital imaging of a GC in the inguinal LN, with collagen fibers in the capsule visible in blue, $EGFP^+$ B1-8^{hi} B cells in green, and FDCs in red, labeled by s.c. injection of Alexa 647-labeled FDC-M1 antibody. The GC is in the center of the field, surrounded by the B cell follicle; plasmablasts are visible in the medulla in the lower half of the field.

Movie 6.2. Dynamics of GC B cells. Intravital imaging of a GC in the inguinal LN 6 d post-boost with NP, with $ECFP^+$ nontransgenic control B cells in blue, $EGFP^+$ B1-8^{hi} B cells in cyan, and FDCs in red, as in **Movie 6.1**. Note that GC B cells are largely restricted to the center of the GC, while control B cells move freely.

Movie 6.3. Dynamics of GC B cells without antigen boost. Intravital imaging of a GC in the inguinal LN, without antigen boost, with $ECFP^+$ nontransgenic control B cells in blue, $EGFP^+$ B1-8^{hi} B cells in cyan, and FDCs in red, as in **Movie 6.1**. Both nontransgenic and B1-8^{hi} B cells move freely in the absence of NP antigen.

Movie 6.4. GC without FDC labeling. Intravital imaging of a GC in the inguinal LN 6 d post-boost with NP, with $ECFP^+$ nontransgenic control B cells in blue, and $EGFP^+$ B1-8^{hi} B cells in cyan. Note that GC B cells are largely restricted to the center of the GC, while control B cells move freely.

Movie 6.5. Dynamics of B1-8^{hi} B cell:FDC contacts. Intravital imaging of a GC in the inguinal LN 6 d post-boost with NP, with $ECFP^+$ nontransgenic control B cells in blue, $EGFP^+$ B1-8^{hi} B cells in green, and FDCs in red, as in **Movie 6.1**. The track of a B1-8^{hi} B cell is denoted in green, repeatedly making brief contacts with the FDC.

Movie 6.6. Dynamics of nontransgenic B cell:FDC contacts. Intravital imaging of a GC in the inguinal LN 6 d post-boost with NP, with $ECFP^+$ nontransgenic control B cells in blue, $EGFP^+$ B1-8^{hi} B cells in green, and FDCs in red, as in **Movie 6.1**. The track of a nontransgenic control B cell is denoted in blue, and is not notably associated with FDCs.

References

Abbas, A. K., Murphy, K. M., and Sher, A. (1996). Functional diversity of helper T lymphocytes. Nature *383*, 787-793.

Agace, W. W. (2006). Tissue-tropic effector T cells: generation and targeting opportunities. Nat Rev Immunol *6*, 682-692.

Alam, S. M., Travers, P. J., Wung, J. L., Nasholds, W., Redpath, S., Jameson, S. C., and Gascoigne, N. R. (1996). T-cell-receptor affinity and thymocyte positive selection. Nature *381*, 616-620.

Allan, R. S., Smith, C. M., Belz, G. T., van Lint, A. L., Wakim, L. M., Heath, W. R., and Carbone, F. R. (2003). Epidermal viral immunity induced by CD8alpha+ dendritic cells but not by Langerhans cells. Science *301*, 1925-1928.

Allan, R. S., Waithman, J., Bedoui, S., Jones, C. M., Villadangos, J. A., Zhan, Y., Lew, A. M., Shortman, K., Heath, W. R., and Carbone, F. R. (2006). Migratory Dendritic Cells Transfer Antigen to a Lymph Node-Resident Dendritic Cell Population for Efficient CTL Priming. Immunity *25*, 153-162.

Allen, C. D., Ansel, K. M., Low, C., Lesley, R., Tamamura, H., Fujii, N., and Cyster, J. G. (2004). Germinal center dark and light zone organization is mediated by CXCR4 and CXCR5. Nat Immunol *5*, 943-952.

Allen, C. D., Okada, T., Tang, H. L., and Cyster, J. G. (2007). Imaging of germinal center selection events during affinity maturation. Science *315*, 528-531.

Anderson, D. C., Schmalstieg, F. C., Arnaout, M. A., Kohl, S., Tosi, M. F., Dana, N., Buffone, G. J., Hughes, B. J., Brinkley, B. R., Dickey, W. D., and et al. (1984). Abnormalities of polymorphonuclear leukocyte function associated with a heritable deficiency of high molecular weight surface glycoproteins (GP138): common relationship to diminished cell adherence. J Clin Invest *74*, 536-551.

Anderson, M. S., Venanzi, E. S., Klein, L., Chen, Z., Berzins, S. P., Turley, S. J., von Boehmer, H., Bronson, R., Dierich, A., Benoist, C., and Mathis, D. (2002). Projection of an immunological self shadow within the thymus by the aire protein. Science *298*, 1395-1401.

Bajenoff, M., Egen, J. G., Koo, L. Y., Laugier, J. P., Brau, F., Glaichenhaus, N., and Germain, R. N. (2006). Stromal cell networks regulate lymphocyte entry, migration, and territoriality in lymph nodes. Immunity *25*, 989-1001.

Bajenoff, M., Granjeaud, S., and Guerder, S. (2003). The strategy of T cell antigen-presenting cell encounter in antigen-draining lymph nodes revealed by imaging of initial T cell activation. J Exp Med *198*, 715-724.

Banchereau, J., Pascual, V., and Palucka, K. A. (2004). Autoimunity through cytokine-induced dendritic cell activation. Immunity *20*, 539-550.

Belz, G. T., Behrens, G. M., Smith, C. M., Miller, J. F., Jones, C., Lejon, K., Fathman, C. G., Mueller, S. N., Shortman, K., Carbone, F. R., and Heath, W. R. (2002). The CD8alpha(+) dendritic cell is responsible for inducing peripheral self-tolerance to tissue-associated antigens. Journal of Experimental Medicine *196*, 1099-1104.

Belz, G. T., Smith, C. M., Kleinert, L., Reading, P., Brooks, A., Shortman, K., Carbone, F. R., and Heath, W. R. (2004). Distinct migrating and nonmigrating dendritic cell populations are involved in MHC class I-restricted antigen presentation after lung infection with virus. Proceedings of the National Academy of Sciences of the United States of America *101*, 8670-8675.

Bennett, C. L., Christie, J., Ramsdell, F., Brunkow, M. E., Ferguson, P. J., Whitesell, L., Kelly, T. E., Saulsbury, F. T., Chance, P. F., and Ochs, H. D. (2001). The immune dysregulation, polyendocrinopathy, enteropathy, X-linked syndrome (IPEX) is caused by mutations of FOXP3. Nat Genet *27*, 20-21.

Benvenuti, F., Hugues, S., Walmsley, M., Ruf, S., Fetler, L., Popoff, M., Tybulewicz, V. L., and Amigorena, S. (2004). Requirement of Rac1 and Rac2 expression by mature dendritic cells for T cell priming. Science *305*, 1150-1153.

Berg, E. L., Robinson, M. K., Warnock, R. A., and Butcher, E. C. (1991). The human peripheral lymph node vascular addressin is a ligand for LECAM-1, the peripheral lymph node homing receptor. J Cell Biol *114*, 343-349.

Bhakta, N. R., Oh, D. Y., and Lewis, R. S. (2005). Calcium oscillations regulate thymocyte motility during positive selection in the three-dimensional thymic environment. Nat Immunol *6*, 143-151.

Billingham, R. E., Brent, L., and Medawar, P. B. (1953). Actively acquired tolerance of foreign cells. Nature *172*, 603-606.

Bjorses, P., Halonen, M., Palvimo, J. J., Kolmer, M., Aaltonen, J., Ellonen, P., Perheentupa, J., Ulmanen, I., and Peltonen, L. (2000). Mutations in the AIRE gene: effects on subcellular location and transactivation function of the autoimmune polyendocrinopathy-candidiasis-ectodermal dystrophy protein. Am J Hum Genet *66*, 378-392.

Blander, J. M., and Medzhitov, R. (2004). Regulation of phagosome maturation by signals from toll-like receptors. Science *304*, 1014-1018.

Blander, J. M., and Medzhitov, R. (2006). Toll-dependent selection of microbial antigens for presentation by dendritic cells. Nature *440*, 808-812.

Bonifaz, L., Bonnyay, D., Mahnke, K., Rivera, M., Nussenzweig, M. C., and Steinman, R. M. (2002). Efficient targeting of protein antigen to the dendritic cell receptor DEC-205 in the steady state leads to antigen presentation on major histocompatibility complex class I products and peripheral CD8+ T cell tolerance. Journal of Experimental Medicine *196*, 1627-1638.

Bonifaz, L. C., Bonnyay, D. P., Charalambous, A., Darguste, D. I., Fujii, S., Soares, H., Brimnes, M. K., Moltedo, B., Moran, T. M., and Steinman, R. M. (2004). In vivo targeting of antigens to maturing dendritic cells via the DEC-205 receptor improves T cell vaccination. J Exp Med *199*, 815-824.

Bousso, P., and Robey, E. (2003). Dynamics of CD8+ T cell priming by dendritic cells in intact lymph nodes. Nat Immunol *4*, 579-585.

Bowen, T. J., Ochs, H. D., Altman, L. C., Price, T. H., Van Epps, D. E., Brautigan, D. L., Rosin, R. E., Perkins, W. D., Babior, B. M., Klebanoff, S. J., and Wedgwood, R. J. (1982). Severe recurrent bacterial infections associated with defective adherence and chemotaxis in two patients with neutrophils deficient in a cell-associated glycoprotein. J Pediatr *101*, 932-940.

Brack, C., Hirama, M., Lenhard-Schuller, R., and Tonegawa, S. (1978). A complete immunoglobulin gene is created by somatic recombination. Cell *15*, 1-14.
Bretscher, P., and Cohn, M. (1970). A theory of self-nonself discrimination. Science *169*, 1042-1049.

Brimnes, M. K., Bonifaz, L., Steinman, R. M., and Moran, T. M. (2003). Influenza virus-induced dendritic cell maturation is associated with the induction of strong T cell immunity to a coadministered, normally nonimmunogenic protein. J Exp Med *198*, 133-144.

Brocker, T., Riedinger, M., and Karjalainen, K. (1997). Driving gene expression specifically in dendritic cells. Advances in Experimental Medicine and Biology *417*, 55-57.

Brunkow, M. E., Jeffery, E. W., Hjerrild, K. A., Paeper, B., Clark, L. B., Yasayko, S. A., Wilkinson, J. E., Galas, D., Ziegler, S. F., and Ramsdell, F. (2001). Disruption of a new forkhead/winged-helix protein, scurfin, results in the fatal lymphoproliferative disorder of the scurfy mouse. Nat Genet *27*, 68-73.

Bujdoso, R., Hopkins, J., Dutia, B. M., Young, P., and McConnell, I. (1989). Characterization of sheep afferent lymph dendritic cells and their role in antigen carriage. Journal of Experimental Medicine *170*, 1285-1301.

Burnet, F. M. (1959). The Clonal Selection Theory of Acquired Immunity. Cambridge *The University Press.*

Campbell, D. J., and Butcher, E. C. (2002). Rapid acquisition of tissue-specific homing phenotypes by CD4(+) T cells activated in cutaneous or mucosal lymphoid tissues. J Exp Med *195*, 135-141.

Campbell, D. J., Kim, C. H., and Butcher, E. C. (2001). Separable effector T cell populations specialized for B cell help or tissue inflammation. Nat Immunol *2*, 876-881.

Campbell, J. J., Bowman, E. P., Murphy, K., Youngman, K. R., Siani, M. A., Thompson, D. A., Wu, L., Zlotnik, A., and Butcher, E. C. (1998a). 6-C-kine (SLC), a lymphocyte adhesion-triggering chemokine expressed by high endothelium, is an agonist for the MIP-3beta receptor CCR7. J Cell Biol *141*, 1053-1059.

Campbell, J. J., Hedrick, J., Zlotnik, A., Siani, M. A., Thompson, D. A., and Butcher, E. C. (1998b). Chemokines and the arrest of lymphocytes rolling under flow conditions. Science *279*, 381-384.

Castellino, F., Huang, A. Y., Altan-Bonnet, G., Stoll, S., Scheinecker, C., and Germain, R. N. (2006). Chemokines enhance immunity by guiding naive CD8+ T cells to sites of CD4+ T cell-dendritic cell interaction. Nature *440*, 890-895.

Celsus, A. C. a., and Spencer, W. t. (1938). De Medicina. Harvard University Press.

Cemerski, S., Das, J., Locasale, J., Arnold, P., Giurisato, E., Markiewicz, M. A., Fremont, D., Allen, P. M., Chakraborty, A. K., and Shaw, A. S. (2007). The stimulatory potency of T cell antigens is influenced by the formation of the immunological synapse. Immunity *26*, 345-355.

Chatila, T. A., Blaeser, F., Ho, N., Lederman, H. M., Voulgaropoulos, C., Helms, C., and Bowcock, A. M. (2000). JM2, encoding a fork head-related protein, is mutated in X-linked autoimmunity-allergic disregulation syndrome. J Clin Invest *106*, R75-81.

Consortium, T. F.-G. A. (1997). An autoimmune disease, APECED, caused by mutations in a novel gene featuring two PHD-type zinc-finger domains. The Finnish-German APECED Consortium. Autoimmune Polyendocrinopathy-Candidiasis-Ectodermal Dystrophy. Nat Genet *17*, 399-403.

Croft, M., Duncan, D. D., and Swain, S. L. (1992). Response of naive antigen-specific CD4+ T cells in vitro: characteristics and antigen-presenting cell requirements. J Exp Med *176*, 1431-1437.

Crowley, C. A., Curnutte, J. T., Rosin, R. E., Andre-Schwartz, J., Gallin, J. I., Klempner, M., Snyderman, R., Southwick, F. S., Stossel, T. P., and Babior, B. M. (1980). An

inherited abnormality of neutrophil adhesion. Its genetic transmission and its association with a missing protein. N Engl J Med *302*, 1163-1168.

Crowley, M., Inaba, K., and Steinman, R. M. (1990). Dendritic cells are the principal cells in mouse spleen bearing immunogenic fragments of foreign proteins. Journal of Experimental Medicine *172*, 383-386.

Cyster, J. G. (1999). Chemokines and the homing of dendritic cells to the T cell areas of lymphoid organs. Journal of Experimental Medicine *189*, 447-450.

Dana, N., Todd, R. F., 3rd, Pitt, J., Springer, T. A., and Arnaout, M. A. (1984). Deficiency of a surface membrane glycoprotein (Mo1) in man. J Clin Invest *73*, 153-159.

Daniels, M. A., Teixeiro, E., Gill, J., Hausmann, B., Roubaty, D., Holmberg, K., Werlen, G., Hollander, G. A., Gascoigne, N. R., and Palmer, E. (2006). Thymic selection threshold defined by compartmentalization of Ras/MAPK signalling. Nature *444*, 724-729.

Denk, W., Strickler, J. H., and Webb, W. W. (1990). Two-photon laser scanning fluorescence microscopy. Science *248*, 73-76.

Di Noia, J., and Neuberger, M. S. (2002). Altering the pathway of immunoglobulin hypermutation by inhibiting uracil-DNA glycosylase. Nature *419*, 43-48.

Dudziak, D., Kamphorst, A. O., Heidkamp, G. F., Buchholz, V. R., Trumpfheller, C., Yamazaki, S., Cheong, C., Liu, K., Lee, H. W., Park, C. G., *et al.* (2007). Differential antigen processing by dendritic cell subsets in vivo. Science *315*, 107-111.

Dustin, M. L. (2008). T-cell activation through immunological synapses and kinapses. Immunol Rev *221*, 77-89.

Dustin, M. L., Tseng, S. Y., Varma, R., Campi, G. (2006) T cell-dendritic cell immunological synapses. Curr Opin Immunol *18*, 512-516.

Dustin, M. L., Rothlein, R., Bhan, A. K., Dinarello, C. A., and Springer, T. A. (1986). Induction by IL-1 and interferon, tissue distribution, biochemistry, and function of a natural adherence molecule (ICAM-1). Journal of Immunology *137*, 245-254.

Efron, B., and . (1979). Bootstrap methods: another look at the jackknife. Ann Statist *7*, 1-26.

Etzioni, A., Frydman, M., Pollack, S., Avidor, I., Phillips, M. L., Paulson, J. C., and Gershoni-Baruch, R. (1992). Brief report: recurrent severe infections caused by a novel leukocyte adhesion deficiency. N Engl J Med *327*, 1789-1792.

Etzioni, A., and Harlan, J. M. (1999). Cell adhesion and leukocyte adhesion defects. In: Ochs, H D; Smith, C I E; Puck, J M (eds) : Primary Immunodeficiency Diseases: A Molecular and Genetic Approach *New York: Oxford University Press*, 375-388.

Evavold, B. D., and Allen, P. M. (1991). Separation of IL-4 production from Th cell proliferation by an altered T cell receptor ligand. Science *252*, 1308-1310.

Finkelman, F. D., Lees, A., Birnbaum, R., Gause, W. C., and Morris, S. C. (1996). Dendritic cells can present antigen in vivo in a tolerogenic or immunogenic fashion. J Immunol *157*, 1406-1414.

Fleeton, M. N., Contractor, N., Leon, F., Wetzel, J. D., Dermody, T. S., and Kelsall, B. L. (2004). Peyer's patch dendritic cells process viral antigen from apoptotic epithelial cells in the intestine of reovirus-infected mice. J Exp Med *200*, 235-245.

Frydman, M., Etzioni, A., Eidlitz-Markus, T., Avidor, I., Varsano, I., Shechter, Y., Orlin, J. B., and Gershoni-Baruch, R. (1992). Rambam-Hasharon syndrome of psychomotor retardation, short stature, defective neutrophil motility, and Bombay phenotype. Am J Med Genet *44*, 297-302.

Garside, P., Ingulli, E., Merica, R. R., Johnson, J. G., Noelle, R. J., and Jenkins, M. K. (1998). Visualization of specific B and T lymphocyte interactions in the lymph node. Science *281*, 96-99.

Gavin, A. L., Hoebe, K., Duong, B., Ota, T., Martin, C., Beutler, B., and Nemazee, D. (2006). Adjuvant-enhanced antibody responses in the absence of toll-like receptor signaling. Science *314*, 1936-1938.

Geener, B. M., and Gowans, J. L. (1962). The output of lymphocytes from the thoracic duct of unanesthetized mice. Br J Exp Path *43*, 424.

Germain, R. N., Miller, M. J., Dustin, M. L., and Nussenzweig, M. C. (2006). Dynamic imaging of the immune system: progress, pitfalls and promise. Nat Rev Immunol *6*, 497-507.

Girard, J.-P., and Springer, T. A. (1996). High endothelial venules (HEVs): Specialized endothelium for lymphocyte migration. Immunol Today *16*, 449-457.

Göppert-Mayer, M. (1931). Ueber Elementarakte mit zwei Quantensprungen. Annalen der Physik *9*, 273-294.

Gowans, J. L., and Knight, E. J. (1964). The Route of Re-circulation of Lymphocytes in the Rat. Proc R Soc Lond B Biol Sci *159*, 257-282.

Guermonprez, P., Valladeau, J., Zitvogel, L., Thery, C., and Amigorena, S. (2002). Antigen presentation and T cell stimulation by dendritic cells. Annual Review of Immunology *20*, 621-667.

Gunn, M. D., Tangemann, K., Tam, C., Cyster, J. G., Rosen, S. D., and Williams, L. T. (1998). A chemokine expressed in lymphoid high endothelial venules promotes the adhesion and chemotaxis of naive T lymphocytes. Proc Natl Acad Sci U S A *95*, 258-263.

Gunzer, M., Schafer, A., Borgmann, S., Grabbe, S., Zanker, K. S., Brocker, E. B., Kampgen, E., and Friedl, P. (2000). Antigen presentation in extracellular matrix: interactions of T cells with dendritic cells are dynamic, short lived, and sequential. Immunity *13*, 323-332.

Gunzer, M., Weishaupt, C., Hillmer, A., Basoglu, Y., Friedl, P., Dittmar, K. E., Kolanus, W., Varga, G., and Grabbe, S. (2004). A spectrum of biophysical interaction modes between T cells and different antigen-presenting cells during priming in 3-D collagen and in vivo. Blood *104*, 2801-2809.

Hadjantonakis, A. K., Macmaster, S., and Nagy, A. (2002). Embryonic stem cells and mice expressing different GFP variants for multiple non-invasive reporter usage within a single animal. BMC Biotechnol *2*, 11.

Hamann, A., Andrew, D. P., Jablonski-Westrich, D., Holzmann, B., and Butcher, E. C. (1994). Role of alpha 4-integrins in lymphocyte homing to mucosal tissues in vivo. J Immunol *152*, 3282-3293.

Hamann, A., Jablonski-Westrich, D., Duijvestijn, A., Butcher, E. C., Baisch, H., Harder, R., and Thiele, H. G. (1988). Evidence for an accessory role of LFA-1 in lymphocyte-high endothelium interaction during homing. J Immunol *140*, 693-699.

Hanna, M. G., Jr. (1964). An Autoradiographic Study of the Germinal Center in Spleen White Pulp During Early Intervals of the Immune Response. Lab Invest *13*, 95-104.

Hauser, A. E., Junt, T., Mempel, T. R., Sneddon, M. W., Kleinstein, S. H., Henrickson, S. E., von Andrian, U. H., Shlomchik, M. J., and Haberman, A. M. (2007). Definition of germinal-center B cell migration in vivo reveals predominant intrazonal circulation patterns. Immunity *26*, 655-667.

Hawiger, D., Inaba, K., Dorsett, Y., Guo, M., Mahnke, K., Rivera, M., Ravetch, J. V., Steinman, R. M., and Nussenzweig, M. C. (2001). Dendritic cells induce peripheral T cell unresponsiveness under steady state conditions in vivo. J Exp Med *194*, 769-779.

Hawiger, D., Masilamani, R., Betelli, E., Kuchroo, V. J., and Nussenzweig, M. C. (2004). Immunological Unresponsiveness Characterized by Increased Expression of CD5 on Peripheral T cells Induced by Dendritic Cells In Vivo. Immunity *20*, 695-705.

Henrickson, S. E., Mempel, T. R., Mazo, I. B., Liu, B., Artyomov, M. N., Zheng, H., Peixoto, A., Flynn, M. P., Senman, B., Junt, T., *et al.* (2008). T cell sensing of antigen dose governs interactive behavior with dendritic cells and sets a threshold for T cell activation. Nat Immunol *9*, 282-291.

Henrickson, S. E., and von Andrian, U. H. (2007). Single-cell dynamics of T-cell priming. Curr Opin Immunol *19*, 249-258.

Himmelweit, F. (1956-1960). Collected papers of paul ehrlich. Pergamon, London.

Holick, M. F., MacLaughlin, J. A., Clark, M. B., Holick, S. A., Potts, J. T., Jr., Anderson, R. R., Blank, I. H., Parrish, J. A., and Elias, P. (1980). Photosynthesis of previtamin D3 in human skin and the physiologic consequences. Science *210*, 203-205.

Holt, P. G., Schon-Hegrad, M. A., and Oliver, J. (1988). MHC class II antigen-bearing dendritic cells in pulmonary tissues of the rat. Regulation of antigen presentation activity by endogenous macrophage populations. Journal of Experimental Medicine *167*, 262-274.

Homey, B., Alenius, H., Muller, A., Soto, H., Bowman, E. P., Yuan, W., McEvoy, L., Lauerma, A. I., Assmann, T., Bunemann, E., *et al.* (2002). CCL27-CCR10 interactions regulate T cell-mediated skin inflammation. Nat Med *8*, 157-165.

Hori, S., Nomura, T., and Sakaguchi, S. (2003). Control of regulatory T cell development by the transcription factor Foxp3. Science *299*, 1057-1061.

Hoshino, K., Takeuchi, O., Kawai, T., Sanjo, H., Ogawa, T., Takeda, Y., Takeda, K., and Akira, S. (1999). Cutting edge: Toll-like receptor 4 (TLR4)-deficient mice are hyporesponsive to lipopolysaccharide: evidence for TLR4 as the Lps gene product. J Immunol *162*, 3749-3752.

Hozumi, N., and Tonegawa, S. (1976). Evidence for somatic rearrangement of immunoglobulin genes coding for variable and constant regions. Proc Natl Acad Sci U S A *73*, 3628-3632.

Huang, A. Y., Qi, H., and Germain, R. N. (2004). Illuminating the landscape of in vivo immunity: insights from dynamic in situ imaging of secondary lymphoid tissues. Immunity *21*, 331-339.

Huang, F. P., Platt, N., Wykes, M., Major, J. R., Powell, T. J., Jenkins, C. D., and MacPherson, G. G. (2000). A discrete subpopulation of dendritic cells transports apoptotic intestinal epithelial cells to T cell areas of mesenteric lymph nodes. J Exp Med *191*, 435-444.

Hugues, S., Fetler, L., Bonifaz, L., Helft, J., Amblard, F., and Amigorena, S. (2004). Distinct T cell dynamics in lymph nodes during the induction of tolerance and immunity. Nat Immunol *5*, 1235-1242.

Iezzi, G., Karjalainen, K., and Lanzavecchia, A. (1998). The duration of antigenic stimulation determines the fate of naive and effector T cells. Immunity *8*, 89-95.

Idoyaga, J., Cheong, C., Suda, K., Suda, N., Kim, J. Y., Lee, H., Park, C. G., and Steinman, R. M. (2008). Cutting Edge: Langerin/CD207 Receptor on Dendritic Cells Mediates Efficient Antigen Presentation on MHC I and II Products In Vivo. J Immunol *180*, 3647-3650.

Inaba, K., Pack, M., Inaba, M., Sakuta, H., Isdell, F., and Steinman, R. M. (1997). High levels of a major histocompatibility complex II-self peptide complex on dendritic cells from the T cell areas of lymph nodes. Journal of Experimental Medicine *186*, 665-672.

Inaba, K., Turley, S., Yamaide, F., Iyoda, T., Mahnke, K., Inaba, M., Pack, M., Subklewe, M., Sauter, B., Sheff, D., *et al.* (1998). Efficient presentation of phagocytosed cellular fragments on the major histocompatibility complex class II products of dendritic cells. Journal of Experimental Medicine *188*, 2163-2173.

Inohara, N., and Nunez, G. (2003). NODs: intracellular proteins involved in inflammation and apoptosis. Nat Rev Immunol *3*, 371-382.

Itano, A. A., and Jenkins, M. K. (2003). Antigen presentation to naive CD4 T cells in the lymph node. Nat Immunol *4*, 733-739.

Itano, A. A., McSorley, S. J., Reinhardt, R. L., Ehst, B. D., Ingulli, E., Rudensky, A. Y., and Jenkins, M. K. (2003). Distinct dendritic cell populations sequentially present antigen to CD4 T cells and stimulate different aspects of cell-mediated immunity. Immunity *19*, 47-57.

Iwata, M., Hirakiyama, A., Eshima, Y., Kagechika, H., Kato, C., and Song, S. Y. (2004). Retinoic acid imprints gut-homing specificity on T cells. Immunity *21*, 527-538.

Jacob, J., Kassir, R., and Kelsoe, G. (1991a). In situ studies of the primary immune response to (4-hydroxy-3-nitrophenyl)acetyl. I. The architecture and dynamics of responding cell populations. Journal of Experimental Medicine *173*, 1165-1175.

Jacob, J., Kelsoe, G., Rajewsky, K., and Weiss, U. (1991b). Intraclonal generation of antibody mutants in germinal centres. Nature *354*, 389-392.

Jaiswal, A. I., Dubey, C., Swain, S. L., and Croft, M. (1996). Regulation of CD40 ligand expression on naive CD4 T cells: a role for TCR but not co-stimulatory signals. Int Immunol *8*, 275-285.

Janeway, C., Travers, P., Walport, M., and Shlomchik, M. (2001). Immunobiology: Fifth edition. New York and London: Garland Science.

Janeway, C. A., Jr. (1989). Approaching the asymptote? Evolution and revolution in immunology. Cold Spring Harb Symp Quant Biol *54 Pt 1*, 1-13.

Janeway, C. A., Jr., and Medzhitov, R. (2002). Innate immune recognition. Annu Rev Immunol *20*, 197-216.

Jenkins, M. K., Pardoll, D. M., Mizuguchi, J., Quill, H., and Schwartz, R. H. (1987). T-cell unresponsiveness in vivo and in vitro: fine specificity of induction and molecular characterization of the unresponsive state. Immunol Rev *95*, 113-135.

Jenkins, M. K., and Schwartz, R. H. (1987). Antigen presentation by chemically modified splenocytes induces antigen-specific T cell unresponsiveness in vitro and in vivo. J Exp Med *165*, 302-319.

Jerne, N. K. (1955). The Natural-Selection Theory of Antibody Formation. Proc Natl Acad Sci U S A *41*, 849-857.

Kaiser, W., and Garrett, C. (1961). Two-photon excitation in CaF2:Eu2+. Phys Rev Lett *7*, 229.

Kang, Y. S., Yamazaki, S., Iyoda, T., Pack, M., Bruening, S. A., Kim, J. Y., Takahara, K., Inaba, K., Steinman, R. M., and Park, C. G. (2003). SIGN-R1, a novel C-type lectin expressed by marginal zone macrophages in spleen, mediates uptake of the polysaccharide dextran. International Immunology *15*, 177-186.

Kantele, A., Zivny, J., Hakkinen, M., Elson, C. O., and Mestecky, J. (1999). Differential homing commitments of antigen-specific T cells after oral or parenteral immunization in humans. J Immunol *162*, 5173-5177.

Karsan, A., Cornejo, C. J., Winn, R. K., Schwartz, B. R., Way, W., Lannir, N., Gershoni-Baruch, R., Etzioni, A., Ochs, H. D., and Harlan, J. M. (1998). Leukocyte Adhesion Deficiency Type II is a generalized defect of de novo GDP-fucose biosynthesis. Endothelial cell fucosylation is not required for neutrophil rolling on human nonlymphoid endothelium. J Clin Invest *101*, 2438-2445.

Katakai, T., Hara, T., Sugai, M., Gonda, H., and Shimizu, A. (2004). Lymph node fibroblastic reticular cells construct the stromal reticulum via contact with lymphocytes. J Exp Med *200*, 783-795.

Kaye, J., Hsu, M. L., Sauron, M. E., Jameson, S. C., Gascoigne, N. R., and Hedrick, S. M. (1989). Selective development of CD4+ T cells in transgenic mice expressing a class II MHC-restricted antigen receptor. Nature *341*, 746-749.

Kelsoe, G. (1996). Life and death in germinal centers (redux). Immunity *4*, 107-111.

Kim, C. H., Rott, L. S., Clark-Lewis, I., Campbell, D. J., Wu, L., and Butcher, E. C. (2001). Subspecialization of CXCR5+ T cells: B helper activity is focused in a germinal center-localized subset of CXCR5+ T cells. J Exp Med *193*, 1373-1381.

Kim, J. M., and Rudensky, A. (2006). The role of the transcription factor Foxp3 in the development of regulatory T cells. Immunol Rev *212*, 86-98.

Kirberg, J., Berns, A., and von Boehmer, H. (1997). Peripheral T cell survival requires continual ligation of the T cell receptor to major histocompatibility complex-encoded molecules. Journal of Experimental Medicine *186*, 1269-1275.

Kissenpfennig, A., Henri, S., Dubois, B., Laplace-Builhe, C., Perrin, P., Romani, N., Tripp, C. H., Douillard, P., Leserman, L., Kaiserlian, D., *et al.* (2005). Dynamics and function of Langerhans cells in vivo dermal dendritic cells colonize lymph node areas distinct from slower migrating Langerhans cells. Immunity *22*, 643-654.

Klonowski, K. D., Williams, K. J., Marzo, A. L., Blair, D. A., Lingenheld, E. G., and Lefrancois, L. (2004). Dynamics of blood-borne CD8 memory T cell migration in vivo. Immunity *20*, 551-562.

Kosco, M. H., Pflugfelder, E., and Gray, D. (1992). Follicular dendritic cell-dependent adhesion and proliferation of B cells in vitro. J Immunol *148*, 2331-2339.

Kosco, M. H., Szakal, A. K., and Tew, J. G. (1988). In vivo obtained antigen presented by germinal center B cells to T cells in vitro. J Immunol *140*, 354-360.

Kosco-Vilbois, M. H. (2003). Are follicular dendritic cells really good for nothing? Nat Rev Immunol *3*, 764-769.

Kretschmer, K., Apostolou, I., Hawiger, D., Khazaie, K., Nussenzweig, M. C., and von Boehmer, H. (2005). Inducing and expanding regulatory T cell populations by foreign antigen. Nat Immunol *6*, 1219-1227.

Kroese, F. G., Wubbena, A. S., Seijen, H. G., and Nieuwenhuis, P. (1987). Germinal centers develop oligoclonally. Eur J Immunol *17*, 1069-1072.

Kuppers, R., Zhao, M., Hansmann, M. L., and Rajewsky, K. (1993). Tracing B cell development in human germinal centres by molecular analysis of single cells picked from histological sections. Embo J *12*, 4955-4967.

Kwan, J., and Killeen, N. (2004). CCR7 directs the migration of thymocytes into the thymic medulla. J Immunol *172*, 3999-4007.

Lanzavecchia, A., and Sallusto, F. (2001). Regulation of T cell immunity by dendritic cells. Cell *106*, 263-266.

Lederberg, J. (1959). Genes and antibodies. Science *129*, 1649-1653.

Lee, J. W., Epardaud, M., Sun, J., Becker, J. E., Cheng, A. C., Yonekura, A. R., Heath, J. K., and Turley, S. J. (2007). Peripheral antigen display by lymph node stroma promotes T cell tolerance to intestinal self. Nat Immunol *8*, 181-190.

Lemaitre, B., Nicolas, E., Michaut, L., Reichhart, J. M., and Hoffmann, J. A. (1996). The dorsoventral regulatory gene cassette spatzle/Toll/cactus controls the potent antifungal response in Drosophila adults. Cell *86*, 973-983.

Lenschow, D. J., Walunas, T. L., and Bluestone, J. A. (1996). CD28/B7 system of T cell costimulation. Annu Rev Immunol *14*, 233-258.

Leonard, W. J., Depper, J. M., Crabtree, G. R., Rudikoff, S., Pumphrey, J., Robb, R. J., Kronke, M., Svetlik, P. B., Peffer, N. J., Waldmann, T. A., and et al. (1984). Molecular cloning and expression of cDNAs for the human interleukin-2 receptor. Nature *311*, 626-631.

Leonard, W. J., Depper, J. M., Robb, R. J., Waldmann, T. A., and Greene, W. C. (1983). Characterization of the human receptor for T-cell growth factor. Proc Natl Acad Sci U S A *80*, 6957-6961.

Liblau, R., Tournier-Lasserve, E., Maciazek, J., Dumas, G., Siffert, O., Hashim, G., and Bach, M. A. (1991). T cell response to myelin basic protein epitopes in multiple sclerosis patients and healthy subjects. Eur J Immunol *21*, 1391-1395.

Lindquist, R. L., Shakhar, G., Dudziak, D., Wardemann, H., Eisenreich, T., Dustin, M. L., and Nussenzweig, M. C. (2004). Visualizing dendritic cell networks in vivo. Nat Immunol *5*, 1243-1250.

Liston, A., Lesage, S., Wilson, J., Peltonen, L., and Goodnow, C. C. (2003). Aire regulates negative selection of organ-specific T cells. Nat Immunol *4*, 350-354.

Liu, L. M., and MacPherson, G. G. (1993). Antigen acquisition by dendritic cells: intestinal dendritic cells acquire antigen administered orally and can prime naive T cells in vivo. Journal of Experimental Medicine *177*, 1299-1307.

Liu, Y. J. (2001). Dendritic cell subsets and lineages, and their functions in innate and adaptive immunity. Cell *106*, 259-262.

Lyons, D. S., Lieberman, S. A., Hampl, J., Boniface, J. J., Chien, Y., Berg, L. J., and Davis, M. M. (1996). A TCR binds to antagonist ligands with lower affinities and faster dissociation rates than to agonists. Immunity *5*, 53-61.

Mackay, C. R., Marston, W. L., and Dudler, L. (1990). Naive and memory T cells show distinct pathways of lymphocyte recirculation. J Exp Med *171*, 801-817.

MacLaughlin, J. A., Anderson, R. R., and Holick, M. F. (1982). Spectral character of sunlight modulates photosynthesis of previtamin D3 and its photoisomers in human skin. Science *216*, 1001-1003.

MacLennan, I. C. (1994). Germinal centers. Annu Rev Immunol *12*, 117-139.
Madrenas, J., and Germain, R. N. (1996). Variant TCR ligands: new insights into the molecular basis of antigen-dependent signal transduction and T-cell activation. Semin Immunol *8*, 83-101.

Madrenas, J., Wange, R. L., Wang, J. L., Isakov, N., Samelson, L. E., and Germain, R. N. (1995). Zeta phosphorylation without ZAP-70 activation induced by TCR antagonists or partial agonists. Science *267*, 515-518.

Mahnke, K., Qian, Y., Knop, J., and Enk, A. H. (2003). Induction of CD4+/CD25+ regulatory T cells by targeting of antigens to immature dendritic cells. Blood *101*, 4862-4869.

Mandala, S., Hajdu, R., Bergstrom, J., Quackenbush, E., Xie, J., Milligan, J., Thornton, R., Shei, G. J., Card, D., Keohane, C., *et al.* (2002). Alteration of lymphocyte trafficking by sphingosine-1-phosphate receptor agonists. Science *296*, 346-349.

Marchesi, V. T., and Gowans, J. L. (1964). The Migration of Lymphocytes Through the Endothelium of Venules in Lymph Nodes: An Electron Microscope Study. Proc R Soc Lond B Biol Sci *159*, 283-290.

Matloubian, M., Lo, C. G., Cinamon, G., Lesneski, M. J., Xu, Y., Brinkmann, V., Allende, M. L., Proia, R. L., and Cyster, J. G. (2004). Lymphocyte egress from thymus and peripheral lymphoid organs is dependent on S1P receptor 1. Nature *427*, 355-360.

Medzhitov, R., Preston-Hurlburt, P., and Janeway, C. A., Jr. (1997). A human homologue of the Drosophila Toll protein signals activation of adaptive immunity. Nature *388*, 394-397.

Mellman, I., and Steinman, R. M. (2001). Dendritic cells: specialized and regulated antigen processing machines. Cell *106*, 255-258.

Mempel, T. R., Henrickson, S. E., and Von Andrian, U. H. (2004). T-cell priming by dendritic cells in lymph nodes occurs in three distinct phases. Nature *427*, 154-159.

Mempel, T. R., Junt, T., and von Andrian, U. H. (2006a). Rulers over randomness: stroma cells guide lymphocyte migration in lymph nodes. Immunity *25*, 867-869.

Mempel, T. R., Pittet, M. J., Khazaie, K., Weninger, W., Weissleder, R., von Boehmer, H., and von Andrian, U. H. (2006b). Regulatory T cells reversibly suppress cytotoxic T cell function independent of effector differentiation. Immunity *25*, 129-141.

Miller, M. J., Hejazi, A. S., Wei, S. H., Cahalan, M. D., and Parker, I. (2004a). T cell repertoire scanning is promoted by dynamic dendritic cell behavior and random T cell motility in the lymph node. Proceedings of the National Academy of Sciences of the United States of America *101*, 998-1003.

Miller, M. J., Safrina, O., Parker, I., and Cahalan, M. D. (2004b). Imaging the Single Cell Dynamics of CD4+ T Cell Activation by Dendritic Cells in Lymph Nodes. J Exp Med *200*, 847-856.

Miller, M. J., Wei, S. H., Cahalan, M. D., and Parker, I. (2003). Autonomous T cell trafficking examined in vivo with intravital two-photon microscopy. Proceedings of the National Academy of Sciences of the United States of America *100*, 2604-2609.

Miller, M. J., Wei, S. H., Parker, I., and Cahalan, M. D. (2002). Two-photon imaging of lymphocyte motility and antigen response in intact lymph node. Science *296*, 1869-1873.

Misslitz, A., Pabst, O., Hintzen, G., Ohl, L., Kremmer, E., Petrie, H. T., and Forster, R. (2004). Thymic T cell development and progenitor localization depend on CCR7. J Exp Med *200*, 481-491.

Mora, J. R., Bono, M. R., Manjunath, N., Weninger, W., Cavanagh, L. L., Rosemblatt, M., and Von Andrian, U. H. (2003). Selective imprinting of gut-homing T cells by Peyer's patch dendritic cells. Nature *424*, 88-93.

Morales, J., Homey, B., Vicari, A. P., Hudak, S., Oldham, E., Hedrick, J., Orozco, R., Copeland, N. G., Jenkins, N. A., McEvoy, L. M., and Zlotnik, A. (1999). CTACK, a skin-associated chemokine that preferentially attracts skin-homing memory T cells. Proc Natl Acad Sci U S A *96*, 14470-14475.

Nagai, T., Ibata, K., Park, E. S., Kubota, M., Mikoshiba, K., and Miyawaki, A. (2002). A variant of yellow fluorescent protein with fast and efficient maturation for cell-biological applications. Nature Biotechnology *20*, 87 - 90.

Nagamine, K., Peterson, P., Scott, H. S., Kudoh, J., Minoshima, S., Heino, M., Krohn, K. J., Lalioti, M. D., Mullis, P. E., Antonarakis, S. E., *et al.* (1997). Positional cloning of the APECED gene. Nat Genet *17*, 393-398.

Negulescu, P. A., Krasieva, T. B., Khan, A., Kerschbaum, H. H., and Cahalan, M. D. (1996). Polarity of T cell shape, motility, and sensitivity to antigen. Immunity *4*, 421-430.

Nossal, G. J., Ada, G. L., Austin, C. M., and Pye, J. (1965). Antigens in immunity. 8. Localization of 125-I-labelled antigens in the secondary response. Immunology *9*, 349-357.

Okada, T., Miller, M. J., Parker, I., Krummel, M. F., Neighbors, M., Hartley, S. B., O'Garra, A., Cahalan, M. D., and Cyster, J. G. (2005). Antigen-Engaged B Cells Undergo Chemotaxis toward the T Zone and Form Motile Conjugates with Helper T Cells. PLoS Biol *3*, e150.

Pabst, R. (1988). The spleen in lymphocyte migration. Immunol Today *9*, 43-45.
Pawley, J. B. e. (2006). Handbook of Biological Confocal Microscopy, 3rd ed. New York, Springer.

Pitkanen, J., Doucas, V., Sternsdorf, T., Nakajima, T., Aratani, S., Jensen, K., Will, H., Vahamurto, P., Ollila, J., Vihinen, M., *et al.* (2000). The autoimmune regulator protein has transcriptional transactivating properties and interacts with the common coactivator CREB-binding protein. J Biol Chem *275*, 16802-16809.

Poltorak, A., He, X., Smirnova, I., Liu, M. Y., Van Huffel, C., Du, X., Birdwell, D., Alejos, E., Silva, M., Galanos, C., *et al.* (1998). Defective LPS signaling in C3H/HeJ and C57BL/10ScCr mice: mutations in Tlr4 gene. Science *282*, 2085-2088.

Probst, H. C., Lagnel, J., Kollias, G., and van den Broek, M. (2003). Inducible transgenic mice reveal resting dendritic cells as potent inducers of CD8+ T cell tolerance. Immunity *18*, 713-720.

Probst, H. C., McCoy, K., Okazaki, T., Honjo, T., and van den Broek, M. (2005). Resting dendritic cells induce peripheral CD8+ T cell tolerance through PD-1 and CTLA-4. Nat Immunol *6*, 280-286.

Purbhoo, M. A., Irvine, D. J., Huppa, J. B., and Davis, M. M. (2004). T cell killing does not require the formation of a stable mature immunological synapse. Nat Immunol *5*, 524-530.

Qi, H., Egen, J. G., Huang, A. Y., and Germain, R. N. (2006). Extrafollicular activation of lymph node B cells by antigen-bearing dendritic cells. Science *312*, 1672-1676.

Qureshi, S. T., Lariviere, L., Leveque, G., Clermont, S., Moore, K. J., Gros, P., and Malo, D. (1999). Endotoxin-tolerant mice have mutations in Toll-like receptor 4 (Tlr4). J Exp Med *189*, 615-625.

Rajewsky, K. (1996). Clonal selection and learning in the antibody system. Nature *381*, 751-758.

Ramiro, A. R., Stavropoulos, P., Jankovic, M., and Nussenzweig, M. C. (2003). Transcription enhances AID-mediated cytidine deamination by exposing single-stranded DNA on the nontemplate strand. Nat Immunol *4*, 452-456.

Ramsey, C., Winqvist, O., Puhakka, L., Halonen, M., Moro, A., Kampe, O., Eskelin, P., Pelto-Huikko, M., and Peltonen, L. (2002). Aire deficient mice develop multiple features of APECED phenotype and show altered immune response. Hum Mol Genet *11*, 397-409.

Read, S., Malmstrom, V., and Powrie, F. (2000). Cytotoxic T lymphocyte-associated antigen 4 plays an essential role in the function of CD25(+)CD4(+) regulatory cells that control intestinal inflammation. J Exp Med *192*, 295-302.

Redmond, W. L., Hernandez, J., and Sherman, L. A. (2003). Deletion of naive CD8 T cells requires persistent antigen and is not programmed by an initial signal from the tolerogenic APC. J Immunol *171*, 6349-6354.

Reiss, Y., Proudfoot, A. E., Power, C. A., Campbell, J. J., and Butcher, E. C. (2001). CC chemokine receptor (CCR)4 and the CCR10 ligand cutaneous T cell-attracting chemokine (CTACK) in lymphocyte trafficking to inflamed skin. J Exp Med *194*, 1541-1547.

Rogers, P. R., Grey, H. M., and Croft, M. (1998). Modulation of naive CD4 T cell activation with altered peptide ligands: the nature of the peptide and presentation in the context of costimulation are critical for a sustained response. J Immunol *160*, 3698-3704.

Sallusto, F., Lenig, D., Forster, R., Lipp, M., and Lanzavecchia, A. (1999). Two subsets of memory T lymphocytes with distinct homing potentials and effector functions. Nature *401*, 708-712.

Scheinecker, C., McHugh, R., Shevach, E. M., and Germain, R. N. (2002). Constitutive presentation of a natural tissue autoantigen exclusively by dendritic cells in the draining lymph node. J Exp Med *196*, 1079-1090.

Schwickert, T. A., Lindquist, R. L., Shakhar, G., Livshits, G., Skokos, D., Kosco-Vilbois, M. H., Dustin, M. L., and Nussenzweig, M. C. (2007). In vivo imaging of germinal centres reveals a dynamic open structure. Nature *446*, 83-87.

Shakhar, G., Lindquist, R. L., Skokos, D., Dudziak, D., Huang, J. H., Nussenzweig, M. C., and Dustin, M. L. (2005). Stable T cell-dendritic cell interactions precede the development of both tolerance and immunity in vivo. Nat Immunol.

Shaw, G. B. (1906). The doctor's dilemma. Echo library, New York.

Shih, T. A., Meffre, E., Roederer, M., and Nussenzweig, M. C. (2002a). Role of BCR affinity in T cell dependent antibody responses in vivo. Nat Immunol *3*, 570-575.

Shih, T. A., Roederer, M., and Nussenzweig, M. C. (2002b). Role of antigen receptor affinity in T cell-independent antibody responses in vivo. Nat Immunol *3*, 399-406.

Shiow, L. R., Rosen, D. B., Brdickova, N., Xu, Y., An, J., Lanier, L. L., Cyster, J. G., and Matloubian, M. (2006). CD69 acts downstream of interferon-alpha/beta to inhibit S1P1 and lymphocyte egress from lymphoid organs. Nature *440*, 540-544.

Sigmundsdottir, H., Pan, J., Debes, G. F., Alt, C., Habtezion, A., Soler, D., and Butcher, E. C. (2007). DCs metabolize sunlight-induced vitamin D3 to 'program' T cell attraction to the epidermal chemokine CCL27. Nat Immunol *8*, 285-293.

Sixt, M., Kanazawa, N., Selg, M., Samson, T., Roos, G., Reinhardt, D. P., Pabst, R., Lutz, M. B., and Sorokin, L. (2005). The conduit system transports soluble antigens from the afferent lymph to resident dendritic cells in the T cell area of the lymph node. Immunity *22*, 19-29.

Skokos, D., Shakhar, G., Varma, R., Waite, J. C., Cameron, T. O., Lindquist, R. L., Schwickert, T., Nussenzweig, M. C., and Dustin, M. L. (2007). Peptide-MHC potency governs dynamic interactions between T cells and dendritic cells in lymph nodes. Nat Immunol *8*, 835-844.

Sloan-Lancaster, J., and Allen, P. M. (1995). Significance of T-cell stimulation by altered peptide ligands in T cell biology. Curr Opin Immunol *7*, 103-109.

Sloan-Lancaster, J., Evavold, B. D., and Allen, P. M. (1993). Induction of T-cell anergy by altered T-cell-receptor ligand on live antigen-presenting cells. Nature *363*, 156-159.

Smith, C. M., Belz, G. T., Wilson, N. S., Villadangos, J. A., Shortman, K., Carbone, F. R., and Heath, W. R. (2003). Cutting edge: conventional CD8 alpha+ dendritic cells are preferentially involved in CTL priming after footpad infection with herpes simplex virus-1. J Immunol *170*, 4437-4440.

Springer, T. A., Thompson, W. S., Miller, L. J., Schmalstieg, F. C., and Anderson, D. C. (1984). Inherited deficiency of the Mac-1, LFA-1, p150,95 glycoprotein family and its molecular basis. J Exp Med *160*, 1901-1918.

Stagg, A. J., Kamm, M. A., and Knight, S. C. (2002). Intestinal dendritic cells increase T cell expression of alpha4beta7 integrin. Eur J Immunol *32*, 1445-1454.

Starr, T. K., Jameson, S. C., and Hogquist, K. A. (2003). Positive and negative selection of T cells. Annu Rev Immunol *21*, 139-176.

Stein, J. V., Rot, A., Luo, Y., Narasimhaswamy, M., Nakano, H., Gunn, M. D., Matsuzawa, A., Quackenbush, E. J., Dorf, M. E., and von Andrian, U. H. (2000). The CC chemokine thymus-derived chemotactic agent 4 (TCA-4, secondary lymphoid tissue chemokine, 6Ckine, exodus-2) triggers lymphocyte function-associated antigen 1-mediated arrest of rolling T lymphocytes in peripheral lymph node high endothelial venules. J Exp Med *191*, 61-76.

Steinman, R. M., Hawiger, D., Liu, K., Bonifaz, L., Bonnyay, D., Mahnke, K., Iyoda, T., Ravetch, J., Dhodapkar, M., Inaba, K., and Nussenzweig, M. (2003a). Dendritic cell function in vivo during the steady state: a role in peripheral tolerance. Ann N Y Acad Sci *987*, 15-25.

Steinman, R. M., Hawiger, D., and Nussenzweig, M. C. (2003b). Tolerogenic dendritic cells. Annual Review of Immunology *21*, 685-711.

Stoll, S., Delon, J., Brotz, T. M., and Germain, R. N. (2002). Dynamic imaging of T cell-dendritic cell interactions in lymph nodes. Science *296*, 1873-1876.

Streeter, P. R., Berg, E. L., Rouse, B. T., Bargatze, R. F., and Butcher, E. C. (1988a). A tissue-specific endothelial cell molecule involved in lymphocyte homing. Nature *331*, 41-46.

Streeter, P. R., Rouse, B. T., and Butcher, E. C. (1988b). Immunohistologic and functional characterization of a vascular addressin involved in lymphocyte homing into peripheral lymph nodes. J Cell Biol *107*, 1853-1862.

Sumen, C., Mempel, T. R., Mazo, I. B., and von Andrian, U. H. (2004). Intravital microscopy: visualizing immunity in context. Immunity *21*, 315-329.

Sun, J. B., Olsson, T., Wang, W. Z., Xiao, B. G., Kostulas, V., Fredrikson, S., Ekre, H. P., and Link, H. (1991). Autoreactive T and B cells responding to myelin proteolipid protein in multiple sclerosis and controls. Eur J Immunol *21*, 1461-1468.

Suri-Payer, E., and Cantor, H. (2001). Differential cytokine requirements for regulation of autoimmune gastritis and colitis by CD4(+)CD25(+) T cells. J Autoimmun *16*, 115-123.

Svensson, M., Marsal, J., Ericsson, A., Carramolino, L., Broden, T., Marquez, G., and Agace, W. W. (2002). CCL25 mediates the localization of recently activated CD8alphabeta(+) lymphocytes to the small-intestinal mucosa. J Clin Invest *110*, 1113-1121.

Szakal, A. K., Kosco, M. H., and Tew, J. G. (1988). A novel in vivo follicular dendritic cell-dependent iccosome-mediated mechanism for delivery of antigen to antigen-processing cells. J Immunol *140*, 341-353.

Takeda, S., Rodewald, H. R., Arakawa, H., Bluethmann, H., and Shimizu, T. (1996). MHC class II molecules are not required for survival of newly generated CD4+ T cells, but affect their long-term life span. Immunity *5*, 217-228.

Talmage, D. W. (1959). Immunological specificity, unique combinations of selected natural globulins provide an alternative to the classical concept. Science *129*, 1643-1648.

Tang, Q., Adams, J. Y., Tooley, A. J., Bi, M., Fife, B. T., Serra, P., Santamaria, P., Locksley, R. M., Krummel, M. F., and Bluestone, J. A. (2006). Visualizing regulatory T cell control of autoimmune responses in nonobese diabetic mice. Nat Immunol *7*, 83-92.

Thery, C., Regnault, A., Garin, J., Wolfers, J., Zitvogel, L., Ricciardi-Castagnoli, P., Raposo, G., and Amigorena, S. (1999). Molecular characterization of dendritic cell-derived exosomes. Selective accumulation of the heat shock protein hsc73. Journal of Cell Biology *147*, 599-610.

Thucydides, a., and Warner, R. t. (1954). History of the Peloponnesian War, Book 2. Penguin Classics; Revised edition.

Uchida, D., Hatakeyama, S., Matsushima, A., Han, H., Ishido, S., Hotta, H., Kudoh, J., Shimizu, N., Doucas, V., Nakayama, K. I., *et al.* (2004). AIRE functions as an E3 ubiquitin ligase. J Exp Med *199*, 167-172.

Ueno, T., Saito, F., Gray, D. H., Kuse, S., Hieshima, K., Nakano, H., Kakiuchi, T., Lipp, M., Boyd, R. L., and Takahama, Y. (2004). CCR7 signals are essential for cortex-medulla migration of developing thymocytes. J Exp Med *200*, 493-505.

Varma, R., Campi, G., Yokosuka, T., Saito, T., Dustin, M. L. (2006). T cell receptor-proximal signals are sustained in peripheral microclusters and terminated in the central supramolecular activation cluster. Immunity *25*:117-127.

Vermaelen, K. Y., Carro-Muino, I., Lambrecht, B. N., and Pauwels, R. A. (2001). Specific migratory dendritic cells rapidly transport antigen from the airways to the thoracic lymph nodes. Journal of Experimental Medicine *193*, 51-60.

Villasenor, J., Benoist, C., and Mathis, D. (2005). AIRE and APECED: molecular insights into an autoimmune disease. Immunol Rev *204*, 156-164.

von Andrian, U. H. (1996). Intravital microscopy of the peripheral lymph node microcirculation in mice. Microcirculation *3*, 287-300.

von Andrian, U. H., and Mempel, T. R. (2003). Homing and cellular traffic in lymph nodes. Nature Reviews Immunology *3*, 867-878.

Warnock, R. A., Askari, S., Butcher, E. C., and von Andrian, U. H. (1998). Molecular mechanisms of lymphocyte homing to peripheral lymph nodes. J Exp Med *187*, 205-216.

Widengren, J., and Rigler, R. (1996). Mechanisms of photobleaching investigated by fluorescence correlation spectroscopy. Bioimaging *4*, 149-157.

Wildin, R. S., Ramsdell, F., Peake, J., Faravelli, F., Casanova, J. L., Buist, N., Levy-Lahad, E., Mazzella, M., Goulet, O., Perroni, L., *et al.* (2001). X-linked neonatal diabetes mellitus, enteropathy and endocrinopathy syndrome is the human equivalent of mouse scurfy. Nat Genet *27*, 18-20.

Wilson, N. S., El-Sukkari, D., and Villadangos, J. A. (2004). Dendritic cells constitutively present self antigens in their immature state in vivo and regulate antigen presentation by controlling the rates of MHC class II synthesis and endocytosis. Blood *103*, 2187-2195.

Wright, D. E., Cheshier, S. H., Wagers, A. J., Randall, T. D., Christensen, J. L., and Weissman, I. L. (2001). Cyclophosphamide/granulocyte colony-stimulating factor causes selective mobilization of bone marrow hematopoietic stem cells into the blood after M phase of the cell cycle. Blood *97*, 2278-2285.

Xu, C., Zipfel, W., Shear, J. B., Williams, R. M., and Webb, W. W. (1996). Multiphoton fluorescence excitation: new spectral windows for biological nonlinear microscopy. Proc Natl Acad Sci U S A *93*, 10763-10768.

Yokosuka, T., Sakata-Sogawa, K., Kobayashi, W., Hiroshima, M., Hashimoto-Tane, A., Tokunaga, M., Dustin, M. L., Saito, T. (2005). Newly generated T cell receptor microclusters initiate and sustain T cell activation by recruitment of Zap70 and SLP-76. Nat Immunol *6*, 1253-1262.

Zhao, X., Deak, E., Soderberg, K., Linehan, M., Spezzano, D., Zhu, J., Knipe, D. M., and Iwasaki, A. (2003). Vaginal submucosal dendritic cells, but not Langerhans cells, induce protective Th1 responses to herpes simplex virus-2. J Exp Med *197*, 153-162.

Zipfel, W. R., Williams, R. M., and Webb, W. W. (2003). Nonlinear magic: multiphoton microscopy in the biosciences. Nat Biotechnol *21*, 1369-1377.